Table of Contents

List of Figures

List of Tables

Nomenclature

Acronyms

ac	Alternating Current
CUT	Core Under Test
dc	Direct Current
FET	Field Effect Transistor
J-A	Jiles-Atherton
OA	Op-Amp
SMPS	Switch Mode Power Supply
THD	Total Harmonic Distortion
ZVS	Zero Voltage Switching

Symbols

Small Characters

a	J-A parameter
c	J-A parameter
a_o	Constant due to inclusions
bo	Constant due to crystal anisotropy
c_{ij}	elastic moduli
e_{ij}	Strains
f	Frequency
f_k	Magnetocrystalline anisotropy energy density
f_a	Anisotropy energy density
k	J-A parameter
k_B	Boltzman constant
m	Magnetic moment, mass
n	Average density of pinning sites
p.f.	Power factor
t	Time

u(a,b,c)	Displacement in Cartesian coordinates
v	core volume, velocity
vf	Volume Fraction
v_f	Vibration amplitude of harmonic at the ac magnetic field excitation frequency
v_n	Vibration amplitude of nth harmonic component up to fifth harmonic and excluding v_f

Capital Letters

A	Cross sectional area
A_i	Amplitude of ith harmonic of vibration
A_L	Inductance factor
B	Flux density
B_{ac}	ac flux density
B_{dc}	dc flux density
B_e	Effective flux density
B_i	Magnetoelastic coupling constants
B_m	Maximum operating flux density
B_{rem}	Remanent flux density
B_{sat}	Saturation flux density
Co	Cobalt
Cu	Copper
D	Fractional energy loss per period of vibration
E	Youngs modulus, percentage error, Energy
E_{pin}	Total energy dissipated through domain wall movement
Fe	Iron
H	Applied magnetic field strength
H_a	Magnetic field strength component due to anisotropy
H_c	Coercive force
H_{dc}	dc magnetic field strength
H_e	Effective magnetic field strength
$H_{\sigma i}$	Magnetic field strength component due to internal stress
I	Current

I_{ac}	ac current
I_{dc}	dc current
J_s	Saturation polarization
K	Anisotropy energy density constant
I_{excite}	Excitation current
L	Inductance
M	Magnetization
M_{air}	Air cored magnetizing inductance
M_{cut}	CUT magnetizing inductance
M_{an}	Anhysteretic magnetization
M_{irr}	Irreversible magnetization
M_{rev}	Reversible magnetization
M_s	Saturation magnetization
Mn-Zn	Manganese-zinc ferrite material
Mg	Magnesium
N	Turns on a winding, domain density p.u. volume
Ni-Zn	Nickel-zinc ferrite material
R(a,b,c)	Position in Cartesian coordinates
R_{FE}	Equivalent core loss resistance
R_W	Winding resistance
T	Temperature
V(t)	Vibration
V_{dc}	dc voltage
V_{excite}	Excitation voltage
V_s	Supply voltage
V_{sense}	Excitation winding emf
W_e	Elastic energy stored at maximum strain
X_l	Leakage reactance
X_m	Magnetizing reactance

Greek Letters

α	J-A parameter, phase shift measurement error
α_{LL}	Landau-Lifschitz damping constant
α_n	Direction cosines of the spontaneous magnetization vector referred to the

	crystal axes
δ	domain wall thickness
ΔW	energy lost per cycle at the expense of W_e
ε_{pin}	Domain wall pinning site energy
ε_{π}	180^o domain wall pinning site energy
γ	Electron gyromagnetic constant
κH	Field induced increase in spontaneous magnetization of domains
θ	Phase shift
λ	Joule magnetostriction
μ_e	effective permeability of a gapped core
μ_i	initial permeability
μ_o	$4\pi \times 10^{-7}$
χ_{diff}	Differential susceptibility
ϕ	Flux
σ	Applied stress

Chapter 1

Introduction

1.1 Research Background

An electronic power supply is essential to the operation of most electrical and electronic products, including computers, office equipment, battery chargers, as well as a wide range of other household and industrial appliances. Its ubiquity is evident through the estimate that 2.9 billion units were used in the U.S. alone in 2003, consuming an estimated 207 billion kWh of electricity [1]. From these estimates it has come to the attention of various environmental protection organizations that even fractional improvements to the efficiency of power supplies offer the opportunity for large energy savings to be achieved. Accordingly, strong regulatory pressures have been have been exerted on manufacturers to improve power supply efficiency levels [2]-[6], and in Europe were estimated to have saved between 1 and 5 TWh of electricity in 2010 [7]. Therefore, to improve on these energy savings research in the area of power supply efficiency has assumed great practical importance.

Because of their low cost, small size, and high efficiency, high frequency switch-mode power supplies, SMPS, are currently the predominant form in which power supplies are implemented [8].

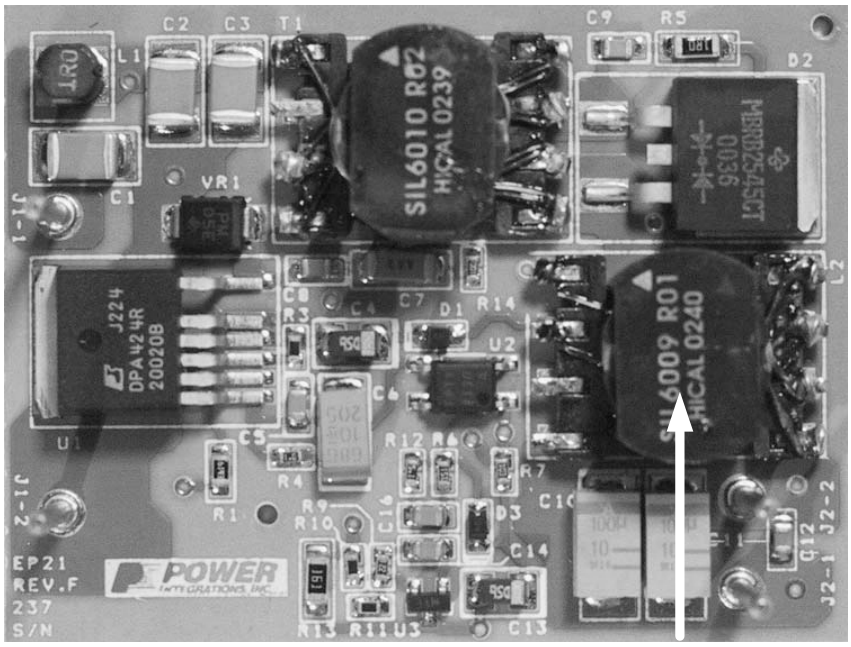

Fig. 1.1 SMPS circuit including dc filter choke, reproduced from [9]

A factor that significantly affects the efficiency and overall size of a SMPS is the performance of its dc filter choke, which, as evident from Fig. 1.1, is typically one of the largest components in a SMPS circuit. A dc filter choke consists essentially of a magnetically soft core around which conductive wire is wound and, within SMPS circuits, is used to limit the short term variations of current at the power supply output [10]. This limitation ensures the current through the winding of a dc filter choke is predominantly dc in nature. As a consequence, the dc component of the magnetic field strength applied to the core is significantly higher than the ac component, and in this condition the core is said to operate under a dc bias. If operated at an excessively high dc bias the inductance of a dc filter choke may decrease to a value below a required minimum, and to preclude such a situation occurring it is often necessary to increase the size of the core. Other factors influencing the core size include: the number of turns fitted to the winding around the core, the temperature rise of the core and winding due to energy losses, and the length of the air gap that can be introduced into the core's magnetic path. Because dc filter chokes are one of the largest and, therefore, most costly components in a SMPS circuit a considerable amount of effort is generally placed on ensuring the size of the core is as small as possible. A simplified relationship between the core size in terms of its volume, the inductance it must provide at a particular current, the maximum flux density it is operated at, and its permeability with an air gap in its magnetic path is given by [11]:

$$\frac{LI^2}{v} = \frac{B_m^2}{\mu_o \mu_e} \tag{1.1}$$

where,

L = dc filter choke inductance (H)

I = current (A)

B_m = maximum operating flux density (T)

v = core volume (m^3)

μ_o = $4\pi \times 10^{-7}$

μ_e = effective permeability of an air-gapped core

From (1.1) it is apparent that the left-most term represents the energy density of the core and, hence, that it is desirable for this to be maximized in order to minimize the core size. One means by which this can be achieved is through lowering μ_e by increasing the air gap in the core. However, practical considerations limit the increase in energy density that can be achieved in this manner, as a larger air gap requires a greater number of turns to attain a given inductance, thus incurring higher winding losses [12]. From (1.1) it is also apparent that the energy density of the dc filter choke is maximized if B_m is chosen to be as close as possible to the saturation flux density, B_{sat}, given an allowable safety margin. The value of B_{sat} differs between the varieties of magnetic materials that are available and, for this reason, the choice of the magnetic material used to implement the core has a direct bearing on the size of a dc filter choke.

Table 1.1 Magnetic Material Characteristics

Material	Part number	B_{sat} (T)	dc Resistivity (Ω /cm)	μ_i
Nanocrystalline	Vitroperm 500F [13]	1.2 [1]	0.000115 [1]	10000 - 150000 [1]
Amorphous alloy	2605SA1[14]	1.56 [1]	0.000137 [1]	45000 [5]
Mn-Zn ferrite	3F3[15]	0.44 [2]	200 [4]	2000 [6]
Mn-Zn ferrite	3C90 [15]	0.47 [2]	500 [4]	2300 [6]
Mn-Zn ferrite	F49 [16]	0.58 [3]	100 [4]	1000 [7]

Notes: [1] Test conditions not stated, [2] 25 °C, 10 kHz, 1200 A/m, [3] 25 °C, 10 kHz, 796 A/m, [4] 25 °C, [5] stated to be "as cast", [6] 25 °C, ≤ 10 kHz, 0.25 mT, [7] 25 °C, 10 kHz, < 0.1 mT

The values of B_{sat} of various magnetic materials that can be used in dc filter choke applications are listed in Table 1.1, along with other magnetic properties of interest including the dc resistivity, and the initial permeability, μ_i. In terms of B_{sat} and μ_i it is apparent that the nanocrystalline and amorphous alloy materials are advantageous in comparison to the Mn-Zn ferrite materials. However, the advantage of high permeability is reduced with the insertion of an air gap into the core which, as shown by (1.1), is required in order to increase the energy density level. Furthermore, it is also apparent from Table 1.1 that Mn-Zn ferrite materials have significantly higher resistivity's than those of the other materials and, therefore, are far less susceptible to eddy current losses. This form of loss increases significantly with frequency for nanocrystalline and amorphous alloy materials and, in addition, increases with the length of the air gap in the core. This particular form of loss is attributable to fringing flux from the air gap entering the core in a direction perpendicular to the ribbon with which nanocrystalline and amorphous alloy cores are wound [17]. Further advantages of Mn-Zn ferrite materials over other material types include its availability in a comparatively wide range of shapes and, importantly, its relatively low cost [18]. For these reasons Mn-Zn ferrite materials are very heavily used to implement the cores of dc filter chokes. However, despite this heavy usage and the influence of core losses on the overall efficiency of SMPS, the core loss characteristics of Mn-Zn ferrite materials under dc bias conditions are not widely known. Moreover, the impact of dc bias conditions on the core losses of Mn-Zn ferrite has previously been completely misrepresented; for example in [10] it is stated that the loss contribution of the ferrite core of a magnetic component progressively falls as dc bias levels are increased. This claim contradicts experimental evidence presented by the author, as well as a small number of other researchers, showing that Mn-Zn ferrite core losses increase significantly with dc bias levels, even as the ac excitation level is maintained constant. This can lead to unfortunate consequences for the magnetic component designer who, in accordance with (1.1), seeks to maximize the energy density of the core of a dc filter choke by running it at a high level of B_m, and thus dc bias, yet is unaware of the increase in core losses this entails. Therefore, there is a need for an investigation into this phenomenon. This Thesis addresses this need through proposing a core loss mechanism for Mn-Zn ferrite materials that increases with increasing dc bias levels. To support the proposed theory the increase in core losses with dc bias levels is modeled in a manner that is consistent with the core loss mechanism. Furthermore, measurement techniques are proposed which allow the core loss mechanism to be monitored at the same time as core losses under dc bias conditions are accurately measured.

In the process of investigating core losses under dc bias conditions a particularly unusual phenomenon was observed involving the distortion of B-H loops into a figure-eight shape. This phenomenon is also investigated in the Thesis.

In Section 1.2 general aspects relating to the nature of Mn-Zn ferrite material and its core loss mechanisms are described, and measured core loss characteristics in the absence of a dc bias are presented.

1.2 The Characteristics of an Mn-Zn Ferrite Material

Ferrite is dark grey, or black in color, and is a very hard, brittle, and chemically inert ceramic material. For magnetically soft ferrites with a cubic crystal structure the general composition is $MeFe_2O_4$, where Me represents one, or several combinations of elements such as manganese, Mn, zinc, Zn, nickel, Ni, cobalt, Co, copper, Cu, iron, Fe, or magnesium, Mg. The most popular combinations are Ni-Zn, and Mn-Zn [19].

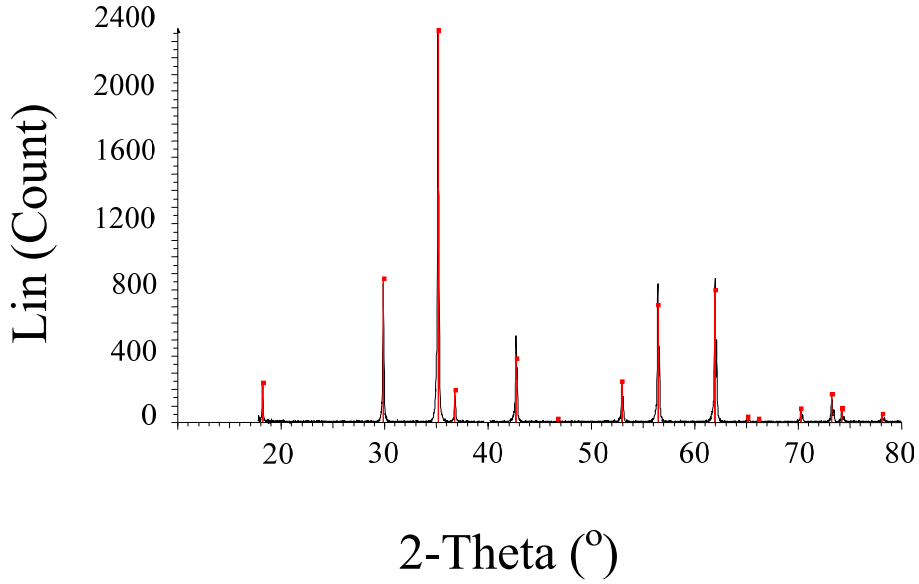

Fig. 1.2 X-ray diffraction results for MMG F49 Mn-Zn material

To investigate the chemical composition and crystal structure of a polycrystalline material such as ferrite, a x-ray diffraction test can be performed. A test of this type projects x-ray beams into a sample of the material, the nature of which is then characterized using the angle, 2-Theta, and intensity, Lin, of the beams reflected from the atoms forming the material's crystal structure [20].

The results of such a test carried out on a MMG F49 Mn-Zn ferrite sample are shown in Fig. 1.2, and enabled it to be identified as having a $Mn_{0.2}Zn_{0.8}Fe_2O_4$ chemical composition, with a face centered cubic crystal structure. This particular Mn-Zn ferrite material is advertised by its manufacturer as being particularly suited to dc filter choke applications due to its level of saturation flux density, B_{sat} which, at 0.58 T, is high in comparison to other Mn-Zn ferrite materials [21]. Therefore, F49 material was tested extensively for the results presented in this Thesis, and a table of its properties is given in Appendix A.

While the properties of a ferrite material such as its level of B_{sat}, permeability, and core loss characteristics are dependent to a large extent on its chemical composition, they are also dependent on the techniques with which it is manufactured [22]. The manufacturing process begins with the intimate mixing of metal oxides of the constituent metals of the ferrite, which are then pre-fired at a temperature of 1000^{o}C in a process known as calcining. The pre-fired material is then broken down, pulverized and, after the addition of bonding materials, is formed into granules suitable for either for pressing or for injection molding or extrusion. Most ferrite parts are formed by pressing, in which case the granules are poured into a die before being compressed. The pressed part is then sintered at a temperature between 1150^{o}C and 1300^{o}C, which is dependent on the grade of ferrite to be produced. This process causes densification and substantial shrinkage of the formed ferrite part, which at this stage has its required magnetic properties. A further manufacturing step may then be employed to give surfaces a smooth finish.

From the above description it is apparent that the manufacturing process contains a number of variables. Those which have the greatest influence on the magnetic properties of the ferrite are the proportions and homogeneity of the initial mixing of metal oxides, and the control of the temperature and atmosphere throughout the sintering period. During the sintering period crystal growth proceeds at points where the particles of the pressed ferrite part are in contact with each other and crystal grains are formed. The crystal structure within ferrites is composed of unit cells that are cubic in shape containing eight molecules of $MeFe_2O_4$ [10], and through building unit cells one atop another a lattice is created. Ideally, a grain is a region in a solid where the crystal structure is perfect, having no defects such as non-magnetic inclusions, pores, or dislocations, and so is in contrast to the boundaries between grains where defects do exist [23]. However, in reality intra-granular defects may be present, and these can be introduced into a ferrite material if crystal growth during the sintering process is too rapid [10]. In this case defects in the form of

pores and impurities can be trapped within a grain. The presence of these defects, both within grains and at grain boundaries, plays a strong role in the magnetization of magnetic materials through the pinning effect that defect sites have on domain walls. As explained in Chapters 3 and 4, defects give rise to energy losses through the pinning and de-pinning of domain walls as they move. For magnetic metals domain wall movement is largely controlled by intra-granular defect distances. However, according to [24], the grains in ferrite materials are comparatively small in size and the material itself is relatively free from intra-granular defects. Therefore, for this type of material domain walls tend to be pinned at grain boundaries.

The energy dissipated due to the pinning of domain walls in the magnetization process contributes to the hysteresis losses of ferrite materials. In turn, these losses create the phenomenon of hysteresis, whereby the response, or magnetization, of the material lags the magnetic field which is applied to it [25]. Hysteresis losses are a form of core loss which is invariant with frequency, but strongly dependent on the amplitude of the magnetic field applied to a core. In addition, frequency dependent losses may also exist, which are discussed further in Chapter 2. For MMG F49 Mn-Zn ferrite material measured results showing the variation in core losses with both the applied ac flux density, and the excitation frequency are given in Fig. 1.3. These results were measured using the technique described in Section 5.4, and at a core temperature of 65^{o}C. At this particular temperature the losses of MMG F49 material ferrite cores are at a minimum, as is apparent from the measured core loss vs. temperature characteristics shown in the Fig. 1.3(b), and show the importance of specifying the temperature at which core loss measurements are made. Accordingly, this specification is stated for all core loss results presented in this Thesis.

In addition to being caused by core losses, hysteresis in the magnetization process can also be caused by anisotropy [26], which, within the context of magnetic materials, refers to the phenomenon whereby certain directions of magnetization are favored over others. Anisotropy energy is that which is required to turn the magnetization from a favored, or easy, direction into another [27], for example that demanded by an applied magnetic field, and can have various causes, and appear in various forms. In this Thesis it is proposed that stress anisotropy, originating through field-induced magnetostriction, influences the magnetization process under dc bias conditions to the extent that distorted B-H loops can be generated. It is further proposed that field-induced magnetostriction can increase hysteresis losses through the core loss

mechanism associated with domain wall pinning. To support both these proposals theoretical considerations and experimental evidence are presented.

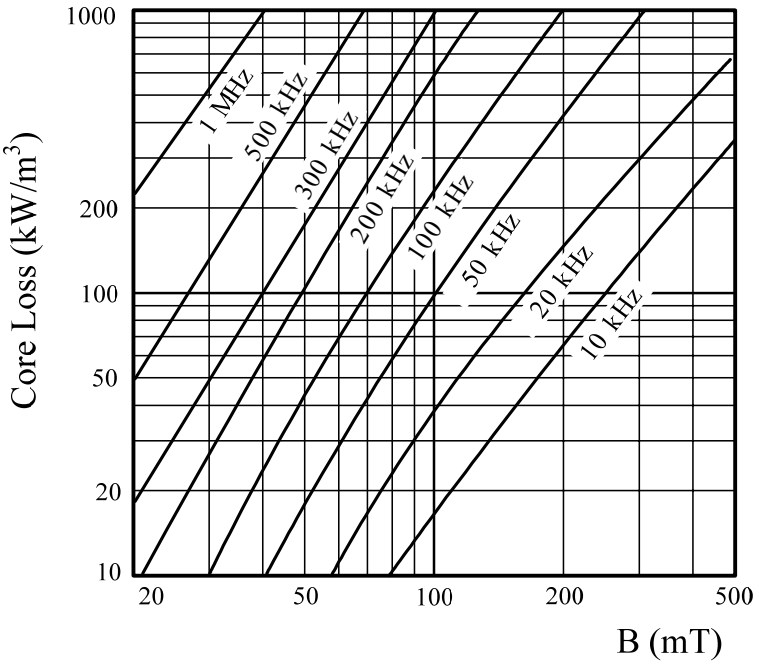

(a)

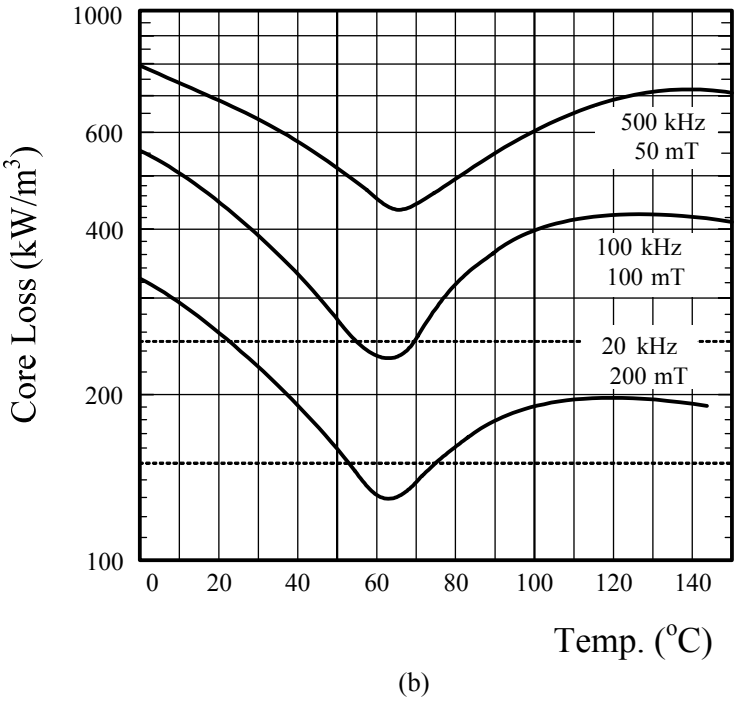

(b)

Fig. 1.3 The variation of core losses (without dc bias) with (a) frequency and flux density, (b) temperature

1.3 The Scope of the Thesis

This Thesis presents the results of an investigation into mechanisms that are operative in the magnetization process of Mn-Zn ferrite materials which, under dc bias conditions, cause core losses to rise significantly above those incurred in the absence of a dc bias. The investigation encompasses a review of previous work in this area, before proposing a core loss mechanism that increases with increasing levels of dc bias, and which is integrated into a model of the magnetization process. In addition, the effects of stress anisotropy are described, and these are also incorporated into the model to predict unusually shaped B-H loops. To verify the proposed core loss mechanism, and the effects of anisotropy on B-H loop shapes, core losses and B-H loops must be accurately measured. For this purpose an accurate measurement circuit is proposed, which also incorporates the means for monitoring a core loss mechanism operating under dc bias conditions, and measured results are presented. These results show a strong correlation between the proposed core loss mechanism and the increase in core losses with dc bias levels and, based on this evidence, confirm the validity of the theoretical work.

The chapters of this Thesis are arranged as follows:

In Chapter 2 a comprehensive review of previous investigations into Mn-Zn ferrite cores losses under dc bias conditions is presented. It includes measured core loss results, undertaken using a variety of core loss measurement circuit types, as well as explanations proposing why core losses increase with dc bias. Both the core loss measurement circuits, as well as the proposed explanations are critically evaluated.

In Chapter 3 explanations for why core losses increase with dc bias are presented which differ from those reviewed in Chapter 2. These explanations are associated with magnetomechanical effects and, therefore, this chapter also includes a description of the nature of field-induced magnetostriction under dc bias conditions. In the course of investigating core losses under dc bias conditions a particularly unusual phenomenon was observed, causing distorted B-H loops to be measured. The mechanism causing this phenomenon is proposed in this chapter.

In Chapter 4 the Jiles-Atherton, J-A, model for taking account of hysteresis in the magnetization process is described. In the description particular emphasis is placed on those parts of the model related to the mechanism causing core losses to increase with dc bias. The J-A model is then

modified to take into account the experimental conditions under which ferrite cores are tested in this Thesis, and used to predict the increase in core losses with dc bias. In addition, the mechanism causing B-H loops to distort under dc bias conditions is modeled, and it is shown that distorted B-H loops can be produced as observed experimentally.

In Chapter 5 three core loss measurement circuits are proposed and described in detail. Each circuit is critically evaluated, and that considered best is selected for making the core loss measurements under dc bias conditions that are presented in this Thesis. In addition, the operation of a laser vibrometer is described, which is used to monitor the magnetostrictive vibration of a ferrite core under test, CUT, under dc bias conditions.

In Chapter 6 core loss results measured under dc bias conditions are presented in association with magnetostrictive vibration waveforms of the CUT. These results are measured at frequencies close to, as well as distant from, magnetomechanical resonance, and show that the increase in core losses with dc bias is related to magnetomechanical effects.

In Chapter 7 measured B-H loops are presented which are distorted into a figure-eight shape under dc bias conditions, and within a narrow frequency range. These B-H loops were measured at the same time as magnetostrictive vibration waveforms of the CUT were generated, using the core loss measurement circuit selected in Chapter 5. Using the two sets of results it is shown that the distorted B-H loops can also be related to magnetomechanical effects.

Chapter 8 concludes the Thesis with a summary of the investigations and findings, and suggests future directions of study.

1.4 References

[1] A. Fanara, "Energy Star®: a Strategy to Encourage Improved Efficiency of Power Supplies," *IEEE Proc. APEC 2004.*, vol.1, 27 Sept. 2004, pp.24-30

[2] Australia Govt. Dept. of Climate Change, "MEPS Requirements for External Power Supplies", www.energyrating.gov.au/eps2.html

[3] California Energy Commission, "Appliance Efficiency Program", www.energy.ca.gov/appliances/index.html

[4] U.S. Dept. of Energy, "Energy Policy and Conservation Act (1975) and Amend.", www1.eere.energy.gov/buildings/appliance_standards/residential/battery_external.html

[5] Natural Resources Canada, "Energy Efficiency Act", www.nrcan.gc.ca

[6] China Standard Cerification Centre, www.cecp.org.cn/english/index.asp

[7] European Commission, "Code of Conduct on Energy Efficiency of External Power Supplies ver. 4", 8 Apr. 2009, www.powerint.com

[8] C. A. Baguley, B. Carsten, and U. K. Madawala, "An Investigation into the Impact of DC Bias Conditions on Ferrite Core Losses", *IEEE Trans. Magn*., vol. 44, no. 2, pp: 246 - 252, Feb. 2008

[9] Power Integrations, "Engineering Prototype Report EPR-21", www.powerint.com/sites/default/files/PDFFiles/epr21.pdf

[10] E. C. Snelling, "Soft Ferrites, Properties and Applications, 2nd ed.", Butterworths, 1988, ISBN 0-408-02760-6 pg 275

[11] N. R. Grossner, "Transformers for Electronic Circuits, Second Ed.", McGraw-Hill, 1983, ISBN 0-07-024979-2, pg.254

[12] B. Carsten, "A New High Saturation Ferrite Increases Switchmode Inductor Energy Density", *Proc. PCIM*, 2006

[13] www.vacuumschmelze.de

[14] www.metglas.com

[15] www.ferroxcube.com

[16] www.mmgca.com

[17] H. Fukunaga, T. Eguchi, Y. Ohta, H. Kakehashi , "Core Loss in Amorphous Cut Cores with Air Gaps," *IEEE Trans. Magn.*, vol.25, no.3, May 1989, pp.2694-2698

[18] B. J. Lyons, J. G. Hayes, M. G. Egan, "Magnetic Material Comparisons for High-Current Inductors in Low-Medium Frequency DC-DC Converters," *IEEE Proc. APEC 2007*, Feb. 25 -Mar. 1 2007, pp.71-77

[19] "Soft Ferrites Data Handbook MA01", Philips Components, 1996

[20] B. E. Warren, "X-Ray Diffraction", Addison-Wesley, 1969

[21] www.mmgca.com/catalogue/MMG-F49.pdf

[22] "Book 1, Ferrite Components and Accessories", MMG Product Catalogue, 1993

[23] P. M. Fishbane, S. Gasiorowicz, S. T. Thorton, "Physics for Scientists and Engineers", Prentice-Hall, 1993, ISBN 0-13-663238-6

[24] M. Le Floc'h, A. M. Konn, "Some of the Magnetic Properties of Polycrystalline Soft Ferrites: Origins and Developments of a Model for the Descriptions of the Quasistatic Magnetization", J. Phys. IV, France, 7, 1997, C1-187-C1-190

[25] G. Bertotti, "Hysteresis in Magnetism", Academic Press, San Diego, Academic Press, 1998, ISBN:0-12-093270

[26] F. Liorzou, B. Phelps, D. L. Atherton, "Macroscopic Modes of Magnetization", IEEE Trans. Magn., vol. 36, no. 2, Mar. 2000, pp.418-428

[27] J. Smit, H. P. J. Wijn, "Ferrites, Physical Properties of Ferrimagnetic Oxides in Relation to their Technical Applications", Philips Technical Library

Chapter 2

Literature Review

2.1 Introduction

In Chapter 1 the importance of minimizing the losses of ferrite cored magnetic components operating under dc bias conditions was described in terms of conservation of energy arguments, as well as those related to economics. These arguments have motivated investigations into the nature of ferrite core losses under dc bias conditions, and a literature review of this previous work is presented in this chapter. The literature review is divided into sections to consider specific aspects related to ferrite core losses under dc bias conditions and, to the knowledge of the author, represents all recent work carried out in this area.

To accurately measure core losses under dc bias conditions certain non-trivial difficulties must be overcome. In Section 2.2 these difficulties are described within the context of circuits that have previously been reported for the measurement of core losses under dc bias conditions. The results of ferrite core loss measurements are also presented in this section. In Section 2.3 previously proposed models and explanations relating ferrite core losses to dc bias conditions are described. In addition, measured core loss results which were presented in conjunction with core loss model predictions are shown. The models are categorized as either empirically based, as reviewed in Section 2.3.1, or physically based, as reviewed in Section 2.3.2. Physical explanations advanced for why ferrite core losses increase dc bias levels are also included in Section 2.3.2.

2.2 Core Loss Measurement Circuits under DC Bias Conditions

Of the ferrite core loss measurement circuits described in this literature review, all except one are based on measurements of the ac current through the excitation winding on a CUT, and the excitation winding emf. Such measurements allow core losses to be determined simply through multiplying the current and winding emf waveforms together on a sample by sample basis and integrating over one cycle, before dividing the result by the magnetic excitation period. Furthermore, using the excitation winding emf and current waveforms, B-H loops are also easily determined, through integrating the winding emf to find the flux density, B, and deriving the magnetic field strength, H, from the measured current. The simplified diagram of a circuit which can measure such quantities, and as used in [1]-[3], is illustrated in Fig. 2.1. Within this circuit current shunt R is used to sense the ac excitation current, and a flux sense winding is used to measure the excitation winding emf. Through measuring the winding emf in this manner voltage drops over the excitation winding resistance are excluded from the core loss measurement thereby eliminating a source of measurement error, as is discussed further in Chapter 5. From Fig. 2.1 it is apparent that a third winding is fitted in addition to the excitation and flux sense windings. This is the dc bias winding, through which dc current is passed in order to bias the CUT. Also apparent is an inductor L, in series with the dc source supplying the bias winding. This component ensures the dc bias has a constant value by attenuating ac ripple currents transformed from the ac excitation winding into the bias winding.

Circuits of the type illustrated in Fig. 2.1 have the advantage of allowing core loss measurements to be quickly and easily made. However, there is a significant disadvantage; small measurement errors in the phase shift between the winding emf and current waveforms can lead to large errors in the measured core loss, or B-H loop shape, if the phase angle between the waveforms is close to 90^{o}. Such errors, which are examined in detail in Chapter 5, commonly originate from the sensing method used to measure the excitation current. Therefore, for the core loss measurement circuit used in [1] under dc bias conditions, a relatively large current shunt of 4 Ω was used to minimize the ratio of its resistance to its reactance. Furthermore, the reactance due to parasitic inductance was itself minimized through implementing the current shunt by paralleling 300 resistors together of 1.2 k Ω each. The phase shift error of this current shunt was estimated to be less than 0.01^{o} at 50 kHz, and using it the core losses under dc bias conditions of Ferroxcube 3F3 [4] and Epcos N27 [5] Mn-Zn ferrite toroidals were measured at core temperatures of 100^{o}C, and an ac excitation frequency of 20 kHz. The core loss measurements were related to the dc, B_{dc},

and ac, B_{ac}, flux densities, and showed that core losses do not depend on B_{dc} at low levels, but increase significantly with B_{dc} at high levels for a given level of B_{ac}. It was stated in [1] that it is not possible to measure the B_{dc} in the CUT without modifying its core, and therefore the value of B_{dc} that was related to the core losses was calculated. However, the equation used to calculate B_{dc} had no dependence on the CUT temperature, which is of importance to the accurate determination of B_{dc} due to the significant variation of permeability with the temperature of ferrite materials. Therefore, it is a shortcoming of this method. The core loss results from [1] for the Ferroxcube 3F3 material core are shown in Fig. 2.2.

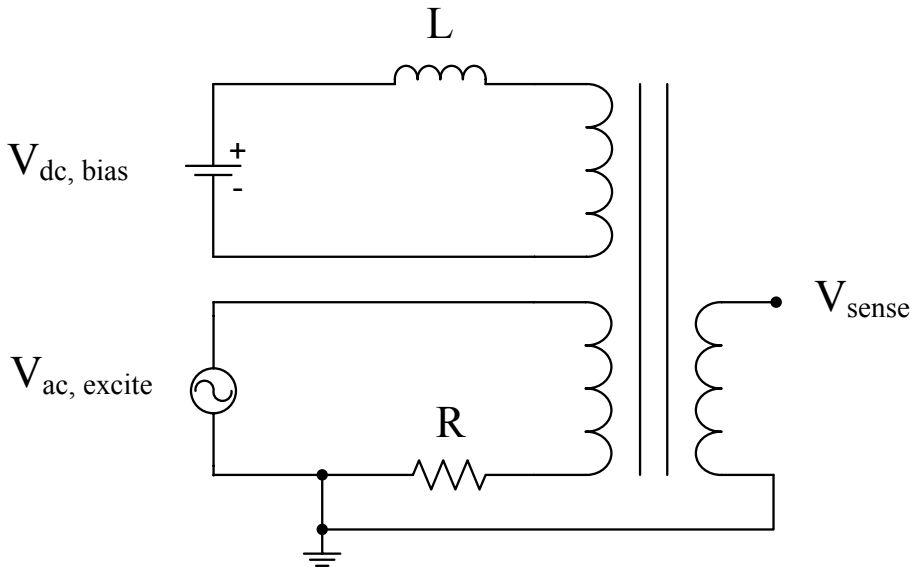

Fig. 2.1 Typical core loss measurement circuit using ac excitation, dc bias, and flux sense windings

In [2] the investigation presented in [1] was extended to determine ferrite core losses under dc bias conditions over a wide frequency range. In this case it was stated that the values of B_{dc} used for the tests were calculated through knowledge of H_{dc}, and the measured magnetization curve. The results, presented for Epcos N27 material, showed core losses increased significantly with dc bias over a frequency range from 10 kHz to 200 kHz, as B_{dc} was varied up to 150 mT and B_{ac} was held constant at 50 mT. Similar trends held for Ferroxcube 3F3 material tested at the same flux densities and at frequencies ranging from 30 kHz to 650 kHz.

A measurement circuit of the type illustrated in Fig. 2.1 was also used in [3], and core losses under dc bias conditions were determined through the measurement of B-H loops. The geometry of the cores tested was not stated, and it was also not stated by which company the cores were

manufactured; however, from the labels used to identify the core materials the manufacturer is believed by the author to be Magnetics Inc [6].

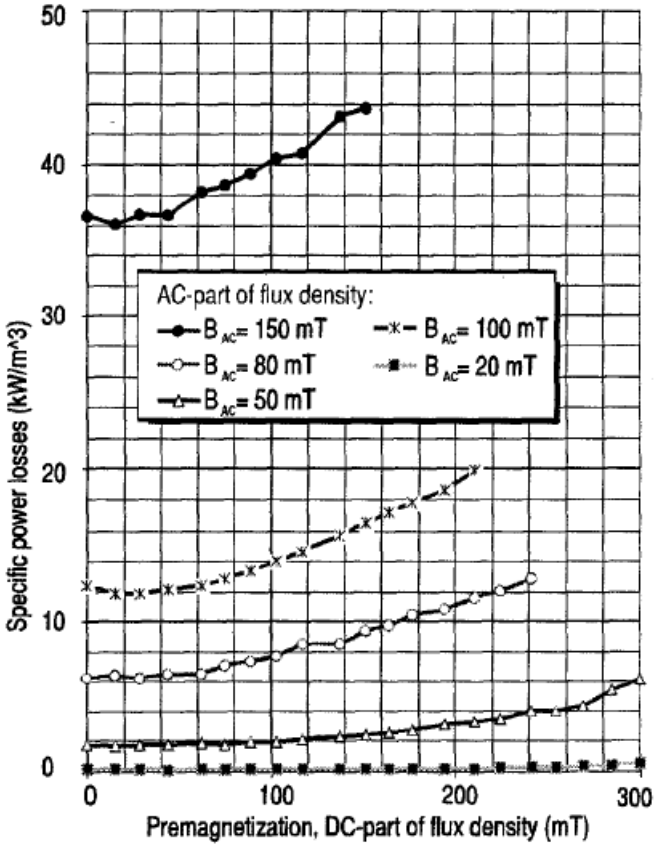

Fig. 2.2 Core loss results measured under dc bias conditions reproduced from [1]

In [3] the importance of accurately measuring the phase shift between the winding emf and current waveforms was conveyed, and for this reason it was stated that a specially designed low inductance current shunt was used. No details of its construction were provided. A further statement was made that the error of the measurement circuit was around +/- 2% at frequencies less than 1 MHz without offering proof. The results of the measurement circuit are reproduced in Fig. 2.3, and it is apparent that the maximum value of B_{dc} used was only 0.025 T; this is significantly below B_{sat} which, as shown in Section 1.1, means the energy density of the CUT is low and the utilization of the core is far from optimal in terms of minimizing its size and cost. Furthermore, it was not stated how the test values of B_{dc} were determined, and the core loss measurements were not related to the CUT temperature. This is of importance due to the significant variation of Mn-Zn ferrite core losses with temperature, as shown by the measured core loss results presented in Chapter 1. As apparent from Fig. 2.3, the test results showed core losses more than doubling at a test frequency of 10 kHz as the ratio of B_{dc}/B_{ac} was increased from

0 to 1, yet rising only slightly with dc bias at 100 kHz. These results were explained by decomposing the total core losses into hysteretic and eddy current components, both theoretically and experimentally, and showing how each of these components varied with dc bias. It was not stated how the experimental values of the core loss components were measured, nor how eddy current losses within ferrite materials become significant at test frequencies of 100 kHz or less. This issue with regard to [3] is addressed in Section 2.3.

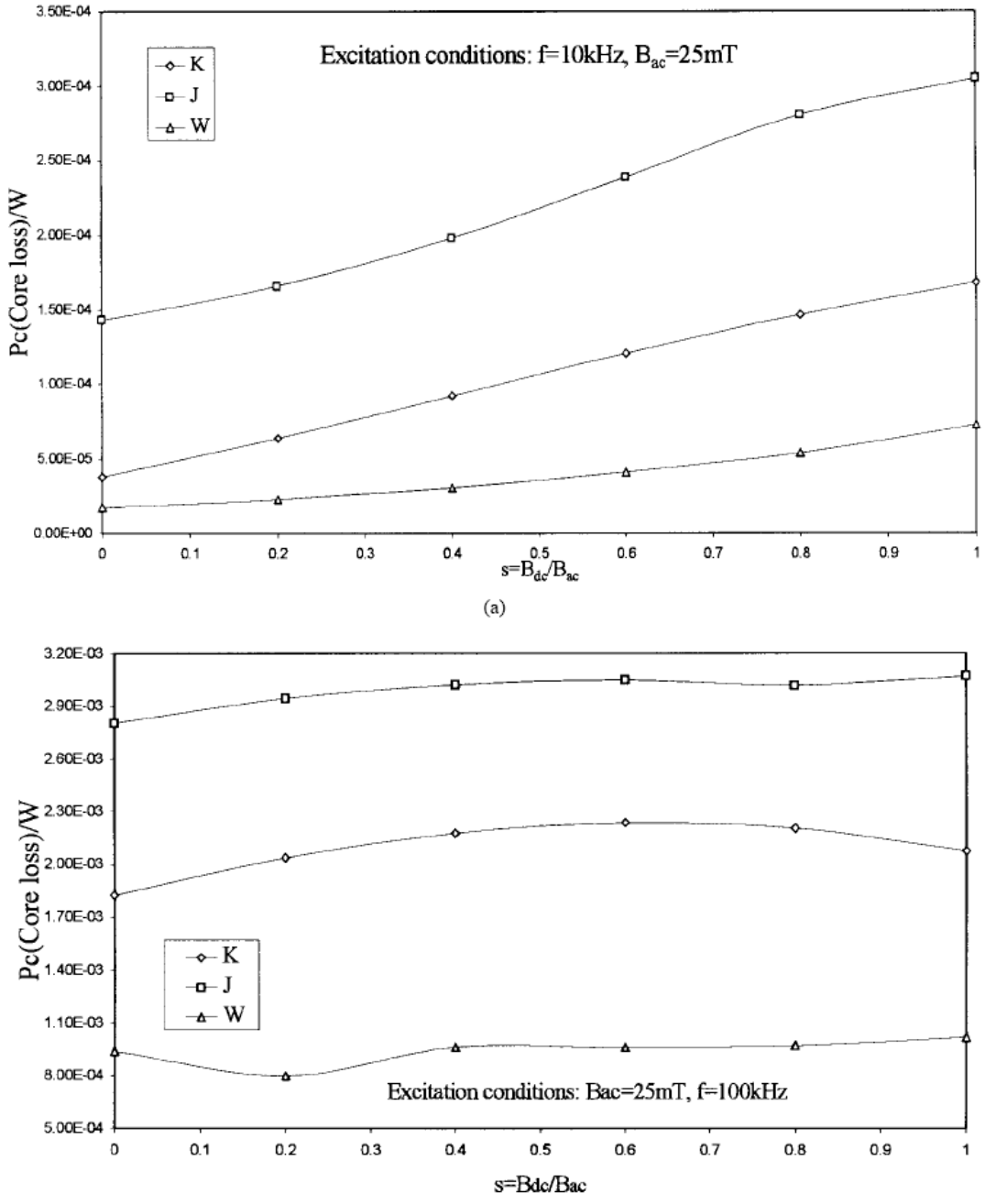

Fig. 2.3 Core loss results measured under dc bias conditions reproduced from [3]

In [7] a large number of measurements were made of the core losses under dc bias conditions of ferrite toroidals in Ferroxcube 3F3 Mn-Zn, and 4F4 Ni-Zn material [4]. The tests were undertaken within a temperature chamber over a wide frequency range, at a very large number of different frequencies, and measured using an impedance analyzer. A simplified diagram of the measurement circuit is shown in Fig. 2.4, from which it is apparent that the impedance probe applies an ac excitation waveform that is dc biased to the CUT. This eliminates the need for the separate dc bias winding necessary in [1]-[3], however, because a flux sense winding is not used the winding losses are measured at the same time as the core losses, and the two cannot be separated. This is a significant disadvantage of this technique, which was stated to be overcome through a calibration procedure. Measurements using the technique showed core losses increased significantly with the dc bias applied to a constant ac excitation waveform for both types of ferrite material that were tested.

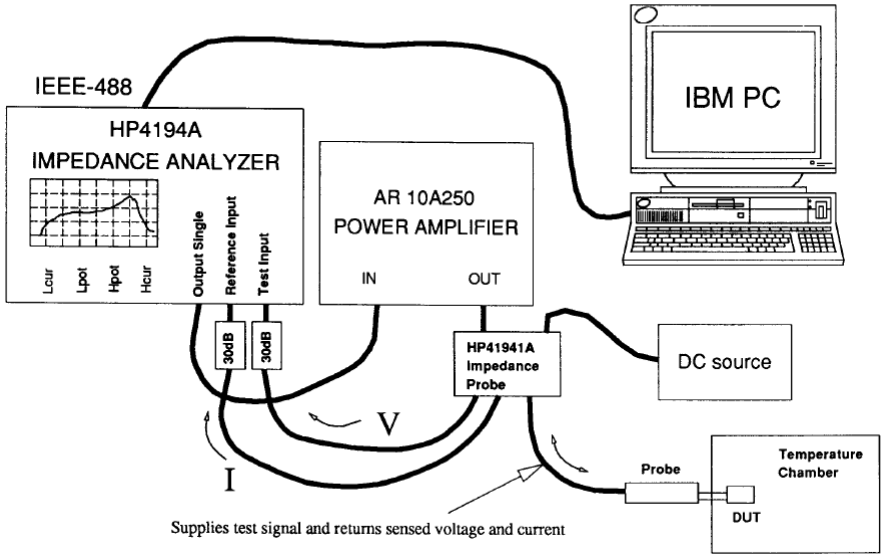

Fig. 2.4 Core loss measurement system reproduced from [7]

In [7] an unusual phenomenon was reported; within a number of different narrow excitation frequency bands it was shown that core losses increased dramatically with dc bias well above and beyond a general level of increase. A graph illustrating the variation in core loss with dc bias is shown in Fig. 2.5. The peaking apparent in the core loss characteristic was attributed solely to the phenomenon of domain wall resonance, occurring as the natural frequency of the domain wall coincided with the amplitude of the applied ac excitation frequency. It was further stated that this phenomenon was only noticeable when a large number of domain walls oscillated in tandem,

which itself occurred when domain walls were stabilized, or stiffened, by a large anisotropy field created externally through the application of a dc bias. It was not stated how the presence of a dc bias created the anisotropy. In addition, no account was taken of the possibility of high core losses due to forms of resonance other than that related to the domain wall, such as magnetomechanical resonance. A resonance of this type occurs when the ac magnetic excitation induces high levels of magnetostrictive vibration, which in turn induces high core losses [19]. This form of resonance is discussed in relation to the measured core loss results presented in Chapter 6.

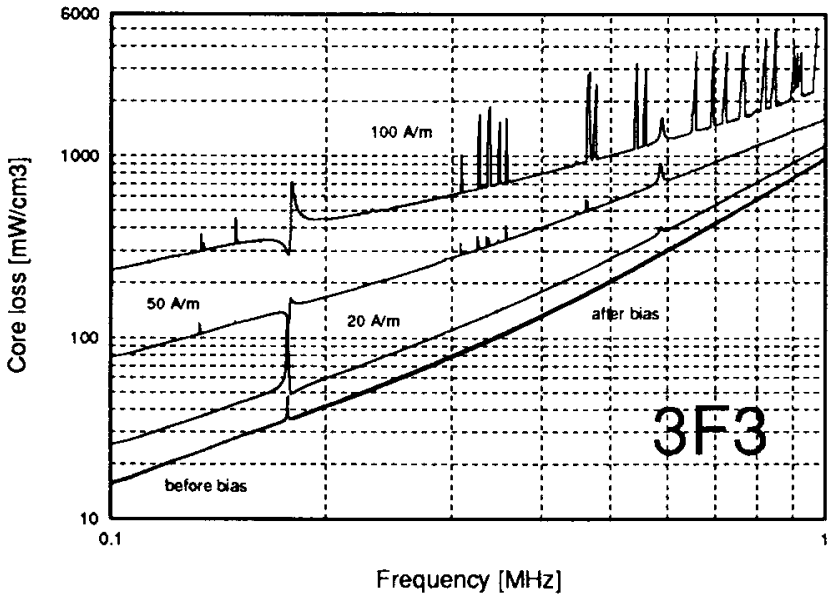

Fig. 2.5 Core loss of Ferroxcube 3F3 material before dc bias, with dc bias, and after dc bias reproduced from [7]

In [8] core loss measurements under dc bias conditions were undertaken through the application of a dc biased ac excitation waveform to the excitation winding on the CUT, which eliminated the need for a separate dc bias winding. In addition a flux sense winding was used to sense the excitation winding emf, which eliminated the error incurred in [7] whereby copper losses were measured at the same time as core losses. In [8] an analysis was presented of the large error in core loss measurements that can occur if the phase shift between the winding emf and current waveforms is close to 90^{o} and is incorrectly measured, and a solution to the problem was proposed. This involved the placement of a capacitor across the flux sense winding to improve the power factor between the winding emf and current waveforms and, therefore, reduce the magnitude of core loss measurement errors due to incorrectly measured phase shifts. However, this form of correction tends to control the magnitude of the core loss measurement error, rather than eliminate it. Furthermore, it introduces other sources of error, as the loss measurement will

include the capacitor losses together with the core losses. Moreover, if the capacitor significantly loads the flux sense winding then the winding resistive losses will be added to the total loss measurement. The core loss measurements presented in [8] were made on a TDK T16-28-13 toroidal core in PC40 material at frequencies ranging from 50 kHz to 500 kHz. The results showed a very significant increase in core loss with dc bias, and are reproduced in Fig. 2.6. The x-axis is not shown in the figure because it was not given in the original paper, however, it is presumed to relate to the B_{ac} test values that were used.

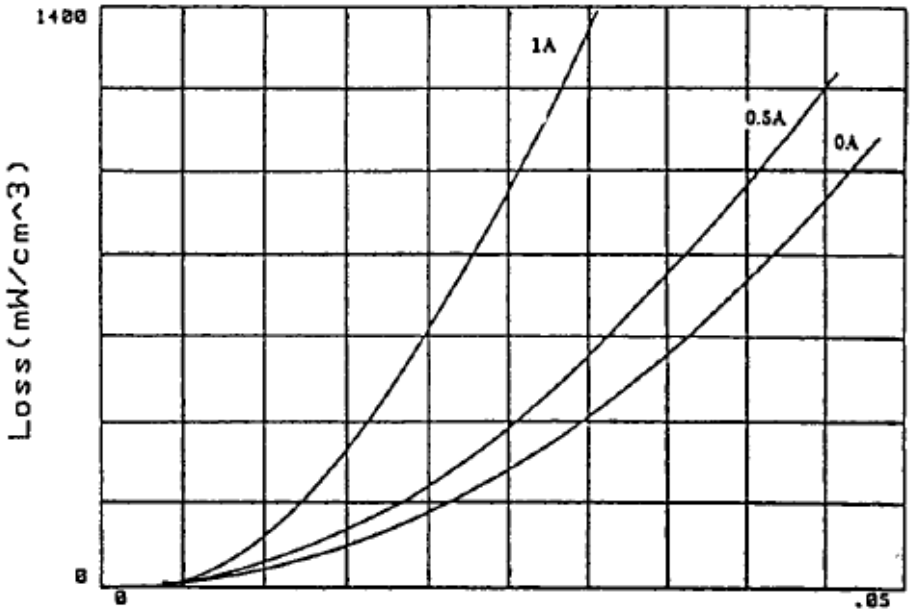

Fig. 2.6 Core losses under dc bias conditions reproduced from [8]

In [9] the core losses under dc bias conditions were measured of an inductor implemented using an EFD20 geometry, Mn-Zn ferrite core in Ferroxcube 3F3 material. A total air gap of 0.1mm was inserted in the core, and the inductor was operated in a SMPS buck-boost converter circuit. Within the cores of inductors operating in such a circuit topology the flux waveform is triangular due to the nature of the current flowing in the excitation winding. Furthermore, the ac component of the excitation winding current is itself dc biased, so eliminating the need for a dc bias winding. The core losses in [9] were determined through measuring the excitation winding current and the winding emf in a method similar to that used in [1], with the exception that a dc bias winding was not used. Consequently, accurate measurement of the phase shift between the winding emf and the excitation current waveforms was required. It was reported that the time delay error due to the phase shift between the winding emf and current sensing channels was less than 5 ns and, therefore, that errors from this particular cause could be ignored. Other actions taken to minimize

phase shift errors included: removing the dc offset voltage introduced by the voltage probe into the winding emf voltage, and using a current shunt with low value of parasitic inductance. However, detail on the placement of the flux sense winding to measure the winding emf was not given. Such detail should be reported for tests undertaken with gapped cores, as used in [9], because fringing flux radiating from air gaps can distort the voltage measured by the flux sense winding, thereby deteriorating the accuracy of the core loss measurement. To overcome this problem the flux sense winding should be placed on a section of the CUT distant from the air gap. However, this introduces another potential problem due to the highly non-uniform geometry of EFD type cores; if the flux sense winding is placed over a section of the CUT in which flux has a greater concentration, then high and inaccurate core loss measurements will result. The various core loss measurements presented in [9] centered about investigations on varying the duty cycle of the magnetic excitation waveform applied to the CUT. While core loss measurements were made under dc bias conditions, no emphasis was placed upon investigating the influence of a dc bias itself on core losses. Therefore, core loss results from [9] are not reproduced here.

In order to obtain core loss results that are representative of a particular ferrite material, it is desirable for the CUT to have a uniform cross sectional area so, that a uniform flux density is maintained throughout the core. Therefore, although the results obtained in [9] characterize the particular losses of an EFD20 type of core in 3F3 material, they are not applicable to 3F3 ferrite material in general due to the non-uniformity of the flux density distribution. This issue is also of note in [10] which, in common with [9], presented core loss measurements made under dc bias conditions with triangular ac flux excitation, and a CUT with a non-uniform cross section. In this case an ungapped ETD44 geometry core in Ferroxcube 3F3 material [4] was used. Core losses were measured with a flux sense winding fitted and using an ac excitation current that itself was dc biased, eliminating the need for a separate dc bias winding.

With regard to determination of B_{dc} for each test in [10], it was stated “To translate a measurable dc bias current into the B field, an anhysteretic curve was first measured at 20 kHz. The core was demagnetized with an ac square wave voltage from saturation to zero, prior to each new test”. A well known method for measuring the anhysteretic magnetization curve involves applying an ac field of gradually decreasing amplitude superimposed on a dc field of interest. As the ac field is reduced to zero, then the magnetization converges on its anhysteretic value for the given dc magnetic field strength, and if both these quantities can be measured then one point on the

anhysteretic magnetization curve can be determined [11]. From the description given in [10] it is not stated how the dc value of the magnetization or B_{dc} for each point on the anhysteretic magnetization curve was determined. In [10] it was also reported that a current transformer implemented using a TX36/23/15 toroidal in 3E25 Mn-Zn ferrite material [4] was used to monitor the dc biased ac excitation current, and that this current transformer is "almost not influenced by dc currents up to 3A". However, simple calculations based on the nominal A_L value of the current transformer core and its cross sectional area, show that this core would be operating at a B_{dc} value of 0.23 T with $3A_{dc}$ through its primary winding. In the opinion of the author this is a high value of B_{dc} at which a ferrite current transformer can still be expected to be linear.

The core loss results under dc bias conditions in [10] showed that core losses are most significantly affected by dc bias conditions at 20 kHz, with this influence lessening at 100 kHz and becoming almost negligible at 500 kHz. It was noted in the [10] that self heating of the CUT at 500 kHz was significant and, because the core loss characteristic of power grade ferrite materials varies significantly with temperature, this compromises any conclusion that can be drawn from the variation in loss at this frequency. The core loss results measured in [10] are reproduced in Section 2.3.1 along with the core loss predictions made using a proposed model.

In [12] an investigation into ferrite core losses under dc bias conditions was undertaken through the application of a dc bias transverse to both a 2 mT ac excitation field, as well as the plane of an Epcos N87 [5] Mn-Zn ferrite toroidal CUT. Core loss measurements were made at test frequencies ranging from 1 kHz to 10 MHz using a suitably designed wattmeter, and at frequencies up to 1 GHz using a transmission line method. Detailed descriptions on either the transmission line method or the wattmeter were not stated explicitly. At frequencies lower than 1 MHz a clear increase in core losses with the application of a transverse dc bias occurred. At frequencies greater than 1 MHz it was found that the core loss characteristics in the presence and the absence of a dc bias tended to converge for reasons given in Section 2.3.2, along with measured core loss results and core loss model predictions.

Whilst the measurements presented in [12] showed that core losses increase with dc bias for frequencies below 1MHz, they were made at a very low ac excitation level of 2 mT. Such an excitation level is low and, therefore, may not induce all the core loss mechanisms experienced

by many cores operating at higher excitation levels. Furthermore, the dc bias applied to the CUTs was transverse to the applied ac field. Such a condition is not normally encountered by ferrite cores used in inductors and transformers under practical dc bias conditions, for which the dc bias is generally co-axial to the applied ac magnetic excitation. The above shortcomings in [12] were overcome in [13] through measurements made on U25 geometry Ferroxcube 3E27 [4] Mn-Zn ferrite cores. Coaxial ac excitation and dc bias conditions were used at frequencies ranging from 20 kHz to 200 kHz and peak to peak ac excitation levels of 100 mT. Such an ac excitation level is common for dc biased inductors operating in SMPS applications. In addition, results were measured with biased symmetrical and asymmetrical triangular ac flux waveforms, which are also typical in SMPS applications. However, although the 3E27 ferrite material tested is a Mn-Zn type, it is a higher permeability and higher loss material relative to the Mn-Zn material grades normally used in SMPS applications. Therefore, it was a somewhat unusual choice of material to be investigated under SMPS conditions [14]. The core losses under these conditions were measured using a calorimetric method, which relates the power dissipated in a CUT to its temperature rise. In this way the core loss measurement was reduced to the measurement of a temperature ramp, which avoids the phase shift error associated with all the core loss measurement circuits previously described. However, other difficulties are introduced, including the distortion of the core loss measurement due to the contribution of the winding losses to the heating of the core, which was not addressed in the paper. In addition the variation in temperature with core loss was not given, which may have affected the measured core loss characteristic due to the significant variation of the core losses with temperature for ferrite materials. Nevertheless, the results that were presented showed that Mn-Zn ferrite core losses increase significantly with dc bias. These results, in addition to the predictions of a core loss model proposed in [14], are given in Section 2.3.2.

2.3 Models and Explanations for Ferrite Core Losses under dc Bias

Of the work presented in Section 2.2, neither models nor physical explanations for the increase in core losses with dc bias were presented in [1] [2] or [8]. In [3], [7], [10], [12], and [13] either empirically based models, or physically based models or explanations were presented. These are described in Sections 2.3.1 and 2.3.2, respectively.

2.3.1 Empirically Based Models

In [10] total ferrite core losses under dc bias conditions were modeled as:

$$P_{total} = P_{hyst} + P_{dcbias} + P_{other} \text{ (W)} \quad (2.1)$$

For (2.1), it was stated that the component P_{dcbias} is the increase in hysteresis loss, P_{hyst}, due to the presence of a dc bias, but which is added to the total losses as a separate component. The physical basis for P_{other} was not described in more detail other than to state its dependency on dB/dt, and its independence of dc bias conditions. The equations given for each of the core loss components, which are not repeated here, are similar to each other in form, with each equation containing a small number of parameters determined through curve fitting. The results of the model are reproduced together with core loss measurements made under dc bias conditions in Fig. 2.7. Fig. 2.7(a) shows core losses at 100 kHz and dc bias current values of 0 A, 0.2 A, 0.8 A, and 1.2 A and it is apparent that a good fit results. Fig. 2.7(b) shows core losses at 500 kHz and dc bias current values of 0 A, 0.2 A, 0.8 A, and 1 A and in this case a poor fit is apparent. This was explained as a decrease in the dependency of ferrite core losses on dc bias conditions at higher frequencies, which was not taken into account by the model. As noted in Section 2.2 however, the authors of [10] state that at 500 kHz significant self heating of the CUT occurred, which would affect the core loss characteristic. Therefore, in the opinion of the author, these core loss results should be viewed with caution.

In common with [10], an empirical core loss model based on the division of total core losses into different components was used in [3], through decomposing measured core losses into hysteretic and eddy current components, and showing how each varied with dc bias. The hysteresis losses were defined in terms of an equation based on a modification of the Steinmetz equation for core loss, using coefficients obtained through curve fitting. The equation defining the eddy current losses was given without showing its derivation and, in common with the hysteresis equation, used parameters obtained through curve fitting. With regard to eddy current losses it was stated that "An alternating flux in a ferrite core will induce eddy currents in that core, and the resulting loss of energy is called eddy-current loss". Furthermore, eddy current losses actually exceeded hysteresis losses for the materials tested at 50 mT and 100 kHz in the absence of a dc bias, in terms of both the experimental and the theoretical results that were given. The results also showed that as dc bias levels increased the hysteresis losses initially increased before decreasing,

while the eddy current losses initially decreased before increasing. However, through consideration of the properties of Mn-Zn ferrite materials, it was shown in [15] that the classical eddy current losses of these materials can be considered as negligible at excitation frequencies below 1 MHz. Consequently, the investigation presented in [3] is not considered relevant to Mn-Zn ferrite material, which is the material investigated in this Thesis.

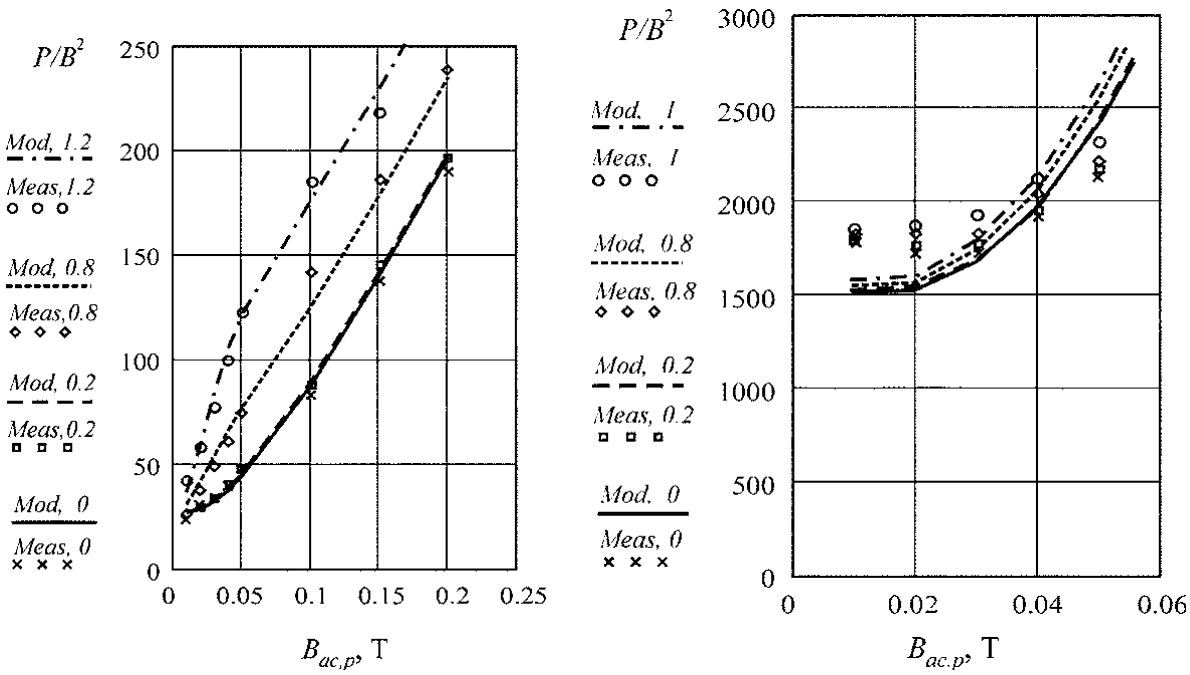

Fig. 2.7 Core loss (P)/peak induction (B) vs. peak Bac for (a) 100 kHz at 0 A, 0.2 A, 0.8 A and 1.2 A dc bias, and (b) 500 kHz at 0 A, 0.2 A, 0.8 A and 1 A dc bias, reproduced from [10]

2.3.2 Physically Based Models and Explanations

Whilst the above empirical models provide a means by which magnetic core losses can be predicted, and thereby are of utility to magnetic component designers, they do not give insight into the physical processes causing core losses to rise under dc bias conditions. Consequently, a need for physically based models exists which relate core losses under dc bias conditions to actual loss inducing mechanisms. In this section such models are reviewed, in addition to explanations describing why ferrite core losses increase with dc bias.

In [7] a model relating ferrite core losses to dc bias conditions was not presented. However, the statement was made that "the magnetic domains oriented in one direction under a dc bias require

more energy to change their orientation, and thus cause more core loss". This is considered by the author to be an explanation for why core losses increase in general with dc bias levels. Furthermore, the statement indicates that a form of anisotropy is responsible for the general increase of core loss with dc bias without stating so explicitly. To the knowledge of the author, the researchers of [7] did not undertake further investigations in this area.

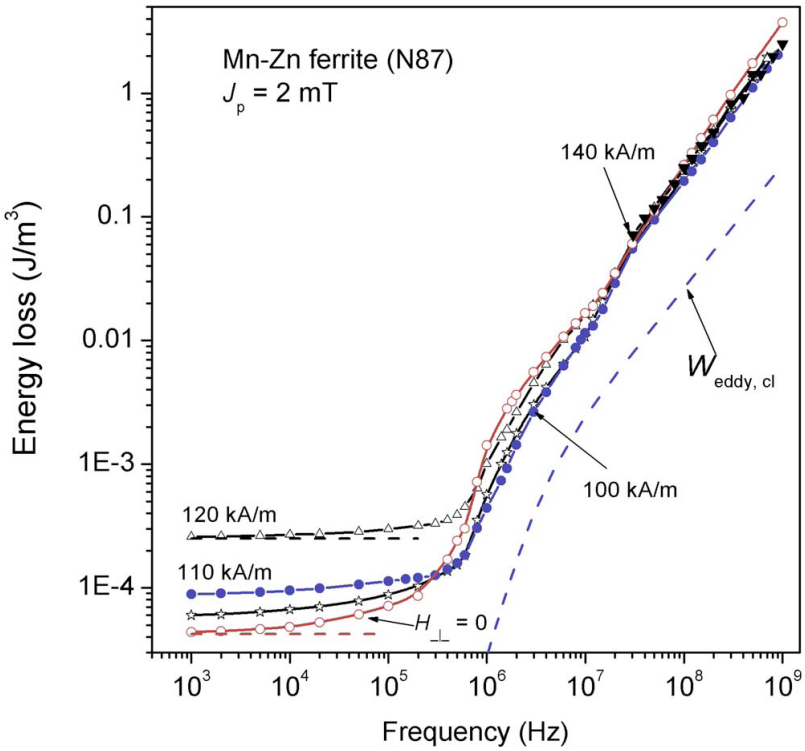

Fig. 2.8 Measured energy losses at various levels of transverse dc bias, and predicted classical eddy current losses reproduced from [12]

In [12] measured ferrite core losses under dc bias conditions were explained in terms of the contributions associated with the domain wall movement and domain rotation magnetization processes. At frequencies less than 1 MHz, for which domain wall movement is significant in the magnetization process well below saturation levels, it was stated that the increased difficulty of domain wall movement under dc bias contributes to an increase in hysteresis losses. This is apparent in Fig. 2.8, which is reproduced from [12], and shows that at the lowest test frequency of 1 kHz, at which the core losses for Mn-Zn ferrite materials are largely made up of hysteresis losses [16], the core losses increase with dc bias. It was further stated that this increase takes place despite the reduction in domain wall activity caused by an increasing dc bias, because "The residual domain wall processes are harder, and generate increased losses because also rotations are more difficult". However, no statement was made as to why this is so. At frequencies higher

than 1 MHz it is apparent from Fig. 2.8 that the dependence of ferrite core losses on dc bias conditions diminishes, as the core loss characteristics in the presence and the absence of a dc bias converge. This was explained to be partially due to an increase in core losses in the classical eddy current form, which were calculated based on the model proposed in [17], and which are labeled in Fig. 2.8 as $W_{eddy,cl}$. However, the largest contribution to core losses in the high frequency region was attributed to resonant phenomena associated with domain rotation processes.

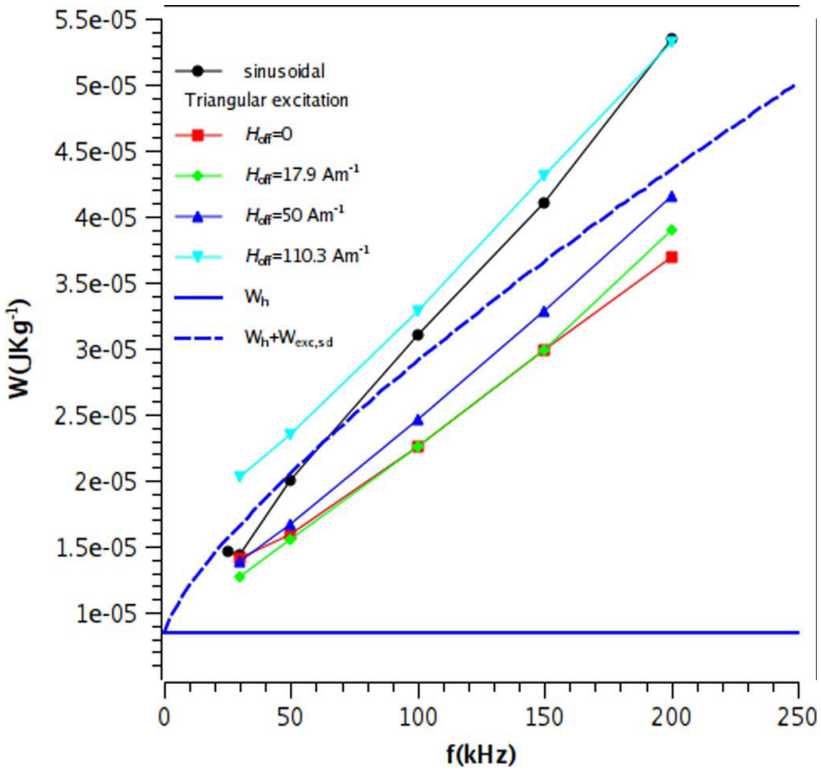

Fig. 2.9 Measured energy losses at various levels of dc bias, and predicted core losses reproduced from [13]

The assumption that excess and classical eddy current losses can be considered negligible at frequencies less than 1 MHz was also followed in [13], which compared measured Mn-Zn ferrite core losses under dc bias conditions to predictions made using a model based on that proposed in [18]. The model proposed in [18] included core loss contributions from a number of mechanisms related to the magnetization process. However, in [13] only the hysteresis, W_h, and the frequency dependent spin damping excess losses, $W_{exc,sd,}$ associated with domain wall motion were summed together to determine a total predicted core loss. A comparison between the predicted and measured losses is given in Fig. 2.9. From this graph it is apparent that measured core losses increase with dc bias levels, shown on the graph as increasing values of H_{off}. It is also apparent that the model makes no allowance for the influence of dc bias conditions, and it was stated in

[13] that it was used for the purpose of giving a qualitative comparison, with further investigations to be undertaken. However, consideration of the equations defining the core loss components used in the model suggest mechanisms which could explain the increase in core losses with dc bias.

The $W_{exc,sd}$ losses calculated in [13] encompass those mechanisms which hinder the motion, and therefore the speed of moving domain walls, with this speed also being dependent on difference between the applied and local coercive fields. In [18] the damping constant associated with this form of loss is defined as:

$$\beta_{sd} = \frac{2J_s \alpha_{LL}}{\mu_o \gamma \delta} \tag{2.2}$$

where,

J_s = saturation polarization (T)

α_{LL} = Landau-Lifschitz damping constant

μ_o = $4\pi \times 10^{-7}$

γ = the electron gyromagnetic ratio

δ = domain wall thickness (m)

From (2.2) it is apparent that the damping of domain wall movement is inversely proportional to the domain wall thickness, which itself is defined as:

$$\delta = \pi \sqrt{\frac{A}{\langle K \rangle}} \tag{2.3}$$

where,

A = stiffness constant

$\langle K \rangle$ = average anisotropy constant (J/m^3)

Consideration of (2.2) and (2.3) together shows that an increase in the anisotropy constant, and therefore the anisotropy field, must act to increase the losses associated with domain wall movement. In addition to acting on the motion of domain walls, anisotropy also influences domain rotation. Although it was stated in [13] that damping due to domain rotation occurs in the

magnetization process at frequencies below 100 kHz, and is in fact predominant above this frequency for Mn-Zn materials [18], this loss mechanism was not included in the model. It is also well known that domain rotation becomes more significant relative to domain wall motion in the magnetization process at higher values of applied magnetic field strength, such as occur at high dc bias levels [11]. Therefore, it is reasonable to conclude that this form of loss can be considered highly relevant to ferrite core losses under dc bias conditions, and is discussed further in Chapter 3.

2.4 Summary

This chapter presented a literature review of previous work undertaken on the measurement of ferrite core losses under dc bias conditions. The measurement circuits used have been briefly described and issues which are relevant to the accurate measurement of core losses under dc bias have been stated. These issues are expanded upon more fully in Chapter 4.

By the majority of researchers, it has been shown that core losses increase in general with dc bias, and that this increase is significant. While a number of empirical models have been presented, such models do not give insight into the physical mechanisms causing the phenomenon. To address this issue some explanations have been presented, which to the author in the case of [3] appear to be incorrect, and in some other cases appear to be general. However, in the cases of [12] and [13], with the aid of [18], more specific reasons for the increase in core loss with dc bias are suggested, though details are not provided; for example in [12] it is stated that losses due to domain wall motion become harder under increasing dc bias conditions because domain wall processes are harder as rotations become more difficult. However, no statement is made as to why this is so. In Chapter 3 detailed reasons for why domain wall motion becomes harder under increasing dc bias conditions are given, and in addition, a loss mechanism affecting domain rotation is proposed.

2.5 References

[1] A. Brockmeyer, “Experimental Evaluation of the Influence of DC-pre-magnetization on the Properties of Power Electronic Ferrites,” *IEEE Proc. APEC ’96,* vol. 1, 3-7 Mar. 1996, pp. 454–460.

[2] A. Brockmeyer and J. Paulus-Neues, "Frequency Dependence of the Ferrite Loss Increase Caused by Premagnetization," *IEEE Proc. APEC '97,* vol. 1, 23-27 Feb. 1997, pp. 375–380

[3] W. K. Mo, D. K. W. Cheng and Y. S. Lee, "Simple Approximations of the DC Flux Influence on the Core Loss of Power Electronic Ferrites and their use in Design of Magnetic Components," *IEEE Trans. on Ind. Elec*., vol. 44, no. 6, Dec. 1997, pp. 788-799

[4] www.ferroxcube.com

[5] www.epcos.com

[6] www.mag-inc.com/home

[7] P. M. Gradzki and F. C. Lee, "Domain Wall Resonance and its Effect on Losses in Ferrites," *IEEE Proc. PESC '91*, 24-27 June 1991*,* pp. 627-632

[8] F. D. Tan, J. L. Vollin and S. M. Cuk, "Effective Control of the Error in a Direct Measurement of Core-Loss Power," *IEEE Trans. on Magn.*, vol. 31, no. 3, May 1995, pp. 2280-2284

[9] H. Y. Chung, F. N. K. Poon, C. P. Liu and M. H. Pong, "Analysis of Buck-boost Converter Inductor Loss using a Simple Online B-H Curve Tracer", *IEEE Proc. APEC 2000,* vol. 2, 6-10 Feb. 2000, pp. 640-646

[10] A. P. Van den Bossche, V. C. Valchev, D. M. Van de Sype, "Ferrite losses of cores with square wave voltage and dc Bias", *J. App. Phys,* 99, 2006, 08M908-1-08M908-3

[11] D. Jiles, "Introduction to Magnetism and Magnetic Materials", Chapman & Hall, London, 1998

[12] F. Fiorillo, M Coisson, C. Beatrice, M. Pasquale, "Permeability and losses from dc to the microwave regime", *J. App. Phys*., vol. 105, 2009, 07a517-1-07A517-3

[13] M. LoBue, F. Mazaleyrat, V. Loyau, "Study of Magnetic Losses in Mn-Zn Ferrites under Biased and Asymmetric Excitation Waveforms", *IEEE Trans. Magn*., vol.46, no.2, Feb. 2010, pp.451-454

[14] Ferroxcube Soft Ferrites and Accessories Handbook, 2009, pg.59

[15] C.Beatrice, F. Fiorillo, F. J. Landgraf, V. Lazaro-Colan, S. Janasi, J Leicht, "Magnetic Loss, permeability dispersion, and role of eddy-currents in Mn-Zn sintered ferrites, *J. Magn. Magn. Mat.*, 320, 2008, e865-e868

[16] D. C. Jiles, Frequency Dependence of Hysteresis Curves in Non-conducting Materials", *IEEE Trans. Magn.,* vol. 29, no. 6, Nov. 1993, pp.3490-3492

[17] O. Bottauscio, M. Chiampi, A. Manzin, "Influence of constitutive parameters in soft ferrites: A modeling analysis by homogenization technique", *J. Mag. Magn. Mat.,* 304, 2006, e746-e748

[18] F. Fiorillo, C. Beatrice, O. Bottauscio, A. Manzin, "Approach to magnetic losses and their frequency dependence in Mn-Zn ferrites", *App. Phys. Lett*., 89, 2006, 122513-1-122513-3

[19] V. J. Thottuvelil, T. G. Wilson, and H. A. Owen, "High-frequency core-loss characteristics of biased Fe B S amorphous metallic alloy tape-wound cores," *IEEE Trans. Magn*., vol. MAG-20, no. 5, Sep. 1984, pp.1329–1331

Chapter 3

Theory of B-H Loop Phenomena under DC Bias

3.1 Introduction

The magnetic moments lying within the domains of a demagnetized CUT will be aligned in easy directions of magnetization, if the CUT has not been subjected to stress and contains few imperfections. These easy directions are determined by the crystal anisotropy and, because the CUT is demagnetized, a large number of domains will exist. However, with the application of a small magnetic field changes occur, as domain walls move in such a manner that those domains aligned most favorably with respect to the applied magnetic field grow at the expense of others. With applied magnetic fields of moderate strength a second magnetization process occurs, domain rotation. During this process magnetic moments within domains rotate into those easy directions of magnetization lying closest to that of the applied magnetic field. Domain rotation takes place after the energy of the applied magnetic field has reached a sufficient level to overcome local forms of anisotropy, and eventually becomes predominant over domain wall motion in the magnetization process. At high applied magnetic fields coherent rotation occurs, as magnetic moments rotate together into alignment with the applied magnetic field [1]. In this chapter it is proposed that both domain wall movement and domain rotation are significantly influenced by the presence of a dc bias, which in turn significantly influences the hysteresis of the magnetization process. It is further proposed that the mechanisms by which these influences manifest exist at microscopic, as well as macroscopic spatial scales relative to the geometry of a CUT.

3.2 DC Bias, Vibration and Hysteresis Losses at Microscopic Levels

In this section particular loss mechanisms operating at a microscopic scale are described that are dependent on the magnetostriction that results under dc bias conditions. Therefore, the section begins with a brief description of the nature of magnetostriction.

Magnetostriction is the manifestation of the influence of the magnetic state of a CUT on its mechanical state and can occur through non-180^o domain wall movement, but primarily takes place through the rotation of magnetic moments [2]. The magnetostrictive strain due to rotation occurs because the individual crystal lattice structures of a polycrystalline CUT spontaneously lengthen in the direction of the domain magnetization. Consequently, as the strain axis of the domain magnetization rotates with the domain magnetization itself as a magnetic field is applied, deformation of the CUT as a whole will result [3]. Deformation can occur in the form of Joule magnetostriction, λ. In this case a fractional change in length, $\Delta l/l$, occurs, with certain dimensions of a CUT expanding, while others contract in such a manner that the volume of the CUT remains constant. Magnetostriction can also occur in the form of volume magnetostriction, in which case the CUT dimensions expand or contract in such a manner as to change the CUT volume. In [4] it is stated that volume magnetostriction is very small and has no influence on the practical behavior of magnetic materials in magnetic fields at, or below saturation. Therefore, it is not considered relevant in this Thesis.

When an ac magnetic field is applied to a CUT, the CUT will vibrate due to the dynamically varying λ caused by domain wall movement and rotation. With the amplitude of the applied ac magnetic field held at a constant level, and with the application of a dc bias, the peak to peak amplitude of λ will increase as more of the magnetization process takes place through domain rotation. The increase in λ with the magnetization level, up to a limiting value reached at saturation, λ_s, is apparent in the λ vs. H characteristic typical of magnetic materials shown in Fig. 3.1 [5].

In the absence of a dc bias λ varies at a fundamental frequency which is twice that of the applied ac magnetic field, and at a low level. With the application of a sufficiently high dc bias the fundamental frequency decreases to become the same as the ac excitation frequency, while the amplitude of the magnetostrictive vibration increases significantly. This can be observed in Fig. 3.2, which shows measured displacement waveforms that occur due to λ without, and with a dc bias. These waveforms were measured using the method described in Chapter 5, at an ac excitation frequency of 20 kHz and on a 30 x 18 x 6 mm Mn-Zn ferrite toroidal in MMG F49 material.

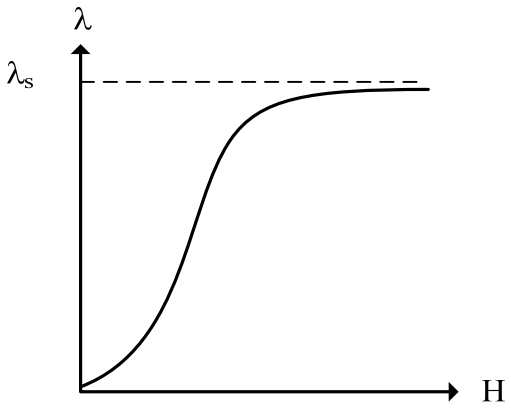

Fig. 3.1 Typical λ vs. H characteristic

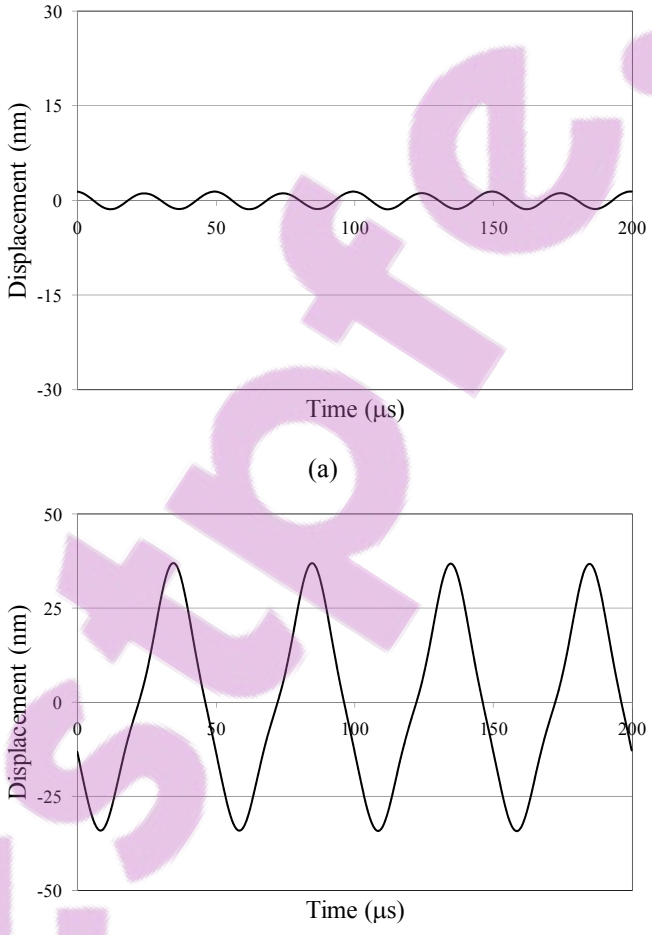

Fig. 3.2 Displacement waveforms measured (a) without and (b) with a high dc bias.

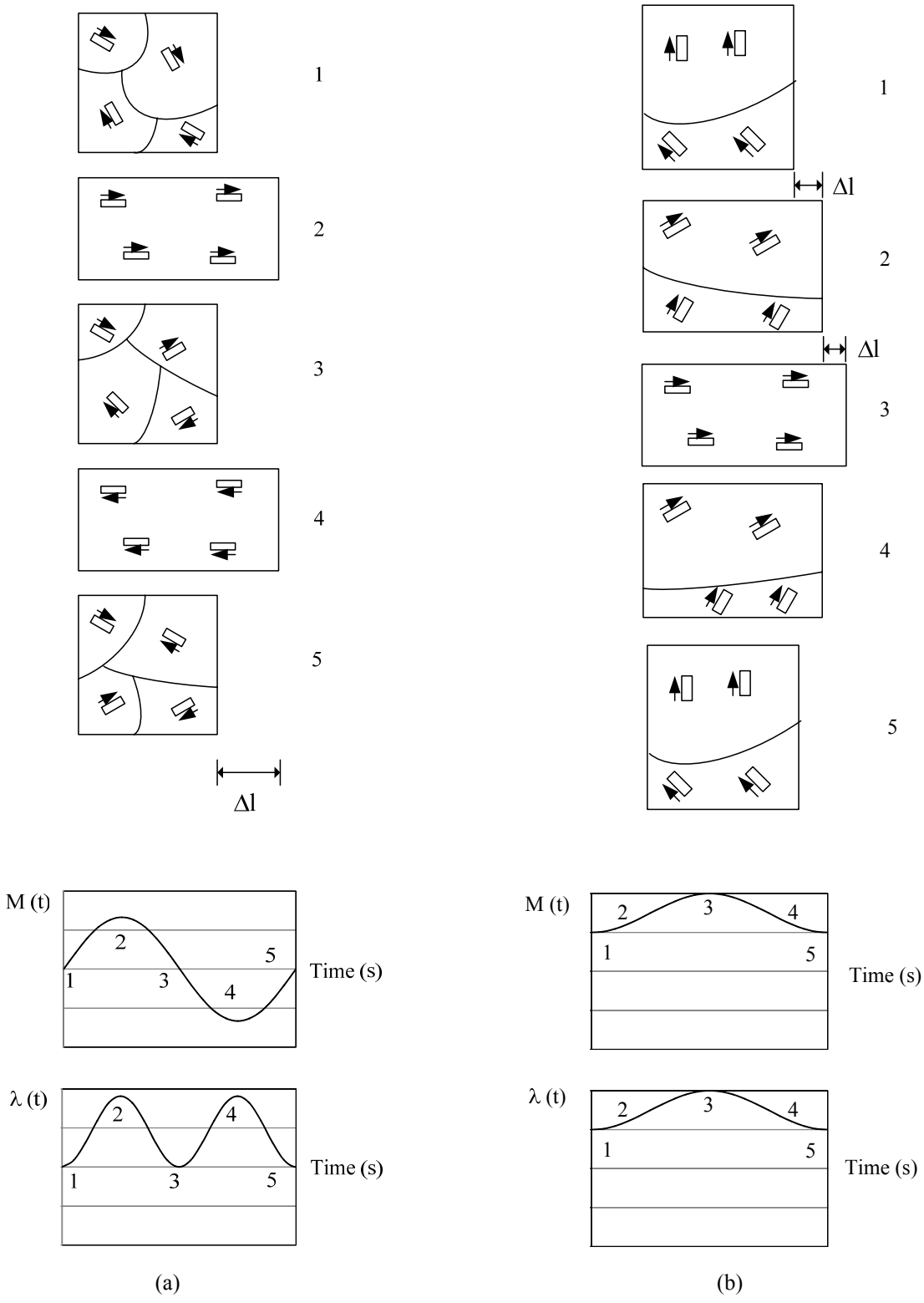

Fig. 3.3 The wall movement and rotation of domain magnetization, accompanying rotation of the axis of spontaneous strain, and the corresponding M(t) and λ(t) waveforms (a) without, and (b) with a dc bias

The change in the frequency of λ with dc bias can be understood with reference to the simplified diagrams in Fig. 3.3. These diagrams illustrate the relationship between λ and the magnetization

process in a CUT at various points on a magnetization waveform, M(t). In Fig. 3.3(a) the ac magnetization process is shown in terms of domain wall movement and domain rotation in the absence of a dc bias, along with the corresponding change in dimensions, Δl, of the CUT. It can be observed that Δl reaches its maximum level at the highest levels of magnetization, which occurs when all magnetic moments are in alignment, as is the case at points 2 and 4. It can also be observed that complete alignment takes place twice within one cycle of M(t) and, therefore, that the frequency of the magnetostrictive vibration of the CUT is twice that of M(t). In Fig. 3.3(b) the magnetization process under dc bias conditions is shown. In this case it is apparent that complete alignment of magnetic moments takes place only once within each cycle of M(t), at point 3. Therefore, under dc bias conditions the frequency of the magnetostrictive vibration of the CUT is the same as that of M(t).

When a material of any type vibrates energy losses within the material can occur at the expense of the elastic energy stored at the maximum strain due to the stress from the vibration. The elastic energy and its losses can be related to one another through [6], [7]:

$$D = \frac{\Delta W}{W_e} \tag{3.1}$$

where,

D = fractional energy loss per period of vibration

W_e = elastic energy stored at maximum strain (J)

ΔW = energy lost per cycle at the expense of W_e (J)

For magnetic materials, the total energy lost during each vibration cycle can include a specific component due to magnetomechanical damping. Magnetomechanical damping, so named due to the damping effect it has on vibrations, originates from the dynamics of domain re-orientation [8], occurring as the result of strain. Furthermore, it is dependent on the magnetomechanical coupling factor, which shows the ease with which elastic energy due to vibration can be converted to magnetic energy, from which state it is dissipated [9]. The losses incurred through magnetomechanical damping have been described by Bozorth as being due to macro and micro-eddy currents, as well as to magnetomechanical hysteresis [2]. Macro-eddy currents result from induction in a magnetic material on a macroscopic scale from the strain due to cyclic vibrations.

However, given the high resistivity of Mn-Zn ferrite material at test frequencies well below 1 MHz, such as those used in the Thesis, this form of damping is not considered relevant. Micro-eddy currents are local eddy currents generated by local changes in magnetization due to the strain of vibration, and exist due to stress induced domain wall displacements. It is stated by Bozorth that this form of loss is inversely proportional to the square of any non-applied internal stress field. Therefore, according to this view, any increase in the non-applied internal stress of a CUT, such as that which occurs due to hardworking, will decrease the micro-eddy current losses due to an applied stress [2]. A similar relationship also holds for magnetomechanical hysteresis losses.

Magnetomechanical hysteresis losses have been attributed to the irreversible jumps of non-180^o domain walls, which occur only if the vibrational stress exceeds the local stress barrier opposing domain wall motion. Furthermore, it has been shown theoretically that the damping due to magnetomechanical hysteresis losses is inversely dependent on the average level of the internal stress field that opposes the movement of non-180^o domain walls [10].

The magnetomechanical loss mechanisms due to vibration that were described above take place as the vibration is induced by an applied stress. In this case losses are able to be inhibited by non-applied stresses internal to a CUT, because such stresses inhibit domain wall movement. Consequently, domain wall movement and, therefore, magnetomechanical losses due to a vibrating applied stress, may be largely suppressed if the non-applied internal stress is sufficiently strong. However, with the application of an ac magnetic field to a CUT, domain wall movement must occur so that the magnetization can change with time. In addition, if the ac magnetic field is dc biased then the magnetostrictive vibration is significantly increased, as shown by Fig. 3.2(b). This situation, in which a CUT is subject to an applied magnetic field in addition to vibration that is magnetostrictive in origin rather than being applied, is not dealt with by the magnetomechanical damping theory outlined above. Therefore, a loss mechanism associated with vibration under dc bias conditions is described below. The Thesis proposes that this mechanism is due to microscopic and non-applied stresses internal to a CUT, which increase with dc bias levels.

As defined in [4], stress can exist within a CUT through being applied externally, or through being internal, or residual, within the core and, therefore, present even when no stress is

externally applied. Residual stresses can be generated in a number of ways, including: by spontaneous magnetization as a CUT is cooled through its Curie temperature and different domains distort in different directions, and by plastic deformation. In this Thesis it is proposed that increasing internal elastic micro-stresses, σ_i, within a CUT can also be generated through the application of a dc biased ac magnetic field to the CUT. In this instance λ will take place in both the static and dynamic senses, as the dimensions of the CUT change with the applied dc and ac magnetic fields respectively. These changes in dimension create regions of irregular σ_i and, therefore, micro-strains. Through interacting with magnetic moments via λ, the σ_i can generate local energy barriers, or domain wall pinning sites, which impede domain wall motion. Because the σ_i are assumed in this Thesis to be elastic and increase with the dc bias applied to an ac magnetic field, increasing levels of dc bias will also result in more pinning sites and, therefore, increased core losses. The mechanism by which increasing σ_i influence core losses is explained below with reference to the disperse field theory.

3.2.1 Stress Anisotropy and Domain Wall Motion Losses under DC Bias

Irregular σ_i induce local variations in stress anisotropy within a CUT, which influence the direction that magnetic moments will be directed in an irregular manner even within a single domain [11]. In this section it is explained how stress anisotropy is created through λ, and why this impacts upon losses due to domain wall motion if the stress anisotropy varies in an irregular manner at a microscopic level.

Magnetic anisotropy can result from several causes. Two causes can be explained with reference to the crystalline structure of a CUT, and the stress that this structure is placed under. Magnetocrystalline anisotropy shows the dependence of the internal energy within a CUT on the direction of magnetic moments [3], and is due to the coupling between the spin and orbital motion of electrons. This coupling means that when an applied field attempts to re-orientate the spin axis of an electron, the orbital motion is also affected. However, the orbital motion is also coupled in a strong manner to the crystal lattice and so resists the attempt to rotate the spin if it is lying in an easy direction of magnetization. The energy required to rotate the spin system away from the easy direction is the magnetocrystalline anisotropy energy, and is dependent on the crystal symmetry. For crystals of the cubic variety, such as occur in polycrystalline ferrite

materials, the equation for magnetocrystalline anisotropy energy density, f_K, has been defined as [12]-[14]:

$$f_K = K\left[\alpha_1^2\alpha_2^2 + \alpha_2^2\alpha_3^2 + \alpha_3^2\alpha_1^2\right] \tag{3.2}$$

where,

α_n = direction cosines of the spontaneous magnetization vector referred to the crystal axes

K = anisotropy energy density constant (ergs/cm^3)

From (3.2) it is apparent that f_K is dependent only on the direction of magnetization relative to the crystal axes, and not on the type or magnitude of the magnetization in any way. However, if the crystal lattice is strained due to λ then, by the same spin-orbital coupling mechanism previously described, further contributions are made to the energy density, in addition to that given by (3.2). These contributions sum to a total, the anisotropy energy density, f_a, and include f_k, as well as a magnetoelastic component that is dependent on the strain of the crystal and is given by [12]:

$$\begin{aligned} f_a = f_K &+ B_1\left[\alpha_1^2 e_{xx} + \alpha_2^2 e_{yy} + \alpha_3^2 e_{zz}\right] + B_2\left[\alpha_1\alpha_2 e_{xy} + \alpha_2\alpha_3 e_{yz} + \alpha_3\alpha_1 e_{zx}\right] \\ &+ \tfrac{1}{2}c_{11}\left[e_{xx}^2 + e_{yy}^2 + e_{zz}^2\right] + \tfrac{1}{2}c_{44}\left[e_{xy}^2 + e_{yz}^2 + e_{zx}^2\right] + c_{12}\left[e_{yy}e_{zz} + e_{xx}e_{zz} + e_{xx}e_{yy}\right] \end{aligned} \tag{3.3}$$

where,

B_i = magnetoelastic coupling constants (ergs/cm^3)

e_{ij} = strains as defined below

c_{ij} = elastic moduli (ergs/cm)

For (3.3) the e_{ij} terms are defined in terms of the displacement of a particular point within a material from an original position described in Cartesian coordinates by **R** (a,b,c). After a displacement occurs the material point will move to position **R'** (a,b,c), and the displacement, **u**(a,b,c), is defined by:

$$\mathbf{R'}(a,b,c) = \mathbf{R}(a,b,c) + \mathbf{u}(a,b,c) \tag{3.4}$$

From the displacement the strains can be defined as [15] :

$$e_{xx} = \frac{\partial u_a}{\partial a}, \quad e_{xy} = e_{yx} = \frac{\partial u_a}{\partial b} + \frac{\partial u_b}{\partial a}$$
$$e_{yy} = \frac{\partial u_b}{\partial b}, \quad e_{yz} = e_{zy} = \frac{\partial u_b}{\partial c} + \frac{\partial u_c}{\partial b} \tag{3.5}$$
$$e_{zz} = \frac{\partial u_c}{\partial c}, \quad e_{xz} = e_{zx} = \frac{\partial u_c}{\partial a} + \frac{\partial u_a}{\partial c}$$

In (3.3) the terms additional to f_K are generally known as the magnetoelastic contribution to the anisotropy energy. This equation shows all the energy density components that influence the local direction of magnetic moments in the absence of an applied external stress; with the application of an external stress an additional and separate contribution is made [14]. Although complex in form, (3.3) shows that the direction of magnetic moments within any small region of a CUT is dependent on the strain, as well as the elastic moduli in that region. Therefore, if an irregular pattern of σ_i exists within a small region with sufficient strength to induce an irregular pattern of strains, the orientations of the magnetic moments in that region will also vary in an irregular manner.

A simplified case of irregular variations of magnetic moments within the local stressed region of a CUT is illustrated in Fig. 3.4, and it is apparent that the magnetization is divergent. In this condition a magnetostatic field will be created, and magnetic charges can be considered to arise [16]. When a domain wall is positioned so that it intersects a region where positive and negative magnetic charges are also present some mixing will occur, resulting in charge neutralization and, thereby, a reduction in the magnetostatic energy [11]. Consequently, such a position will be favored by the domain wall under equilibrium conditions, for which a minimum energy condition is sought, and becomes a domain wall pinning site. This is known as the disperse field theory [1], and can be applied to explain the increase in loss due to domain wall movement under dc bias conditions. When an ac magnetic field is applied to a CUT causing λ, which induces irregular σ_i and, therefore, regions containing magnetic charges, these regions will act as pinning sites for domain walls. With the addition of a dc bias to the ac magnetic field further regions of irregular σ_i will be induced, as the level of magnetostrictive vibration increases, creating a higher density of domain wall pinning sites and increasing the pinning site strengths. Because a higher density of stronger pinning sites will demand increased energy levels from the applied magnetic field in order to allow domain walls to be released, higher losses will be experienced. Consequently, increased losses due to domain wall motion will be incurred with increasing dc bias conditions.

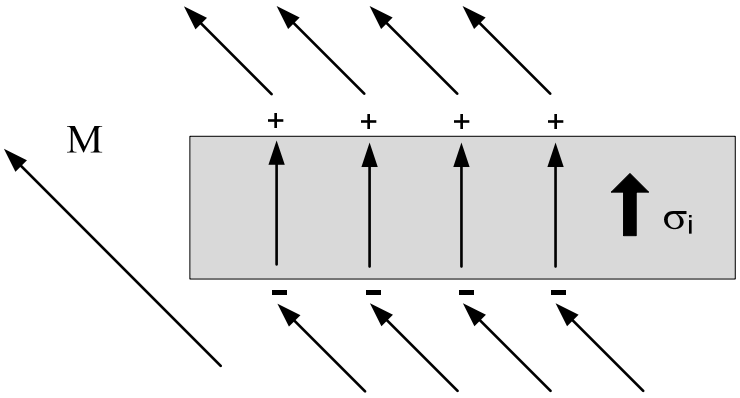

Fig. 3.4 The deviation of magnetic moments due to an irregular σ_i in a local region

3.2.2 Vibration Frequency and Hysteresis Losses under DC Bias

In addition to being dependent on magnetostrictive vibration amplitude, it is also proposed that the strength and density of domain wall pinning sites within a CUT is dependent on the frequency of the vibration. As described in Section 3.2.1, a CUT subjected to an applied ac magnetic field in the absence of a dc bias will vibrate at twice the frequency it would in the presence of a dc bias. Therefore, with the application of an initial and low level of dc bias it can be expected that that core losses will correspondingly decrease as the magnetostrictive vibration frequency decreases. However, as the dc bias is increased beyond very low levels, the decrease in core losses associated with the decrease in the magnetostrictive vibration frequency will be increasingly offset by the increase in the vibration amplitude. This increase will eventually cause core losses to rise with dc bias levels. The proposed theory that core losses are dependent on the magnetostrictive vibration frequency, as well as the amplitude under dc bias conditions, is based on experimental evidence presented in Chapter 6.

The core loss mechanism dependent on the magnetostrictive vibration frequency at low levels of dc bias is proposed to operate through impeding the motion of domain walls. If the ac excitation levels are low in conjunction with the level of dc bias, it is reasonable to assume that the variations in core loss with dc bias are solely dependent on domain wall pinning sites and, therefore, domain wall movement. However, as dc bias levels become sufficient to bring a CUT towards its saturation level, domain wall motion will become less prominent in the magnetization

process relative to domain rotation [1]. In Section 3.2.3 a core loss mechanism influencing the domain rotation process under dc bias conditions is proposed.

3.2.3 Internal Stress, Domain Rotation and Hysteresis Losses under DC Bias

The mechanical movement associated with vibration can influence the magnetic state of a CUT through changing the anisotropy energy, as shown previously using (3.3). With this equation it was explained in Section 3.2.1 how variations in σ_i at a microscopic scale lead to pinning sites, which inhibit the movement of domain walls and, thus, cause core losses to increase with dc bias levels. However, the changes in anisotropy energy caused by the dc bias and vibration can also influence the magnetic state of the CUT through changing the ease with which domain rotation can take place.

Consider a CUT that is excited with a low level of ac excitation, and placed under a dc bias of sufficient strength to bring the core near to its saturation level. In such a high field region it can be assumed that changes in magnetization occur predominantly through domain rotation, and the magnetization can be approximated by a law of approach to saturation. This situation has been modeled using [2]:

$$I = I_S - \frac{a_o}{H} - \frac{b_o}{H^2} + \kappa H \qquad (3.6)$$

where,

I	=	intensity of magnetization (magnetic moment/cm^3)
I_s	=	saturation intensity of magnetization (magnetic moment/cm^3)
H	=	applied magnetic field strength (Oe)
a_o	=	constant due to inclusions
b_o	=	constant dependent on crystal anisotropy
κH	=	field induced increase in spontaneous magnetization of domains

The term b_o in this equation has been attributed to crystal anisotropy, which opposes the action of an applied field. For a polycrystalline magnetic material with crystals orientated at random, b_o has been approximated through an averaging process taking into account all the crystal orientations [2]. It has also been demonstrated that an addition to b_o must be allowed for due to the increase in internal stress that occurs when a magnetic material is severely strained; for

example, when nickel is hammered [2]. In this way, the increase in internal stresses is accounted for by increasing the term associated with anisotropy in (3.6) and, therefore, will increase the size of the B-H loop of the nickel, and so the measured core loss. Although this example is extreme, it is nevertheless analogous to that of σ_i generated by vibration due to magnetostriction under dc bias in ferrite. Therefore, it is reasonable to conclude that higher levels of dc bias and, therefore, vibration and σ_i, will generate an anisotropy which hinders domain rotation. Consequently, it is proposed that increasing levels of σ_i under dc bias conditions have the same general effect on core losses whether acting through the agency of domain wall movement, or domain rotation.

Based on the theory presented in Section 3.2, it is proposed that core loss mechanisms can be invoked by dc bias conditions that increase the difficulty with which domain wall movement and domain rotation can take place. However, under high dc bias conditions experimental results, presented in Chapter 7, show that a B-H loop can cross over on itself. In this case energy is returned from the CUT back to the magnetic excitation supply circuit for a small portion of the magnetic excitation cycle. Although it is believed that this phenomenon derives from magnetomechanical effects, it is not explained by the theory presented in Section 3.2. Therefore an explanation for this phenomenon is proposed in Section 3.3.

3.3 DC Bias, Vibration and Hysteresis at Macroscopic Levels

As described in Section 3.2 hysteresis loss mechanisms can be incurred due to stresses and strains taking place at a microscopic scale. However, in this section it is proposed that the influence of vibration on magnetization can also manifest at a macroscopic scale through inducing an anisotropy that acts on a large number magnetic moments within a CUT in a uniform manner. In this case the stress anisotropy due to magnetostrictive vibration can have a significant influence on differential susceptibility measurements, as illustrated by the simplified analysis below.

Consider a CUT within which the magnetization, **M,** in Fig. 3.5, is dominated by a large domain that varies through rotation; such a situation representative of that occurring under high dc bias conditions. Also shown in Fig. 3.5 are the vectors **H** due to the applied magnetic field strength, and $\mathbf{H_a}$ due to a uniaxial stress anisotropy, which lie at angles ϕ and α with respect to **M**. Not shown are the magnetic field strengths associated with the crystal, magnetostatic and exchange energies, which are assumed not to exist in this simplified system to allow the relationship

between $\mathbf{H_a}$ and $\mathbf{H}$ to be clearly shown. For this system to attain a stable equilibrium the total energy density of the system must be a minimum [16], which is the summation of stress anisotropy energy density, f_σ, which can be derived from (3.3) if λ is assumed to be isotropic and is given by [16]:

$$f_\sigma = -\frac{3}{2}\lambda_S \sigma \cos^2 \alpha , \tag{3.7}$$

and the energy density associated with the $\mathbf{H}$ field, f_H, given by [16]:

$$f_H = -HM\cos\phi \tag{3.8}$$

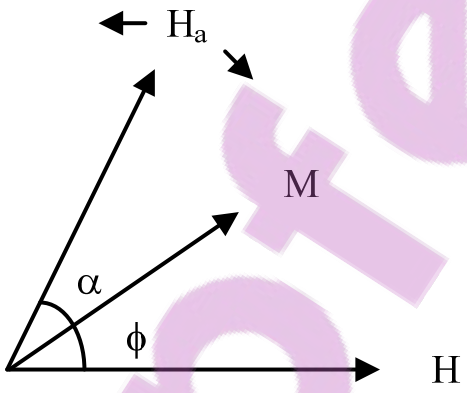

Fig. 3.5 H_a, M and H vectors shown in relationship to one another

From these equations it is apparent that f_σ will be at a minimum if $\mathbf{M}$ is in alignment with $\mathbf{H_a}$; conversely f_H will be a minimum if $\mathbf{M}$ is in alignment with $\mathbf{H}$. Therefore, it is apparent that a competition exists between the $\mathbf{H}$ and $\mathbf{H_a}$ vectors if they are non-aligned with each other. If the CUT is then strained in such a way that the strain axis and, therefore, $\mathbf{H_a}$ is moved away from $\mathbf{H}$, $\mathbf{M}$ will be induced to move away from $\mathbf{H}$ in order to minimize the energy of the system. However, if the strain is such that the $\mathbf{H_a}$ is moved closer to $\mathbf{H}$, then $\mathbf{M}$ will be brought closer in alignment to $\mathbf{H}$. In this way $\mathbf{H_a}$ can dramatically affect the differential susceptibility, χ_{diff}, if this is measured as:

$$\chi_{diff} = \frac{\Delta \mathbf{M}}{\Delta \mathbf{H}} , \tag{3.9}$$

because χ_{diff} takes no account of the influence of $\Delta\mathbf{H_a}$ on $\Delta\mathbf{M}$.

The above analysis is applicable under dynamic conditions if the rate at which $\mathbf{H_a}$ is changed by a stress anisotropy due to magnetostrictive vibration is assumed to be much slower than the rate at which magnetic moments rotate. This assumption, referred to as rate-independence [11], is discussed further in Chapter 4, and was also applied in [18] to model the effect of shock waves on the rotation of magnetization.

Experimental results showing the impact of changes in anisotropy on magnetization under dynamic conditions have previously been presented in [17]-[19]. In [17] the investigation was carried out by firstly applying a dc magnetic field of sufficient strength to a polycrystalline ferrite CUT to bring it to saturation, before using an explosive charge to generate a shock wave perpendicular to the dc magnetic field. The change in magnetization due to the shock wave was then monitored through pick-up coils. A reduction in magnetization was observed and attributed to compression, shock heating, and the rotation of the direction of the magnetization due to the shock induced anisotropy generated by the vibration. In this case the changes in magnetization due to vibration took place through an external stress applied through explosive charges. In this Thesis it is proposed that magnetostrictive vibration under high dc bias conditions can be of such significance that, according to the stress anisotropy analysis presented in this section, the magnetization of large and significant domains is rotated in a coherent manner by the vibration. However, the situation under dc bias conditions, for which the ac excitation is provided by an ac voltage, has an important and distinct difference to that investigated using explosive charges; in [17] the magnetic moments were dynamically free to rotate in response to the vibration, whereas under dc biased, ac voltage excitation conditions, they are not. This allows for the possibility for χ_{diff} to vary dramatically within one cycle from the stress anisotropy associated with magnetostrictive vibration to the extent that distorted B-H loops can be measured. An example of such a B-H loop measured under dc bias conditions, with the dc magnetic field strength component removed, is given in Fig. 3.6. Significant variations in χ_{diff} are apparent in the tail of the B-H loop where it crosses over on itself. This phenomenon is investigated further in Chapters 4 and 7.

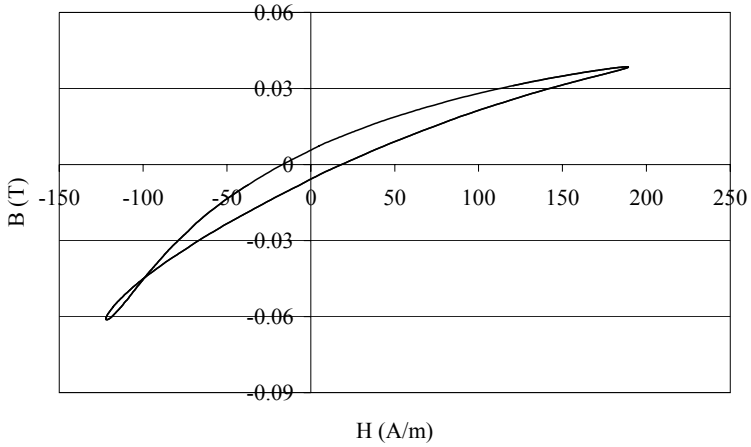

Fig. 3.6 BH loop measured with ac excitation of 0.05T at 37 kHz, and constant dc bias of 247A/m

3.4 Other Losses Related to Vibration under DC Bias

It has been shown that the presence of impurities, such as carbon and nitrogen atoms within an iron crystal lattice, can result in increased losses as the impure atoms jump between energetically preferred positions on the axes of the lattice. However, according to literature, and to the knowledge of the author, this phenomenon has not been found in non-metals [20], and, therefore, is not investigated in this Thesis.

3.5 Summary

In this chapter the nature of magnetostrictive vibration was described in the absence, as well as the presence, of a dc bias and related to mechanisms occurring at a microscopic level that impact upon the magnetization process. In the absence of a dc bias it was shown diagrammatically that the magnetostrictive vibration occurs at twice the frequency of the ac component of the applied magnetic field, and drops to half this value when a dc bias is applied. With the application of an initial dc bias at a low level it was proposed that core losses can decrease, in correspondence with the reduction in the frequency of the magnetostrictive vibration. This was attributed to the dependence of the density and strength of domain wall pinning sites on the vibration frequency. With increasing levels of dc bias it was stated that an increase in the level of the magnetostrictive vibration takes place, as domain rotation becomes more prominent in the magnetization process, so generating higher levels of irregular stress internal to the CUT. Through this mechanism it was proposed that an increasing number of domain wall pinning sites are created, thus contributing to an increase in core losses with dc bias. In addition to acting on the losses due to domain wall

motion, it was also proposed that magnetostrictive vibration could also influence the losses associated with domain rotation at a microscopic scale.

At a macroscopic scale it was proposed that the stress anisotropy resulting from magnetostrictive vibration can influence the magnetization process under dc bias conditions, and an analysis was presented in this regard. By the stress anisotropy mechanism it was proposed that B-H loops can be distorted under dc bias conditions. This phenomenon, in addition to the influence of dc bias conditions on core losses, is investigated in further in Chapter 4.

3.6 References

[1] D. C. Jiles, "Introduction to Magnetism and Magnetic Materials", London, Chapman Hall, 1998

[2] R. M. Bozorth, "Ferromagnetism", IEEE Press, 1993, ISBN 0-7803-1032-2

[3] S. Chikazumi, "Physics of Magnetism", New York, John Wiley & Sons, 1964

[4] B. D. Cullity, "Introduction to Magnetic Materials" Addison-Wesley, Massachusetts, 1972, ISBN 0-201-01218-9

[5] E. du Tremolet de Lacheisserie, "Magnetostriction, Theory and Applications of Magnetoelasticity", CRC Press, 1993, ISBN 0-8493-6934-7

[6] R. D. Adams, "Damping of ferromagnetic materials at direct stress levels below the fatigue limit", *J. Phys. D: App. Phys*., vol. 5, 1972, pp. 1877-1889A.

[7] A. Ercuta, "Magnetomechanical damping in stress-relieved Ni: the effect of the dc magnetic field", *J. Phys.: Condens. Matter*, 20, 2008, pp. 1-9.

[8] N. Good, J. Dooley, and B. Fultz, "Magnetomechanical damping by polycrystalline TbDy", *J. App. Phys*., vol. 91, no. 10, 15 May, 2002, pp. 7824-7826.

[9] K. B. Hathaway, A. E. Clark, J. P. Teter, "Magnetomechanical Damping in Giant Magnetostriction Alloys", *Met. And Mat. Trans. A,* vol. 26, issue 11, Nov. 1995, pp. 2797-2801.

[10] J. Degauque, "Magnetic Domains", *Mat. Sci. Forum*, vol. 366-368, 2001, pp.453-482

[11] G. Bertotti, "Hysteresis in Magnetism", Academic Press, San Diego, 1998, ISBN: 0-12-093270-9

[12] C. Kittel, "Physical Theory of Ferromagnetic Domains", *Rev. Mod. Phys*., vol. 21, no. 4, Oct. 1949, pp.541-583

[13] E. W. Lee, “Magnetostriction and Magnetomechanical Effects”, Repts. Progr. Phys. XVIII, 1955, pp.184-229

[14] G. F. Dionne, “Determination of Magnetic Anisotropy and Porosity from the Approach to Saturation of Polycrystalline Ferrites”, *J. App. Phys.,* vol. 40, no. 4, Mar. 1969, pp.1839-1848

[15] W. S. Weiglhofer, A. Lakhtakia, “Introduction to Complex Mediums for Optics and Electromagnetics”, SPIE Press, 2003, ISBN 0-8194-4947-4, pp.225-244

[16] A. H. Morrish, "The Physical Principles of Magnetism", IEEE Press, 2001

[17] J. W. Shaner, “Shock Induced Demagnetisation of YIG”, *J. App. Phys*., vol. 39, no. 2, 1 Feb. 1968, pp.492-493

[18] I. C. Bartel, Theory of Strain-Induced Anisotropy and the Rotation of the Magnetization in Cubic Single Crystals”, *J. App. Phys*., vol. 40, no. 2, Feb. 1969, pp.661-669

[19] D. E. Grady, G. E. Duvall, “Shock-Induced Anisotropy in Ferromagnetic Material. II. Polyscrystalline Behaviour and Experimental Results for YIG”, *J. App. Phys*., vol. 43, no. 4, Apr. 1972

[20] J. L. Snoek, “New Developments in Ferromagnetic Materials”, Elsevier 1949

Chapter 4

Modeling of B-H Loops under DC Bias

4.1 Introduction

In [1] a model is described with the ability to generate the sigmoid shaped B-H loops that are typical of magnetic materials under symmetrical magnetic excitation conditions. Commonly referred to as the Jiles-Atherton, J-A, model, it assumes the magnetization process is anhysteretic for an ideal magnetic material. Under this condition the magnetization curve is a single valued and, therefore, reversible function of the magnetic field strength [2]. For non-ideal magnetic materials the J-A model assumes magnetization losses exist, which make the magnetization process hysteretic and, thus, irreversible. In this case the total magnetization, M, of a magnetic material will consist of an irreversible component, M_{irr}, in addition to a reversible component, M_{rev}. The J-A model mathematically describes the total magnetization process, including the anhysteretic magnetization, M_{an}, as well as the M_{rev} and M_{irr} components, using a small number of parameters and equations formulated on physical considerations. These equations and parameters are described in this chapter, along with the rationale underlying their existence, and are used to propose a model that predicts the increase in core losses with dc bias levels. In addition the model is able to predict the figure-eight shaped B-H loop phenomenon described in Chapter 3.

4.2 The J-A Model and the Nature of Hysteresis under DC Bias

The magnetization process over an excitation cycle generating a B-H loop can be described in terms of a series of jumps between metastable energy states of a magnetic system [3]. In a

metastable state the thermodynamic forces acting on a magnetic system are in equilibrium and a thermodynamic potential, such as the Landau free energy, G_L, will be at a local minimum for a short period of time. Therefore, the metastable state is characterized by the thermodynamic relation:

$$\left[\frac{\partial G_L}{\partial M}\right]_{H,T} = 0\,, \tag{4.1}$$

which states that in equilibrium the variation of G_L with respect to the magnetization, M, is zero, while the H-field and temperature, T, are held constant. The time period can end if the thermodynamic forces include a contribution from an applied magnetic field, which is changed to a sufficiently large degree. Following such a change the magnetic system loses its stability, as the local energy state it occupies no longer exists as a minimum, and a jump is made to the nearest new local energy minimum. If the jump is so rapid in time that for its duration the applied magnetic field can be considered as constant, then it can be assumed that time plays no role during the jump. In this case the only important feature is the sequence of local energy equilibria that are visited [3], and the magnetic system may be described as being rate-independent. Under this condition the applied magnetic field simply forces the magnetic system to pass from one local energy minimum to the next. However, if the rate at which the applied magnetic field varies is increased so that rate-dependent effects are incurred, such as the inducement of eddy currents in magnetic materials, then a rate-independent approach can no longer be applied.

Following a change to an applied magnetic field the time period occupied in a local energy equilibrium can also end if thermal agitation causes the magnetic system to relax to a thermodynamic equilibrium [3]. If the rate at which the applied field is varied is so slow that a sequence of thermodynamic, rather than local, energy equilibria are traced then the magnetization process will be anhysteretic. In this case losses are not incurred, disallowing the measurement of the phenomenon of hysteresis. Therefore, there exists a frequency bandwidth within which the rate of change of the applied magnetic field is sufficiently slow to avoid rate-dependent effects, yet is fast enough to prevent the magnetic system relaxing to a thermodynamic equilibrium.

In [4] it is stated that the time-independent hysteresis loop of a Mn-Zn ferrite core in Ferroxcube 3C80 material is identical to that occurring at 1 kHz. Time-independence in this context is

considered to be equivalent to rate-independence by the author and, therefore, 1 kHz is assumed in this Thesis to be a frequency which allows rate-independent B-H loops to be modeled for Mn-Zn ferrite materials. This assumption is reasonable if the jumps between local energy equilibria of the magnetic system of a Mn-Zn CUT are assumed to take place through Barkhausen jumps [3], which are relatively undamped due to the low eddy current losses of Mn-Zn ferrite at 1 kHz. Furthermore, the assumption is supported by the core loss results shown in Table 4.1, which were measured using the technique described in Section 5.5 in the absence of a dc bias, at an ac excitation level of 0.05 T, and on a 25x15x10 mm toroidal CUT in MMG F49 Mn-Zn ferrite material. The results show core losses increased by a factor of 1.94 as the frequency was increased from 1 kHz to 2 kHz, and demonstrate that the energy lost per cycle remained approximately constant as the frequency was doubled. Consequently, the area contained within the B-H loops at 1 kHz and 2 kHz must be approximately equal, and both B-H loops can be considered as rate-independent. A comparison between the core losses at 1 kHz and 10 kHz shows an increase by a factor of 12.36, which is greater than the factor by which the frequency increased. This demonstrates a rate-dependence, which is even more pronounced with a comparison between the losses at 1 kHz, and 20 kHz. At higher frequencies, such as 20 kHz, the approximation that the applied magnetic field is constant during Barkhausen jumps no longer holds, and modifications must be made to the rate-independent J-A model.

Table 4.1 Core Losses with no dc Bias at 0.05T

Frequency (kHz)	Measured Core Loss (kW/m^3)
1	0.577
2	1.121
5	3.057
10	7.132
20	17.661

The rate-independent J-A model has previously been modified to account for rate-dependent effects through the use of an equation of motion for moving domain walls [4]. With this equation the damping, and thus the loss, associated with domain wall movement is taken into consideration. Therefore, the issue arises as to whether the increase in core losses with dc bias should be modeled using a rate-independent, or a rate-dependent J-A model. Resolution of this issue is achieved through measuring core losses under dc bias conditions at 1 kHz, to observe whether the

mechanisms causing core losses to increase with dc bias are operative at this low frequency. A core loss characteristic measured at 1 kHz under dc bias conditions is shown in Fig. 4.1. For these measurements the CUT was initially demagnetized before an ac excitation level of 0.05 T was applied. The dc bias was then increased monotonically from zero to a maximum, then decreased back to zero using the technique described in Section 5.5. The characteristic shows core losses decreasing with the initial application of a dc bias, before increasing significantly at higher dc bias levels. This trend is typical of other core loss characteristics measured under dc bias conditions at higher frequencies, which are presented in Chapter 6. Therefore, it shows that the mechanisms causing core losses to increase with dc bias conditions are rate-independent. This is consistent with the theory proposed in Chapter 3, which stated that the increase in core losses with dc bias can be explained by an increase in the level of irregular stress within a CUT, which in turn creates more domain wall pinning sites. Although an increase in domain wall pinning sites generates higher losses, it does not slow the speed of moving domain walls during the Barkhausen jumps between local energy equilibria of a magnetic system. Therefore, according to the definition of rate-independent magnetization in [3], the core loss mechanisms described in Chapter 3 can be accounted for within a rate-independent model. This allows the rate-independent J-A model to be used to simulate the effects of dc bias conditions on the core losses of Mn-Zn ferrite materials.

Of importance to the J-A model is the nature of M_{an}, because once a curve characterizing this quantity is determined, the model only needs to be completed with the introduction of hysteresis into the magnetization process [5]. M_{an} is described in Section 4.3.

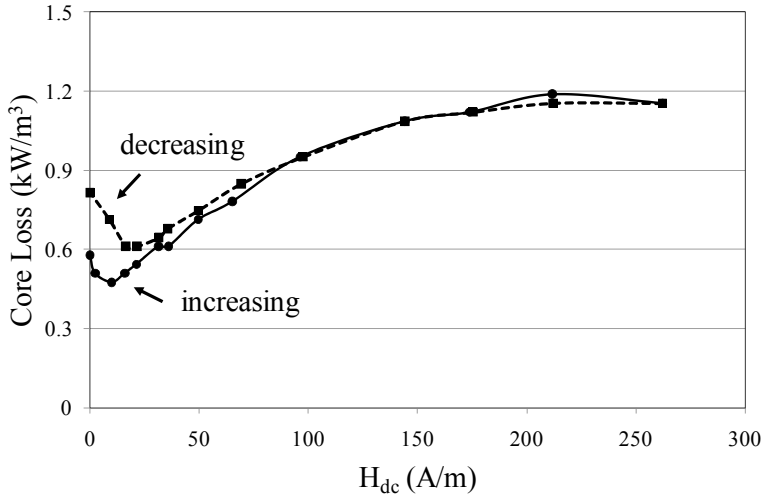

Fig. 4.1 Core losses measured under dc bias conditions for a 25x15x10 mm toroidal CUT at 1 kHz, 0.05T

4.3 The Anhysteretic Magnetization

In Section 4.2 metastable states were described as local equilibrium energy states, which were occupied for short periods of time until the applied magnetic field was changed to a sufficient degree. However, over relatively longer time periods, and in the absence of changes to the applied magnetic field, thermal agitation allows a magnetic system to progress from a local equilibrium to a lower energy state. If the lower energy state corresponds to a global minimum it is known as a thermodynamic equilibrium [3]. The locus of points joining thermodynamic equilibria at various applied magnetic field values represents the M_{an} curve [5], the movement along which does not depend on previous history of the magnetic system, and is reversible. It can be regarded as the path that would be followed if a magnetic material were free from the hysteresis generating phenomena that create domain wall pinning sites and, thus, domain wall movement losses. A simplified diagram comparing a M_{an} curve to an initial magnetization curve is shown in Fig. 4.2, and it is apparent that the permeability of the M_{an} curve is higher than that of the initial magnetization curve at magnetization levels below saturation [5].

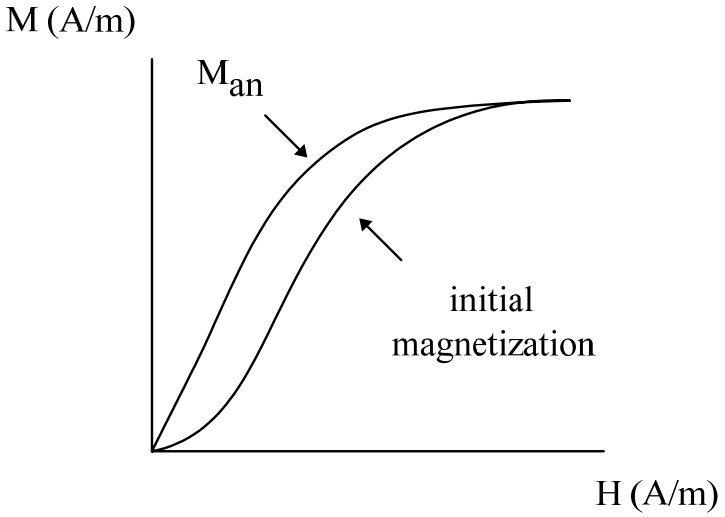

Fig. 4.2 Anhysteretic and initial magnetization curves

In [6] it is stated that the expression for M_{an} used in the J-A model is derived under the assumption that a magnetic material is composed of an array of pseudo-domains with fixed domain walls. As a consequence, the net magnetization of each pseudo-domain is only allowed to change through domain rotation, which must be reversible to avoid hysteresis. These changes are brought about by variations in the effective magnetic field strength, H_e. M_{an} can be defined as a function of H_e by [1]:

$$M_{an} = M_s\left[\coth\left(\frac{H_e}{a}\right) - \left(\frac{a}{H_e}\right)\right] \tag{4.2}$$

where,

a	=	J-A parameter (A/m)
H_e	=	effective magnetic field strength (A/m)
M_{an}	=	anhysteretic magnetization (A/m)
M_s	=	saturation magnetization (A/m)

The constant, a, in (4.2) is a parameter of the J-A model that is proportional to temperature, domain density and the saturation magnetization, and can be determined through experimental measurements. The H_e field consists of contributions derived from a number of domain energy terms including the applied magnetic field energy, and the stress anisotropy energy. The effect of stress anisotropy on the magnetization process has previously been described in Chapter 3 and, within the framework of the J-A model, can influence the total magnetization process through acting on M_{an}. This influence is expressed by defining the total magnetization in terms of two components according to:

$$M = M_{rev} + M_{irr} \tag{4.3}$$

where,

M	=	total magnetization (A/m)
M_{irr}	=	irreversible magnetization (A/m)
M_{rev}	=	reversible magnetization (A/m)

then expressing M_{rev} and M_{irr} as variables dependent on M_{an}. Physically, the influence of M_{an} on M can be understood with knowledge that each point on the M_{an} curve represents a minimum and, therefore, optimal energy state for a CUT to exist in. Consequently, domain walls will move, or bend in such a manner as to minimize the difference between the actual magnetization, and M_{an}. The bending of domain walls can be a lossless and, therefore, reversible process and so is associated with M_{rev}. However, domain wall movement incurs losses and so is associated with M_{irr}. The importance of domain wall pinning to both these components of magnetization, is discussed further in Section 4.4.

4.4 Magnetization and the J-A Model

M_{rev} is considered predominant over M_{irr} at low levels of the magnetization process as the domain walls bend up to, but not beyond, the point where they have expanded sufficiently to break free from their previous pinning sites to new ones. A simplified diagram illustrating how an 180^o domain wall can bend when pinned at both ends is given in Fig. 4.3. Because this domain wall is pinned, it can only be reversibly deformed by the action of an applied magnetic field, and in [1] its geometry was analyzed in conjunction with physical considerations to represent M_{rev} by:

$$M_{rev} = c\left(M_{an} - M_{irr}\right) \tag{4.4}$$

where,

c = J-A parameter

Essentially, (4.4) shows that the amount of bending of a domain wall that takes place is linearly dependent on the difference between M_{an} and M_{irr} at a given magnetic field strength. Equation (4.4) can be differentiated to give the change in M_{rev} with H as:

$$\frac{dM_{rev}}{dH} = c\left(\frac{dM_{an}}{dH} - \frac{dM_{irr}}{dH}\right) \tag{4.5}$$

where,

H = applied magnetic field strength (A/m)

As described in [1], both c, and the M_{an} curve can be determined experimentally.

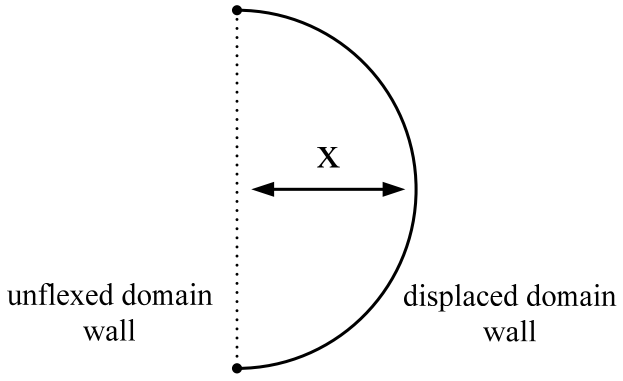

Fig. 4.3 Bending of a domain wall between two pinning sites

The magnetization component M_{irr} exists when domain wall motion is impeded and, in common with M_{rev}, also arises due to domain wall pinning. In this case each incidence of de-pinning that takes place as a domain wall moves results in a Barkhausen jump, and contributes a loss of energy to the magnetization process. This lost energy is related to the anhysteretic magnetization energy and the irreversible magnetization energy, through:

$$\int M_{irr} dB_e = \int M_{an}(H_e) dB_e - k \int \left(\frac{dM_{irr}}{dB_e} \right) \tag{4.6}$$

where,

B_e = effective flux density (T)

k = J-A parameter (A/m)

Equation (4.6) states that the magnetization energy, which is the leftmost term in (4.6), is that which would be obtained in the anhysteretic case, less the hysteresis losses incurred through the movement of domain walls. For (4.6) the field H_e is given by:

$$H_e = H + \alpha M \tag{4.7}$$

where,

α = inter-domain coupling parameter

The term αM in (4.7) gives the contribution to H_e arising from the magnetic interaction between domains, with the terms B_e, H_e, H, and M related to each other by the equation:

$$B_e = \mu_o H_e = \mu_o (H + \alpha M) \tag{4.8}$$

where,

μ_o = $4\pi \times 10^{-7}$

By differentiating (4.6) with respect to B_e, introducing a directional parameter δ, then differentiating with respect to H, the change in magnetization with respect to H can be represented by [7]:

$$\frac{dM_{irr}}{dH} = \frac{1}{\delta k - \alpha\left(M_{an} - M_{irr}\right)}\left(M_{an} - M_{irr}\right) \tag{4.9}$$

The directional parameter δ used in (4.9) takes the values +1 for dH/dt > 0 and -1 for dH/dt < 0.

Through the addition of (4.9) with (4.5), the change in M with H can be found as:

$$\frac{dM}{dH} = \frac{dM_{irr}}{dH} + \frac{dM_{rev}}{dH} \tag{4.10}$$

From (4.9) it is apparent that d M_{irr}/dH is dependent on the difference between M_{an} and M_{irr}. Of key importance to the development of (4.9) is the theory that the losses in a magnetic material due to domain wall pinning can be represented by the third term in (4.6). This term is derived by considering a pinning site located at a domain wall separating magnetic moments **m** and **m′,** with **m** lying in the direction of the applied field, and **m′** aligned at an arbitrary angle θ. The energy required to overcome the pinning site may then be regarded as proportional to the change in energy per unit volume of the **m′** domain caused by rotating its moments into the field direction i.e.:

$$\Delta E = \mathbf{m} \cdot \mathbf{B_e} - \mathbf{m'} \cdot \mathbf{B_e} \tag{4.11}$$

With the consideration that the pinning energy of a site, ε_{pin}, is equal to ΔE, then (4.11) can be simplified to:

$$\varepsilon_{pin} \propto mB_e\left(1 - \cos\theta\right) \tag{4.12}$$

where,

m = magnetic moment of a domain (Wb-m)

Equation (4.12) can only hold for an 180° domain wall if $\varepsilon_\pi \propto 2mB_e$, where ε_π is the pinning energy of an 180° domain wall. Therefore, in [1], (4.12) was re-cast in terms of ε_π as:

$$\varepsilon_{pin} = \frac{1}{2}\varepsilon_\pi(1-\cos\theta) \tag{4.13}$$

By assuming an average density of pinning sites throughout the CUT and an average pinning energy per site, an equation was derived for the total energy dissipated through domain wall movement. For a domain wall of a given area which is moved a distance x between domains whose moments lie at an angle θ, the dissipated energy, E_{pin}, is given by:

$$E_{pin}(x) \propto \int_0^x \frac{n\langle\varepsilon_\pi\rangle}{2}(1-\cos\theta)A\,dx \tag{4.14}$$

where,

A = domain wall area (m^2)

$\langle\varepsilon_\pi\rangle$ = average pinning energy of pinning sites for 180° domain walls (J)

n = average density of pinning sites throughout the CUT

By allowing the net change, dM, in magnetization to be represented by:

$$dM = m(1-\cos\theta)A\,dx \tag{4.15}$$

then the equation for E_{pin} can be given by:

$$E_{pin}(M) = k\int_0^M dM \tag{4.16}$$

where, $k = \frac{n\langle mB_e\rangle}{m}$ (A/m) and is a J-A parameter that is determined experimentally. As noted in [1], parameter k is not constrained to be constant and may vary as a function of H. This allows for k to be varied as a function of the dc bias, and is addressed further in Section 4.5.

4.5 The J-A model under dc Bias Conditions

The discussions in the previous section on M_{an}, and the J-A parameters a and k under symmetrical excitation conditions, are extended in this section to include the influence of dc bias conditions. Through this influence it is proposed that the effect of a dc bias on core losses in the magnetization process can be modeled.

4.5.1 Parameters k and a under DC Bias Conditions

When used with correctly determined parameters the J-A model can accurately reproduce measured symmetrical B-H loops which reach, or are close to, saturation magnetization levels. For smaller symmetric B-H loops [8], and dc biased B-H loops the J-A model can be inaccurate, as simulated B-H loops fail to close at the loop tips. However, in [9] a generalization was presented to resolve this shortcoming, and involves the determination of volume fractions vf , and vf′, which are constants for any pair of dc biased B-H loop H-field extrema. The use of volume fractions achieves the closure of dc biased B-H loops through limiting dM/dH by modifying (4.9) to:

$$\frac{dM_{irr}}{dH} = vf\frac{1}{\delta k - \alpha\left(M_{an} - M_{irr}\right)}\left(M_{an} - M_{irr}\right) \tag{4.17}$$

and modifying (4.5) to:

$$\frac{dM_{rev}}{dH} = vf' \cdot c\left(\frac{dM_{an}}{dH} - \frac{dM_{irr}}{dH}\right) \tag{4.18}$$

Reference [9] describes how the volume fractions can be calculated, which have a value of 1 in the limit for symmetric B-H loops traversing between positive and negative saturation levels. A modification to the volume fraction approach, which also allowed for B-H loop closure, has been applied in [10] to the J-A model. Included in the modifications was the introduction of a dependency of parameters a and k on the ratio:

$$b = \frac{0.5\left|M_{max} - M_{min}\right|}{M_s} \tag{4.19}$$

where,

M_{max} = maximum magnetization of the dc biased hysteresis loop (A/m)

M_{min} = minimum magnetization of the dc biased hysteresis loop (A/m)

M_s = saturation magnetization (A/m)

The justification for modifying parameter a was stated as the need to take into account the size of domains aligned with the applied magnetic field, and parameter k was related to the distribution of domain wall pinning sites within a material [11]. However, a physical effect causing domain wall pinning sites and, therefore, parameter k to vary was not given. A statement was made that dissipation mechanisms different from domain wall movement could exist at magnetic field levels above the knee of B-H loops due to domain nucleation and annihilation; however, this was related to parameter a rather than parameter k. In this Thesis it is proposed that both these parameters can be modified in a manner that is consistent with the real physical effects experienced by a CUT under dc bias conditions, as described below.

The number of domain wall pinning sites in a material is dependent on the presence of irregular stress within a CUT [1]. Therefore, it is proposed that parameter k must increase with dc bias levels, as the dc bias induces higher magnetostrictive vibration, greater levels of irregular stress at a micro-structural level within a CUT and, thus, higher core losses, as described in Chapter 3.

In the demagnetized state it has been stated that parameter a is proportional to the domain density [12]. This statement is obvious from the definition [6]:

$$a = \frac{Nk_B T}{\mu_o M_s} (A/m) \tag{4.20}$$

where,

N = domain density per unit volume

k_B = Boltzman constant (1.38×10^{-23} JK^{-1})

T = temperature (K)

M_s = saturation magnetization (A/m)

Furthermore, in [6] it is stated that parameter a should be a constant of a material, which is dependent in part on the material microstructure. However, from (4.20) it is apparent that parameter a must decrease with the application of a dc bias to an ac excitation waveform, as the number of domains in existence in a material and, therefore, N decreases in the approach to saturation. A procedure for determining parameters a and k, as well as the other parameters of the J-A model, is described in Section 4.5.2.

4.5.2 The J-A Parameter Values under DC Bias Conditions

One parameter of the J-A model, M_s, can be determined by measurement, or through resorting to values published in ferrite material data sheets. For the determination of the other parameters an iterative procedure was described in [7]. However, this procedure is sensitive to the initial parameter values that are entered and, furthermore, may not converge [8]. Therefore, in this Thesis a modified procedure was used, which involves setting the value of parameter k equal to the coercive force, H_c, of a symmetrical B-H loop, before determining the parameters α, a, and c with an iterative numerical algorithm similar to that described in [17]. The numerical algorithm is given in Appendix B, and the parameter values generated by this procedure are used as a first approximation, before being optimized iteratively to achieve a good fit between measured and predicted symmetric B-H loops. With the application of a dc bias to the B-H loop the value of parameter a is decreased, while that of k is increased. These adjustments are made in an iterative manner consistent with the description given in Section 4.5.1.

4.5.3 The Influence of Vibration on M_{an} at a Macroscopic Level

In Section 3.3 a description was given of the manner by which the mechanical state of a CUT can influence its magnetic state. The fact that interactions of this type can take place is well known and, according to [13], the influence of an applied stress on the magnetization of a magnetic material is known as the magnetomechanical effect. In the theory presented in [13], the magnetomechanical effect is explained through a law of approach due to domain wall movement. According to this explanation, the magnetization of a CUT will change in response to a constant applied stress by approaching the M_{an} curve. Furthermore, this law is supported by experimental evidence in [14], showing that the action of an applied compressive stress is to change the magnetization and bring it closer to the M_{an} curve. As illustrated schematically in Fig. 4.4, the action of a compressive stress applied from either position A (demagnetized state), B (positive

remanence), or C (negative remanence), is to cause the magnetization to move closer to position X on the M_{an} curve.

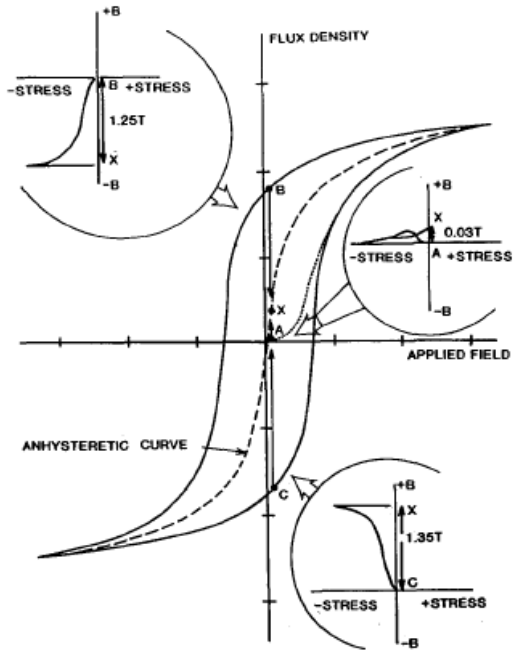

Fig. 4.4 Schematic representation of the characteristics of a ferromagnetic material in the B-H plane and the influence of magnetic history on the stress-magnetization behavior, reproduced from [14]

In [13] the hypothesis was made that the magnetization will approach M_{an} under an applied stress because the elastic energy supplied to a CUT by the applied stress causes domain walls to be released from their pinning sites. In addition, an equation was developed for the rate of change of magnetization with stress, given by:

$$\frac{dM}{d\sigma} = \frac{\sigma}{E\xi}(1-c)(M_{an} - M_{irr}) + \frac{dM_{an}}{d\sigma} \tag{4.21}$$

where,

σ = applied stress (Pa)

E = Youngs modulus

ξ = constant (Joules p.u. volume)

From (4.21) it is apparent that the rate at which M will approach M_{an} is dependent on the difference between M_{an} and M_{irr}.

The theory of the law of approach proposed in [13] is based on the assumption that hysteresis originates mainly from domain wall pinning, and is applicable to major, symmetric B-H loops. However, experimental evidence presented in [15] showed this law does not appear to apply to asymmetric B-H loops, and that the law of approach to M_{an} with the application of stress does not hold. In [15] it was concluded that the magnetization changed in response to an applied stress so as to approach an equilibrium value, which did not coincide with the M_{an}. It was further suggested that the rotation of magnetic moments within a CUT plays a role in the magnetization process, though largely contributing in a reversible, or lossless, manner. In addition, the hypothesis promoted in [13] that an applied stress releases domain walls from their pinning sites is discordant to the theory proposed in this Thesis; in particular, the theory that magnetostrictive vibration under dc bias conditions creates regions of irregular stress at a microscopic level and, thus, a greater number of pinning sites of increased energy levels. Therefore, in this Thesis it is contended that the theory of the magnetomechanical effect as proposed in [13] does not hold within the context of a Mn-Zn ferrite CUT experiencing magnetostrictive vibration under dc bias conditions.

In Section 3.3 it was proposed that stress anisotropy can act on a large number of magnetic moments in a uniform manner. Because stress anisotropy is a domain energy term and, therefore, has an associated H-field [16], $H_{\sigma i}$, it can be modeled through the addition of $H_{\sigma i}$ to the H_e field existent within a CUT. As explained in [13], the modification of the H_e field by a stress field impacts upon the shape of the M_{an} curve, because the M_{an} curve is dependent on the H_e field. In this way the effects of stress anisotropy at a macroscopic level can be incorporated into the J-A model. The addition of an applied stress field component to H_e has previously been proposed in [6] for a J-A model with an H-field input. However, this differs from the macroscopic magnetomechanical effect modeled in this Thesis in that the stress is assumed to be internal and generated by the nature of the magnetostrictive vibration of the CUT. Furthermore, it is necessary to apply an inverse J-A model, which operates with a B-field input rather than an H-field input, because the experimental set-up described in Section 5.5, and used to gather the results presented in this Thesis, applies a controlled B-field to the CUT under dc bias conditions.

Therefore, a modified J-A model is proposed in Section 4.6, which uses a B-field input, and also takes into account an $H_{\sigma i}$ field.

4.6 The Modified J-A Model

According to [17] the four equations of the J-A method are (4.2)-(4.4), which were discussed in Sections 4.3 and 4.4, in addition to:

$$\frac{dM_{irr}}{dH_e} = \frac{M_{an} - M_{irr}}{\delta k} \tag{4.22}$$

which is originates from (4.6) and (4.8). The model proposed in this section derives from (4.2)-(4.4), and it is assumed that the H_e field existent within a CUT that is also subject to stress is modified from (4.7) to:

$$H_e = H + \alpha M + H_{\sigma i} \tag{4.23}$$

as explained in Section 4.5. The term $H_{\sigma i}$, is considered to be the average of localized regions of internal stress in the core, which sum to a non-zero value, and are assumed to be aligned in the same axis as the applied magnetic field.

Using (4.3) and (4.4), and taking the derivative with respect to H gives:

$$\frac{dM}{dH} = \frac{dM_{irr}}{dH} + c\left(\frac{dM_{an}}{dH} - \frac{dM_{irr}}{dH}\right) \tag{4.24}$$

The term dM_{an}/dH in (4.24) can be defined as:

$$\frac{dM_{an}}{dH} = \frac{dM_{an}}{dH_e}\frac{dH_e}{dH} \tag{4.25}$$

Based on (4.23) the derivative of H_e with respect to H is:

$$\frac{dH_e}{dH} = 1 + \alpha\frac{dM}{dH} + \frac{dH_{\sigma i}}{dH} \tag{4.26}$$

Using (4.26), then (4.25) can be re-defined as:

$$\frac{dM_{an}}{dH} = \frac{dM_{an}}{dH_e}\left[1 + \alpha\frac{dM}{dH} + \frac{dH_{\sigma i}}{dH}\right] \tag{4.27}$$

In a similar manner dM_{irr}/dH is given by:

$$\frac{dM_{irr}}{dH} = \frac{dM_{irr}}{dH_e}\left[1 + \alpha\frac{dM}{dH} + \frac{dH_{\sigma i}}{dH}\right] \tag{4.28}$$

Through substituting (4.27) and (4.28), into (4.24) then dM/dH is given by:

$$\frac{dM}{dH} = \frac{\left(1 - c + \frac{dH_{\sigma i}}{dH} - c\frac{dH_{\sigma i}}{dH}\right)\frac{dM_{irr}}{dH_e} + c\left(1 + \frac{dH_{\sigma i}}{dH}\right)\frac{dM_{an}}{dH_e}}{1 - \alpha c\frac{dM_{an}}{dH_e} - \alpha(1-c)\frac{dM_{irr}}{dH_e}} \tag{4.29}$$

where according to [17]:

$$\frac{dM_{an}}{dH_e} = \frac{M_s}{a}\left[1 - \coth^2\left(\frac{dM}{dH}\right) + \left(\frac{a}{H_e}\right)^2\right] \tag{4.30}$$

and dM_{irr}/dH_e is given by (4.22). Equation (4.29) can be solved numerically with an H-field input to give the magnetization of a magnetic specimen. It is further modified as follows to be suitable for a B-field input. The differential equation dM/dB can be defined as:

$$\frac{dM}{dB} = \frac{dM}{dH}\frac{dH}{dB} \tag{4.31}$$

Given that $B = \mu_o(H + M)$ then:

$$\frac{dM}{dB} = \frac{\frac{dM}{dH}}{\mu_o\left(1 + \frac{dM}{dH}\right)} \tag{4.32}$$

Substituting for dM/dH using (4.29) gives:

$$\frac{dM}{dB} = \frac{\left(1 - c + \frac{dH_{\sigma i}}{dH}(1-c)\right)\frac{dM_{irr}}{dB_e} + \frac{c}{\mu_o}\left(1 + \frac{dH_{\sigma i}}{dH}\right)\frac{dM_{an}}{dH_e}}{1 + \frac{dM_{an}}{dH_e}\left[c\left(1 + \frac{dH_{\sigma i}}{dH}\right) - \alpha c\right] + \mu_o \frac{dM_{irr}}{dB_e}\left[1 - c - \alpha + \alpha c + \frac{dH_{\sigma i}}{dH}(1-c)\right]} \tag{4.33}$$

where,

$$\frac{dM_{irr}}{dB_e} = \frac{1}{\mu_o}\frac{dM_{irr}}{dH_e} \tag{4.34}$$

Equation (4.33) is similar to that given in [17] with the exception of the dH_σ/dH terms. By solving (4.33) numerically the change in magnetization with an applied B-field can be determined while taking into magnetomechanical effects.

In [7] it is stated that unphysical solutions can be obtained from a J-A model with an H-field input when the H-field is changed at either of the tips of an unbiased B-H loop. The unphysical solutions occur in the form of a negative differential susceptibility, and result if the H-field is reduced from the B-H loop tip in the first quadrant and M_{irr} is below M_{an}, or if the H-field is increased from the B-H loop tip in the third quadrant and M_{irr} is above M_{an}. To prevent this occurring it was proposed that $dM_{irr}/dH = 0$ under these conditions. This permits M to change only through the reversible process of domain wall bending, as illustrated in Fig. 4.3. This solution is implemented in the B-field input model described in this section with the use of dM_{irr}/dB_e. It is achieved through setting $dM_{irr}/dB_e = 0$ if M_{irr} is below M_{an} at the uppermost tip of a B-H loop as the B-field is reduced, or if M_{irr} is above M_{an} at the lowest tip of a B-H loop as

the B-field is increased. Through (4.28) and (4.34) it can be seen that when $dM_{irr}/dB_e = 0$, then $dM_{irr}/dH = 0$, thereby implementing the solution described in [7].

The model derived in this section is used to predict the effects of dc bias conditions on core losses in Section 4.7, in addition to the distorted figure-eight shaped B-H loops occurring under dc bias conditions in Section 4.8.

4.7 B-H Loops under DC Bias Conditions

In this section the influence of increasing levels of irregular stress within a CUT under dc bias conditions is predicted using the modified J-A model under dc bias conditions. This influence is investigated through changes to parameters a, and k.

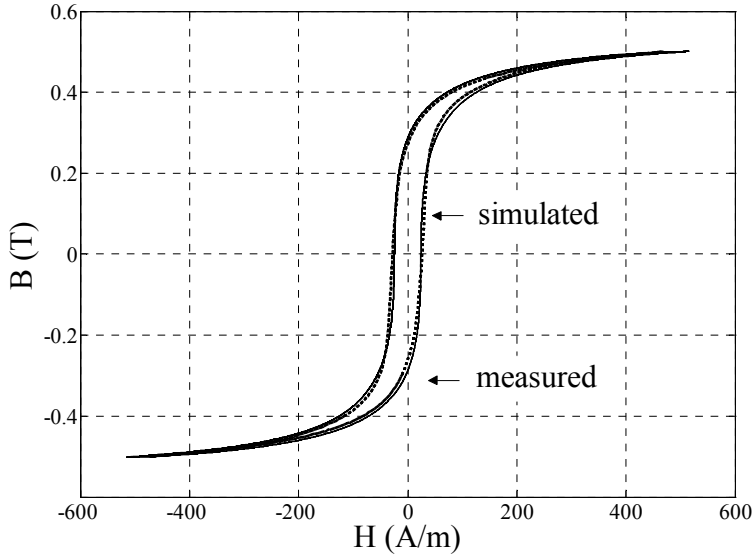

Fig. 4.5 B-H loops measured under various dc bias conditions

Fig. 4.5 shows a major B-H loop measured at 1 kHz for a 25x15x10 mm toroidal CUT in MMG F49 Mn-Zn material, which reaches a peak excitation level of 0.5 T. Also shown is a simulated B-H loop generated using the modified inverse J-A model described in Section 4.6, and with parameters determined using the procedure described in Section 4.5. The model parameters used were: $M_s = 445000$ A/m, $a = 72$ A/m, $\alpha = 0.0005$, $c = 0.48$, $k = 50$ A/m, and the $H_{\sigma i}$ field was set to zero. It is apparent that the simulated and measured major B-H loops are in agreement.

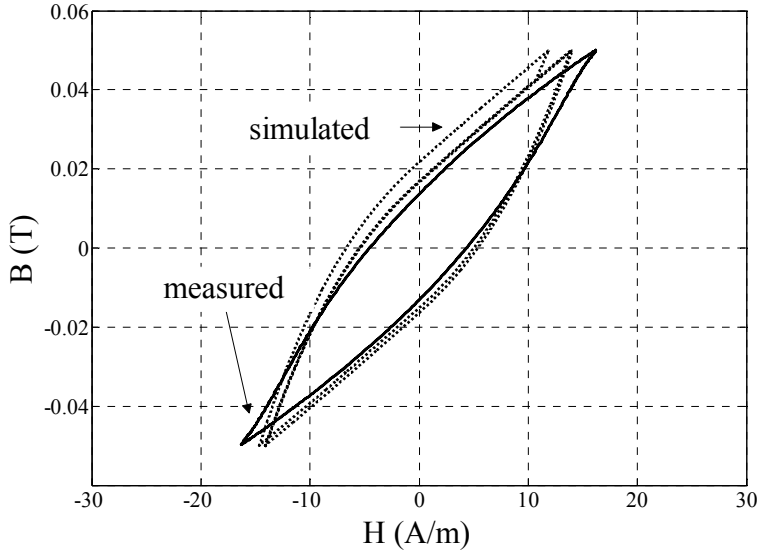

(a)

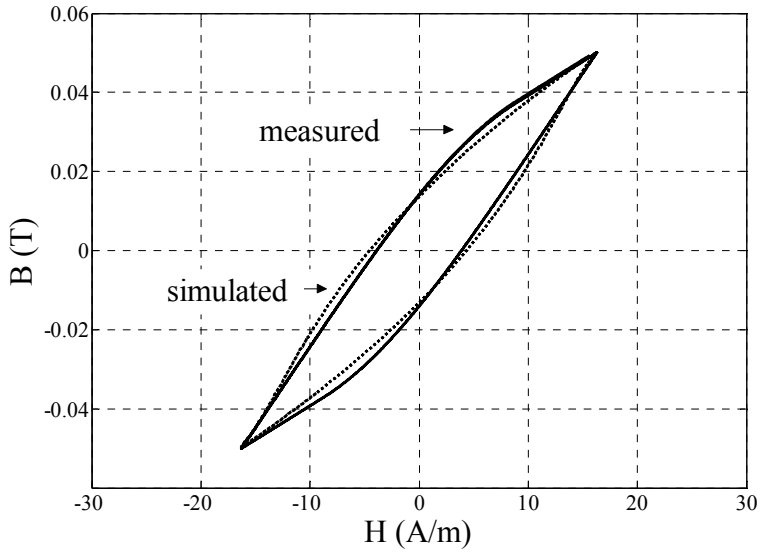

(b)

Fig. 4.6 Measured and simulated B-H loops (a) using parameters derived for major B-H loop, (b) using revised parameters

Measured and simulated minor B-H loops are shown in Fig. 4.6 at 1 kHz, a level of ac excitation of 0.05 T, and in the absence of a dc bias. The simulated B-H loop in Fig. 4.6(a) uses the same J-A parameters as used for Fig. 4.5, and it is apparent that its agreement with the measured B-H loop is poor. However, through applying the numerical algorithm described in Section 4.5.2 new parameter values can be determined that improve the agreement, as shown in Fig. 4.6(b). For this

B-H loop the model parameters used were: M_s = 445000 A/m, a = 91 A/m, α = 0.00032, c = 0.66, k = 13.5 A/m.

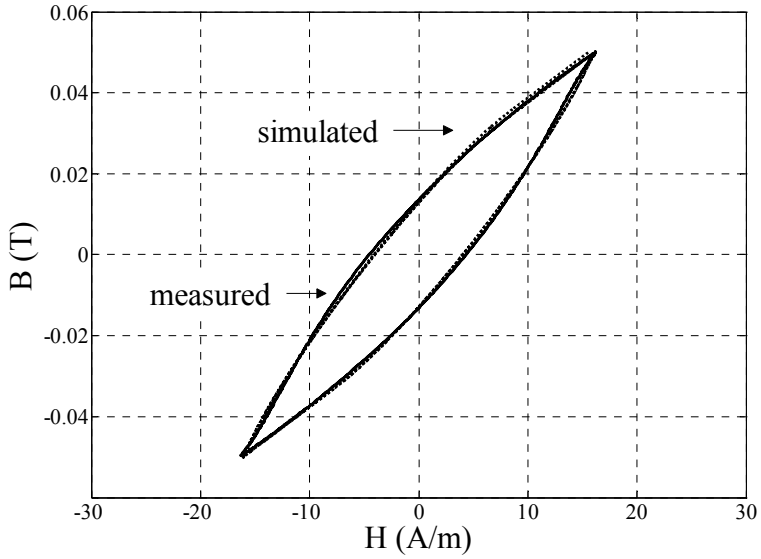

Fig. 4.7 Measured and simulated B-H loops using revised parameters, with k varying at twice the frequency of the applied magnetic field

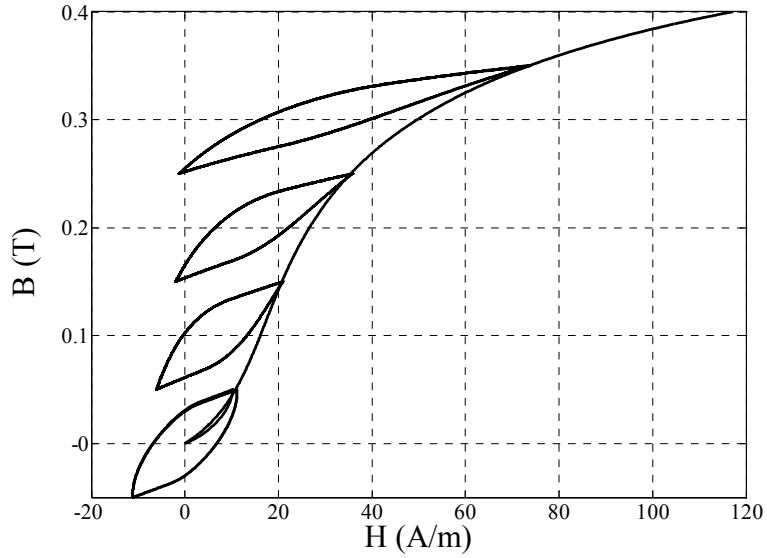

Fig. 4.8 B-H loops modeled under increasing dc bias conditions

The approach of varying all parameters of a J-A model, except M_s, as the amplitude of the applied magnetic field is changed is similar to that followed in [8]. However, the changes in parameters a, c and k between the higher and lower levels of magnetic excitation can be justified

through physical considerations. At low levels of excitation, which are distant from saturation in the absence of a dc bias, a greater number of domains can be assumed to exist in a CUT [3] which, according to (4.20), justifies the increase in parameter a. At low levels of excitation in the absence of a dc bias it can also be assumed that the more of the magnetisation process takes place through reversible domain wall bending, thereby justifying the increase in parameter c and the decrease in parameter k. The fit between the measured and simulated results shown in Fig. 4.6(b) can be improved further through making parameter k variable and dependent on the frequency of the magnetostrictive vibration; this reflects the dependency of domain wall pinning sites on the magnetostrictive vibration frequency, as described in Chapter 3. In the absence of a dc bias this frequency will be 2 kHz, which is twice that of the applied magnetic field for reasons also described in Chapter 3. As discussed in Section 4.2, and based on the core loss measurements in Table 4.1, 2 kHz is considered to be a frequency at which Barkhausen jumps occur at a much faster rate than variations in parameters such as k. Therefore, this allows the rate-independent J-A model to be applied. Accordingly, parameter k is given the value $13+5\cos(2.\pi.2000.t)$ and, as a result, a better fit occurs between the simulated and measured results, as apparent from Fig. 4.7. This supports the proposed theory in Chapter 3 that the number of domain wall pinning sites in a CUT is dependent on elastic variations of irregular stress, and that these variations are partially dependent on the magnetostrictive vibration frequency.

To predict the impact of dc bias conditions on the magnetisation process an initial magnetisation curve was generated, and B-H loops were simulated at various dc bias levels. Because the initial magnetization curve reaches high levels of magnetization, the same parameter values were used as for the major B-H loop shown in Fig. 4.5, which also reaches high levels of magnetization. The B-H loop not subject to a bias in Fig. 4.8 used the same parameter values as for Fig. 4.7. Through progressively increasing the value of parameter k with the dc bias level, decreasing the value of parameter a, and leaving all other parameters unchanged it is apparent that the B-H loops increase in area, reflecting an increase in core losses. In addition, it is also apparent that the upper tips of the modeled B-H loops lie on the initial magnetization curve. A comparison between the values of parameters a and k used for the B-H loops shown in Fig. 4.8 is given in Table 4.2. It is apparent that as the level of dc bias is increased, the values of parameters a and k become closer to the values used to simulate the symmetric B-H loop shown in Fig. 4.5, which traverses between high positive and negative levels of magnetization.

Table 4.2 J-A Parameters a and k used for Fig. 4.7

B-H Loop	Parameter a	Parameter k
i	91	13+5cos(2π2ft)
ii	84.5	19
iii	80.5	22
iv	74	25

4.8 Simulated Figure-eight B-H Loops under DC Bias

In this section the modified J-A model is used to show that the figure-eight shaped B-H loops described in Chapter 3 take place through the magnetomechanical interactions that occur as the stress anisotropy resulting from magnetostriction influences the H-field. This is achieved through introducing a $H_{\sigma i}$ field component to the H_e field under dc bias conditions. In addition, it is assumed that the $H_{\sigma i}$ field is dependent on the nature of the magnetostrictive vibration waveform which generates the stress anisotropy. In Chapter 7 experimental results are presented showing that the magnetostrictive vibration waveform becomes asymmetric and changes rapidly with time when a figure-eight B-H loop is measured. Such a measured waveform is shown in Fig. 4.9, and this waveform is used to model the $H_{\sigma i}$ field. The Fast Fourier Transform of the asymmetric magnetostrictive vibration waveform can be written as:

$$\begin{aligned} V(t)= & A_1\cos(2\pi ft-\theta_1)+A_2\cos(2\pi 2ft-\theta_2)+A_3\cos(2\pi 3ft-\theta_3)+A_4\cos(2\pi 4ft-\theta_4) \\ & +A_5\cos(2\pi 5ft-\theta_5)+A_6\cos(2\pi 6ft-\theta_6)+A_7\cos(2\pi 7ft-\theta_7) \end{aligned} \tag{4.35}$$

where,

$V(t)$ = vibration (m/s)

A_i = amplitude of the i^{th} harmonic (m/s)

f = 34.6 kHz

t = time (s)

with the harmonic components of V(t) as defined in Table 4.3.

Table 4.3 Harmonic Components of Vibration Velocity

Harmonic	Amplitude (mm/s)	θ (degrees)
1	18.34	725.2
2	5.122	1451
3	4.021	2100
4	1.059	2787
5	0.676	3184
6	0.537	3580
7	0.226	3959

The term V(t) is then converted to $H_{\sigma i}$ through scaling by a constant factor S, which is determined through an iterative process and used in the modified J-A model.

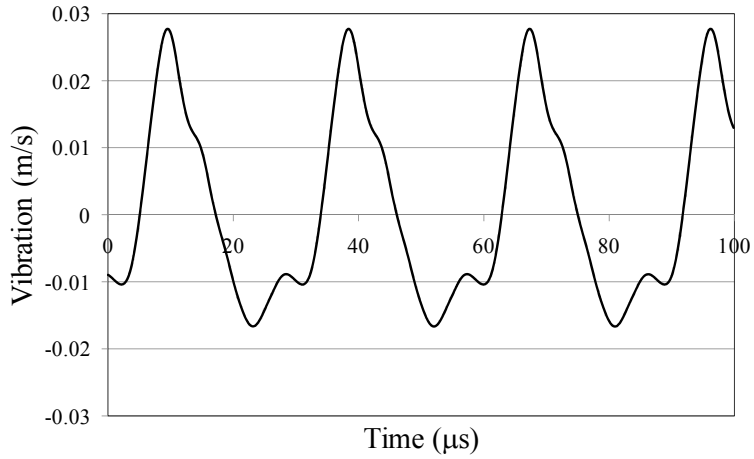

Fig. 4.9 Vibration waveform measured when a figure-eight shaped B-H loop is measured

The J-A parameters used with the modified model were: M_s = 445000 A/m, a = 72 A/m, α = 0.0005, c = 0.48, k = 50 A/m. Fig. 4.10 shows B-H loops simulated using the modified model with a sinusoidal ac excitation of 0.05 T, a high dc bias of 139 A/m, and with $H_{\sigma i}$ waveforms given for values of S = 0, and S = 700. In addition, a leading phase shift of 74.7^o was added to the $H_{\sigma i}$ waveform relative to the B-field. As explained in Chapter 5, the actual phase relationship between the measured magnetostrictive vibration and magnetic excitation waveforms was unable to be determined using the experimental setup; therefore, the phase shift added to the $H_{\sigma i}$ waveform was determined through an iterative process. For the simulated B-H loops the dc bias component has been removed, and the loops are located about zero for ease of comparison.

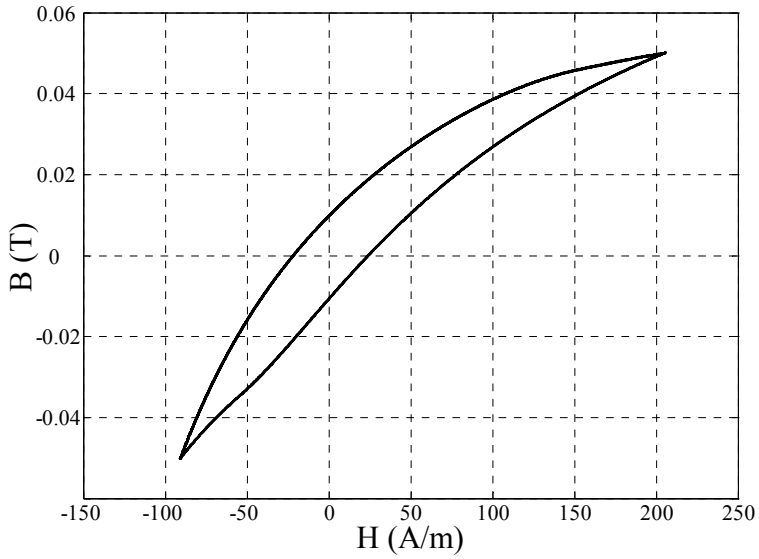

(a)

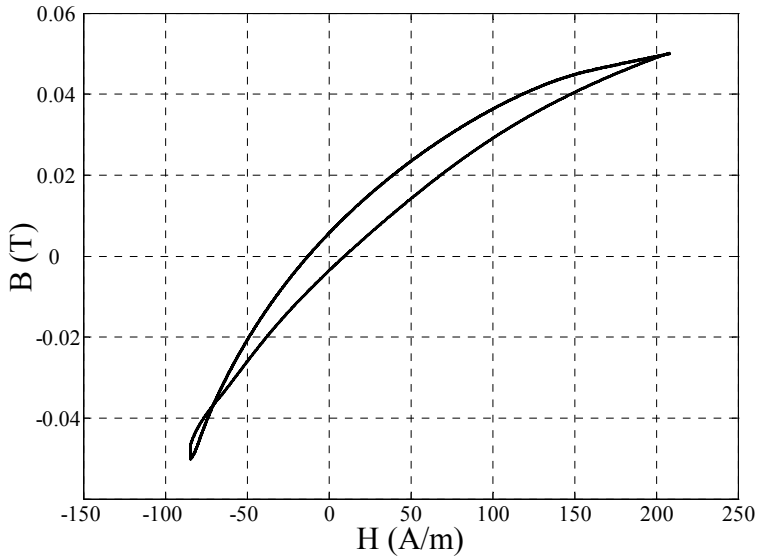

(b)

Fig. 4.10 Simulated B-H loops with (a) S = 0, and no $H_{\sigma i}$, (b) S = 750 and a 29.9^o phase shift added to $H_{\sigma i}$

From Fig. 4.10(a) it is evident that the B-H loop has a conventional shape when S = 0. However, from Fig. 4.10(b) it is apparent that as the magnitude of S and, therefore, that of $H_{\sigma i}$, is increased, a crossover in the tail of the B-H loop is generated, giving it a figure-eight shape. This shows that figure-eight B-H loops can be generated through magnetomechanical interactions under asymmetrical magnetostrictive vibration conditions. The $H_{\sigma i}$ field used to generate the figure-eight shaped B-H loop is shown in Fig. 4.11.

Because the modified J-A model used in this chapter is an inverse type, the simulated B-field is identical to the input B-field of the model. Therefore, the distortion of the B-H loop shape that is brought about by the presence of an $H_{\sigma i}$ field can only occur as the result of changes in the H-field. This is illustrated in Fig. 4.12, which shows H-field waveforms in the presence, and the absence of the $H_{\sigma i}$ field. From these simulated results it is apparent that the influence of the $H_{\sigma i}$ field is to increase the phase shift of the H-field during the lower portion of its cycle. It is shown in Chapter 7 that similar phase shifts can be measured experimentally when a figure-eight B-H loop is generated. This agreement between the experimental measurements and the simulated results supports the predictive ability of the modified model.

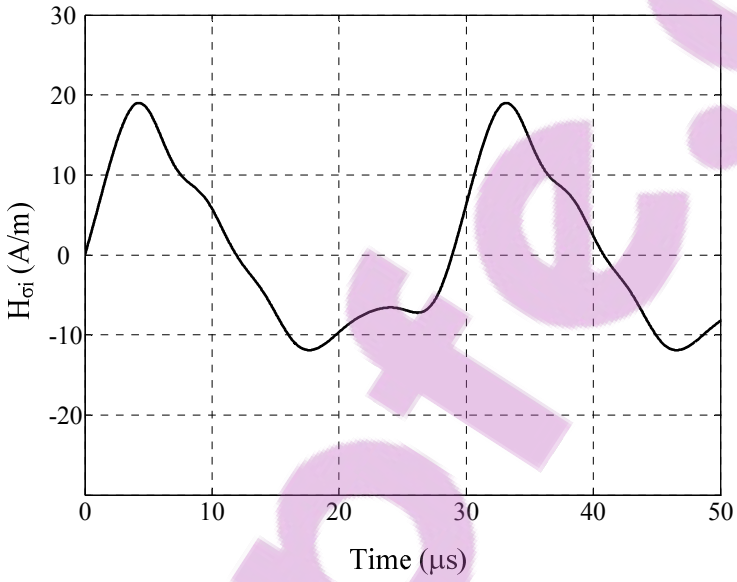

Fig. 4.11 Simulated $H_{\sigma i}$ field waveform

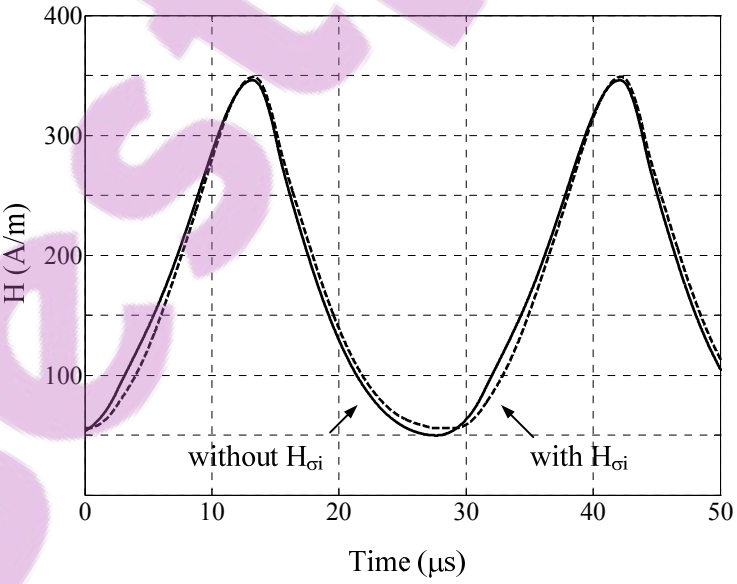

Fig. 4.12 Simulated H field waveforms, derived in the presence and absence of a $H_{\sigma i}$ field

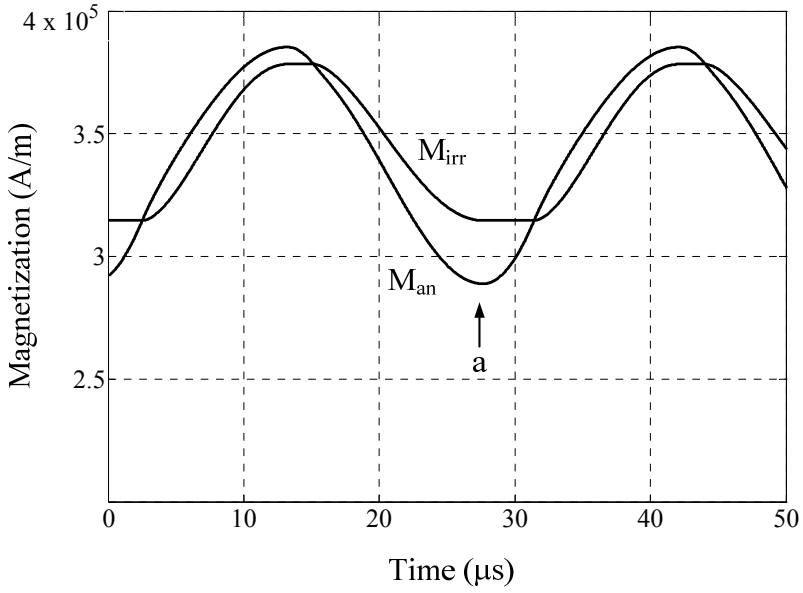

(a)

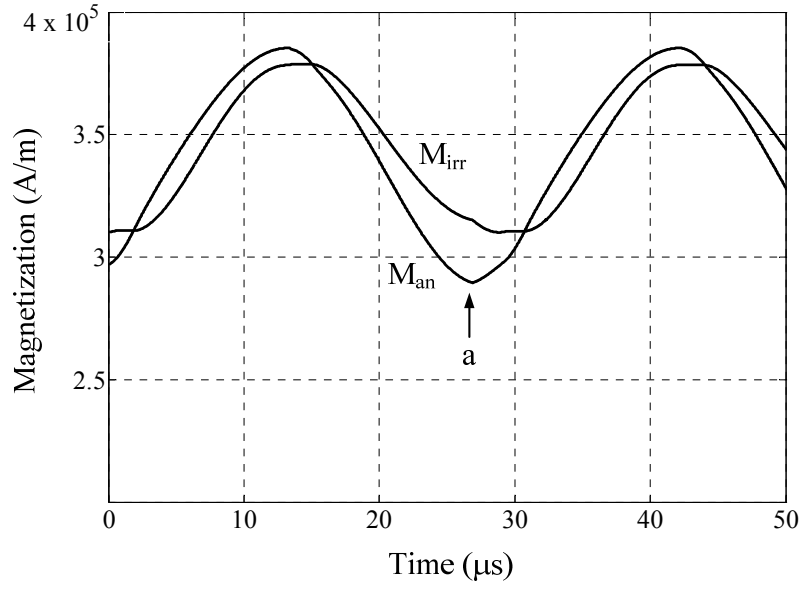

(b)

Fig. 4.13 Simulated Man and Mirr waveforms in the (a) absence, and (b) presence of a $H_{\sigma i}$ field

Within the framework of the J-A model the means by which figure-eight B-H loops are generated can be investigated, and key relationships can be determined. Simulated M_{an} and M_{irr} waveforms generated by the modified model are shown in Fig. 4.13. Fig. 4.13(a) was generated in the absence of a $H_{\sigma i}$ field, and it is evident that M_{irr} is constant for a short period of time after point a until M_{an} becomes greater than M_{irr}. A similar period for which M_{irr} is constant also occurs at the peak of the M_{irr} waveform. These periods are a consequence of setting $dM_{irr}/dB_e = 0$ in the modified model if M_{irr} is below M_{an} at the uppermost tip of a B-H loop as the B-field is reduced,

or if M_{irr} is above M_{an} at the lowest tip of a B-H loop as the B-field is increased, for reasons discussed in Section 4.5. As a result, M_{irr} is disallowed from varying as a function of the applied magnetic field for certain portions of an excitation cycle. However, in the presence of an $H_{\sigma i}$ field it is clear from Fig. 4.13(b) that M_{irr} continues to decrease during the time period immediately after point a, despite the fact that M_{irr} is greater than M_{an}. The reason why M_{irr} decreases can be explained with reference to changes induced in M_{an} by the $H_{\sigma i}$ field.

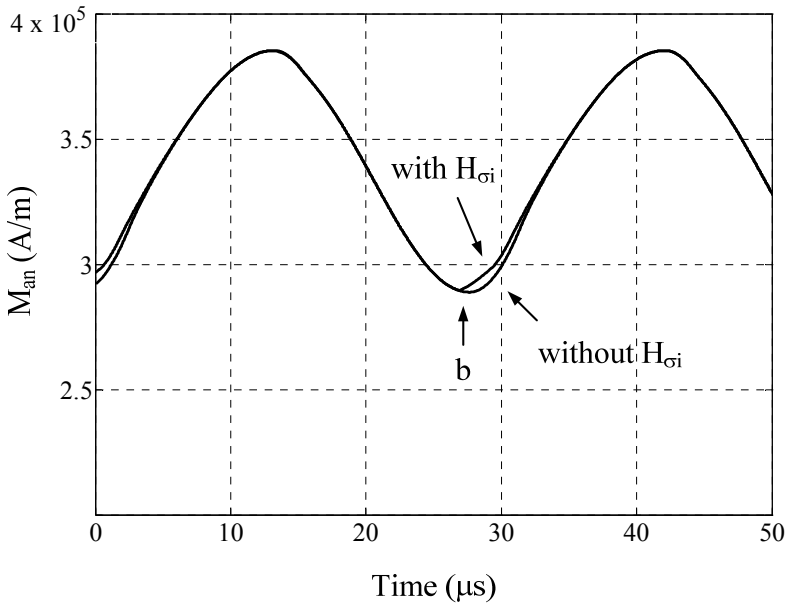

Fig. 4.14 Simulated M_{an} waveforms with , and without a $H_{\sigma i}$ field

When the $H_{\sigma i}$ field changes at a rapid rate in the manner shown in Fig. 4.11, then rapid changes are also induced in M_{an}. This is apparent in Fig. 4.14, which compares simulated M_{an} waveforms in the presence, and the absence, of a $H_{\sigma i}$ field. At point b it is apparent that the presence of the $H_{\sigma i}$ field causes dM_{an}/dt to increase. The rapid increase in dM_{an}/dt in turn generates a rapid increase in dM_{rev}/dt according to:

$$\frac{dM_{rev}}{dt} = c\left(\frac{dM_{an}}{dt} - \frac{dM_{irr}}{dt}\right), \tag{4.36}$$

which is derived from (4.4). Therefore, if the change of dM_{rev}/dt is greater than that of dM/dt, then dM_{irr}/dt must fall according to:

$$\frac{dM}{dt} = \frac{dM_{rev}}{dt} + \frac{dM_{irr}}{dt}, \tag{4.37}$$

which is derived from (4.3). The reduction in M_{irr} does not change the shape of the M waveform because M is constrained to be largely sinusoidal in nature. This is apparent through the relation [2]:

$$B = \mu_o (H + M) \tag{4.38}$$

and with the knowledge that H is much smaller than B/μ_o and M, and B is constrained to be sinusoidal, as explained previously in this section. Therefore, the decrease in M_{irr} as M_{an} is increasing manifests as a phase shift in the H-field waveform, as illustrated in Fig. 4.12, which corresponds to a transfer of energy from the core back to the magnetic excitation source.

The results presented in this section predict the generation of figure-eight shaped B-H loops. Furthermore, with knowledge of its key relationships, the reason why figure-eight B-H loops are generated can be understood from a perspective that is logical in a mathematical sense. From a physical perspective it can be understood that during part of the magnetic excitation cycle mechanical energy is transferred to magnetic energy in such a way that the magnetization process is aided, causing the energy demanded from the H-field to be reduced.

4.9 Summary

In this chapter the J-A model has been described, with an emphasis placed on the parameters a and k of the model, as well as the means by which M_{an} is derived. At a microscopic level it was proposed that under increasing dc bias conditions parameter k must correspondingly increase, as increased domain wall pinning sites are created for the reasons explained in Chapter 3. At a macroscopic level it was proposed that M_{an} is altered by the nature of the stress anisotropy generated by asymmetrical vibration waveforms, which influence the shape of B-H loops. A modified inverse J-A model was then derived with the capacity to take into account the phenomena induced under dc bias conditions, and used to simulate the increase in core losses incurred under dc bias, in addition to the figure-eight shaped B-H loop phenomenon described in Chapter 3.

The verification of the theory described in Chapter 3, as well as the model and simulated results presented in this chapter require the use of techniques that allow core losses and B-H loops under dc bias conditions to be accurately measured. Such techniques are described in Chapter 5.

4.10 References

[1] D. C. Jiles, D. L. Atherton, "Theory of Ferromagnetic Hysteresis", *J. Magn. Magn*, 61, 1986, pp. 48-60

[2] D. Jiles, 'Introduction to Magnetism and Magnetic Materials', Chanpman and Hall, London, U.K., 1998, ISBN 0 412 79860 3

[3] G. Bertotti, "Hysteresis in Magnetism", Academic Press, San Diego, 1998, ISBN: 0-12-093270-9

[4] D. C. Jiles, "Frequency Dependence of Hysteresis Curves in "Non-Conducting" Magnetic Materials", *IEEE Trans. Magn.,* vol. 29, no. 6, No. 1993, pp. 3490-3492

[5] F. Liorzou, B. Phelps, D. L. Atherton, "Macroscopic Models of Magnetization", *IEEE Trans. Magn.,* vol.36, no.2, Mar. 2000, pp.418-428

[6] M. J. Sablik, D. C. Jiles, "Coupled Magnetoelastic Theory of Magnetic and Magnetostrictive Hysteresis," *IEEE Trans. Magn.*, vol.29, no.4, Jul. 1993, pp.2113-2123

[7] D. C. Jiles, J. B. Thoelke, M. K. Devine, "Numerical Determination of Hysteresis Parameters of Magnetic properties Using the Theory of Ferromagnetic Hysteresis", *IEEE Trans. Magn*., vol. 28, no. 1, Jan. 1992, pp. 27-35

[8] D. Lederer, H. Igarashi, A. Kost, T. Honma, "On the Parameter Identification and Application of the Jiles-Atherton Hysteresis Model for Numerical Modelling of Measured Characteristics", *IEEE Trans. Magn*., vol. 35, no. 3, May 1999, pp.1211-1214

[9] D. C. Jiles, "A Self Consistent Generalised Model for the Calculation of Minor Loop Excursions in the Theory of Hysteresis", *IEEE Trans. Magn*., vol. 28, no. 5, Sept. 1992, pp.2602-2604

[10] K. Chwastek, "Modelling Offset Minor Hysteresis Loops with the Modified Jiles-Atherton Description", J. Phys. D: Phys. 42(2009), pp. 1-5

[11] K. Chwastek, J. Szczyglowski, W. Wilczynski, "Modelling Dynamic Hysteresis Loops in Steel Sheets", Compel, vol. 28, no. 3, pp.603-612

[12] M. J. Sablik, D. Stegemann, A. Krys, "Modeling Grain Size and Dislocation Density Effects on Harmonics of the Magnetic Induction", J. App. Phys, vol. 89, no. 11, 1 Jun. 2001, pp.7254-7256

[13] D. C. Jiles, “Theory of the Magnetomechanical Effect”, J. Phys. D: Appl. Phys. 28, 1995, pp.1537-1546

[14] K. C. Pitman, “The Influence of Stress on Ferromagnetic Hysteresis”, *IEEE Trans. Magn*., vol. 26, no. 5, pp.1978-1980

[15] M. G. Maylin, P. T. Squire, “Departures from the Law of Approach to the Principal Anhysteretic in a Ferromagnet”, *J. App. Phys.*, vol.73, no.6, Mar. 1993, pp.2948-2955

[16] T. L. Gilbert, "A Phenomenological Theory of Damping in Ferromagnetic Materials," *IEEE Trans. Magn.* , vol.40, no.6, Nov. 2004, pp. 3443- 3449

[17] J. P. A. Bastos, N. Sadowski, “Electromagnetic Modeling by Finite Element Methods”, New York, Marcel Dekker, ISBN: 0-8247-4269-9

Chapter 5

Core Loss Measurement Techniques

5.1 Introduction

In the preceding two chapters core loss mechanisms operative under dc bias conditions were proposed, and incorporated into a modified J-A model to allow the influence of dc bias conditions on core losses to be predicted. The experimental verification of this work requires the accurate measurement of Mn-Zn ferrite core losses under dc bias conditions, and for this purpose a number of techniques exist. These include: calorimetric techniques, field based techniques which rely on the measurement of the Poynting Vector, and circuit based techniques which rely on the accurate sensing of the winding emf and excitation current waveforms. However, all of these techniques are prone to measurement errors which, for the field and circuit based techniques in particular, are difficult to minimize [1], [2]. The existence of core loss measurement errors is especially significant in the case of low permeability ferrite cores for which losses are small in relation to the excitation VA that is required. Therefore, it is critical to closely monitor and account for sources of error in any ferrite core loss measurement set-up.

This chapter explains why the measurement of core losses under dc bias conditions is difficult, and briefly describes a variety of core loss measurement methods that can be employed, highlighting their advantages and disadvantages. Three measurement techniques are then proposed to overcome many of the disadvantages associated with other techniques.

These measurement techniques are discussed and evaluated, with particular emphasis placed on the ease, accuracy, and speed with which measurements can be made.

5.2 Core Loss Measurement

Average core losses can be measured by exciting a winding on the ferrite CUT, determining the product of the winding emf and the excitation current, and integrating the result over one cycle. However, this procedure is prone to large core loss measurement errors if the CUT is a low permeability, low loss type, and the phase shift between the winding emf, and excitation current, I_{excite}, waveforms is measured incorrectly. It has previously been shown that the relationship between the core loss and phase shift measurement errors is given by [3]:

$$E = \frac{100 \cdot [\cos(\theta + \alpha) - \cos\theta]}{\cos\theta} \qquad (5.1)$$

where,

E = percentage error in the measurement of core loss

θ = phase shift between the winding emf and I_{excite} waveforms (degrees)

α = error in the measurement of θ (degrees)

From (5.1) it is apparent that the closer is θ to 90^o, the greater is E for a given value of α. To illustrate the impact of phase shift measurement errors an example is given using the equivalent circuit of a CUT, which is shown in Fig. 5.1.

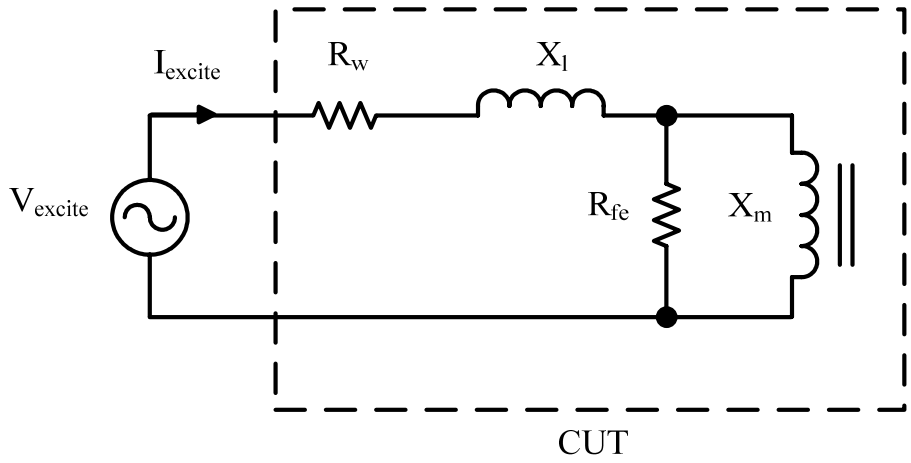

Fig. 5.1 Equivalent circuit of the CUT

Based on the manufacturer's specified properties listed in Table 5.1, Table 5.2 gives the calculated core loss resistances, R_{fe}, and magnetizing reactances, X_m, at 100 ^oC, of E20/10/5 cores in Ferroxcube 3C90, and 3F3 materials [4], which are wound with 10 turns and excited sinusoidally. Also given in Table 5.2 is the power factor, p.f., associated with Fig. 5.1, and calculated using (5.2). For the derivation of these results the calculated winding resistance, R_w, is 0.0189Ω (using 180 x 0.05mm Pack Feindrahte litz wire [5]), and the leakage reactance, X_l, is assumed to be 1% of X_m.

$$\text{p.f.} = \cos\left[\arctan\left(\frac{X_l R_{fe}^2 + X_l X_m^2 + X_m R_{fe}^2}{R_W R_{fe}^2 + R_w X_m^2 + X_m^2 R_{fe}}\right)\right] \tag{5.2}$$

Table 5.1 Ferroxcube E20/10/5 Parameters and Specified Core Losses

Material	Ungapped A_L (nH)	Effective area (mm^2)	Core loss (W) at		
			25 kHz 0.2 T 100 ^oC	100 kHz 0.1 T 100 ^oC	400 kHz 0.05T 100 ^oC
3C90	1500	31.2	≤ 0.15	≤ 0.17	-
3F3	1400	31.2	-	-	≤ 0.28

Table 5.2 Properties and Calculated Parameters of E20/10/5 and 3F3 Ungapped Cores

Frequency (kHz)	Material	B (mT)	A_L (nH)	Loss (W)	R_{FE} (Ω)	X_M (Ω)	pf
25	3C90	200	1500	0.15	320	23.6	0.073
100	3C90	100	1500	0.17	1130	94.3	0.083
400	3F3	50	1400	0.28	2745	351.9	0.126

It is apparent from Table 5.2 that the calculated p.f.s are low, and therefore that the associated θ are close to 90^o. From these results, the error in the measurement of θ, which results in a 5% error in the measurement of core loss, can be determined with the aid of (5.1); for 3C90 material this error is 0.21^o at 25 kHz and 0.24^o at 100 kHz, while for 3F3 material it is 0.36^o at

400 kHz. These errors correspond to time delays of 23.4 ns at 25 kHz, 6.59 ns at 100 kHz, and 2.53 ns at 400 kHz. It is apparent that these very small time delays require the voltage and current sensing channels to be phase/time matched to a high degree in order to make accurate core loss measurements.

From (5.1) it is intuitively obvious that the sensitivity of E to α can be reduced by decreasing θ. This can be achieved by minimizing gaps within the magnetic path of the CUT, as this decreases the excitation VA required to generate a given level of core loss [1]. However, the reductions in θ that can be achieved in this way are limited and, in addition, the method does not allow the core losses of gapped cores to be measured. To illustrate the impact of core gaps on core loss measurement errors, an example is given based on the results presented in Table 5.3. This shows the calculated R_{fe}, X_m, and p.f. of the same core types as used for the example based on Table 5.1, with the exception that the CUTs are gapped so that the A_L value is reduced to 100 nH. With the introduction of a core gap, the leakage reactance is assumed to increase to 2% of X_m.

Table 5.3 Properties and Calculated Parameters of E20/10/5, 3C90 and 3F3 Gapped Cores

Freq (kHz)	Material	B (mT)	A_L (nH)	Loss (W)	R_{fe} (Ω)	X_m (Ω)	pf
25	3C90	200	100	0.15	320	1.57	0.017
100	3C90	100	100	0.17	1130	6.28	0.0084
400	3F3	50	100	0.28	2745	25.1	0.0097

From Table 5.3 it is apparent that the p.f. is dramatically reduced by the introduction of a core gap. Consequently, the maximum error allowed in the phase shift/time delay measurement in order to achieve accuracy in the core loss measurement to within a 5% margin is only 0.0476^o/5.3 ns at 25 kHz and 0.0241^o/669 ps at 100 kHz for the 3C90 material, and 0.0278^o/193 ps at 400 kHz for 3F3 material. In practical terms, the phase shift/time delay matching of the voltage and current sensing channels to a degree equal to or better than that given by the above figures is not a tractable engineering task.

Core losses can also be measured through the determination of the B-H loop of the CUT [1] or through the use of a network analyzer [3]. However, because both these techniques rely on the accurate sensing of the winding emf, the excitation current, and the phase shift between these two waveforms, they suffer the same principle disadvantage as the preceding technique.

A technique that has been proposed to decrease the sensitivity of E to α involves the placement of capacitors across the excitation winding of the CUT in order to reduce the value of θ [6]. However, in this case the magnitude of the potential error is controlled rather than eliminated. A similar technique involves sizing a capacitor to resonate with the excited winding [1] to tune out the winding inductance, leaving an equivalent loss resistance. Power loss can then be measured as the product of the input current and voltage applied to the resonant circuit. In addition to reducing θ, and therefore sensitivity of E to α, this also has the advantage of lowering the VA required to excite the CUT. However, this technique results in distorted measurements at high levels of excitation, for which the CUT traverses a non-linear region of the B-H loop. Other disadvantages include: the requirement for a large number of low loss capacitors in order to test over a wide frequency range, the need for large capacitors for tests at low frequencies, and the inclusion of winding and capacitor losses in the total loss figure that is measured. Furthermore, the technique is laborious as it requires the resonating capacitor to be changed for every new test frequency.

Core losses can also be measured using calorimetric techniques [7]-[9], for which a CUT is placed in a well insulated measurement chamber, usually containing a dielectric fluid that is stirred to enhance thermal uniformity. Magnetic losses are then determined by measuring the temperature rise of the thermal mass within the chamber, which includes the excited and heat generating CUT. This technique, which does not require the difficult measurement of θ, is suitable for the determination of core losses with any shape of excitation waveform, and does not require the use of instrumentation that has high accuracy at high frequencies. However, a significant disadvantage is the long duration of time that is required to allow the CUT to reach a steady state operating temperature. Other disadvantages are: the inclusion of winding losses in the measurement, the need to limit the temperature rise in order to avoid changes in temperature causing changes in core losses, and the high degree of experimental virtuosity

required. A technique, which overcomes these disadvantages, and many of the others explained in this section, is proposed in Section 5.3.

5.3 The Mutual Inductance Neutralization Technique

As explained in Section 5.2, the high susceptibility to errors in the measurement of ferrite core losses when using circuit based techniques occurs because the phase shift between the I_{excite} and winding emf waveforms is very close to 90^o. The measurement technique presented in this section overcomes this difficulty by reducing the phase angle between the I_{excite} and winding emf waveforms using an air cored mutual inductor.

5.3.1 Power Factor Improvement using Mutual Inductance Neutralization

The improvement to the p.f. between the winding emf, V_{sense}, and the I_{excite} waveforms under ac excitation conditions and in the absence of a dc bias is achieved using the "mutual inductance neutralization" technique illustrated in Fig. 5.2(a). The technique is implemented using an adjustable air cored mutual inductor with windings of a relative phasing such that when V_{sense} in Fig. 5.2(a) is measured, the reactive voltage drop across the air cored mutual inductance, M_{air}, cancels that across the CUT, M_{cut}. As apparent from the equivalent circuit shown in Fig. 5.2(b), this leaves only an in-phase resistive core loss component, R_{fe}, in the V_{sense} voltage, which therefore means V_{sense} is in-phase with I_{excite}. Through integration of the product of the V_{sense} and I_{excite} waveforms over one cycle, the CUT core losses can be accurately determined. From Fig. 5.2(b) it is also apparent that the self inductances and winding resistances of the CUT, L_a, L_b, R_a, R_b, as well as those of the mutual inductor, L_1, L_2, R_1, and R_2 have no effect on the phase relationship between V_{sense} and I_{excite} if the instrument used to measure V_{sense} has a sufficiently high impedance. Based on Fig. 5.2(b) the p.f. of the measurement circuit can be calculated using (5.3), and Fig. 5.2(c) can be obtained.

$$\text{p.f.} = \cos\left[\arctan\left[\left(\frac{\omega M_{cut} R_{fe}^2}{R_{fe}^2 + \omega^2 M_{cut}^2} - \omega M_{air}\right) \Big/ \left(\frac{\omega^2 M_{cut}^2 R_{fe}}{R_{fe}^2 + \omega^2 M_{cut}^2}\right)\right]\right] \tag{5.3}$$

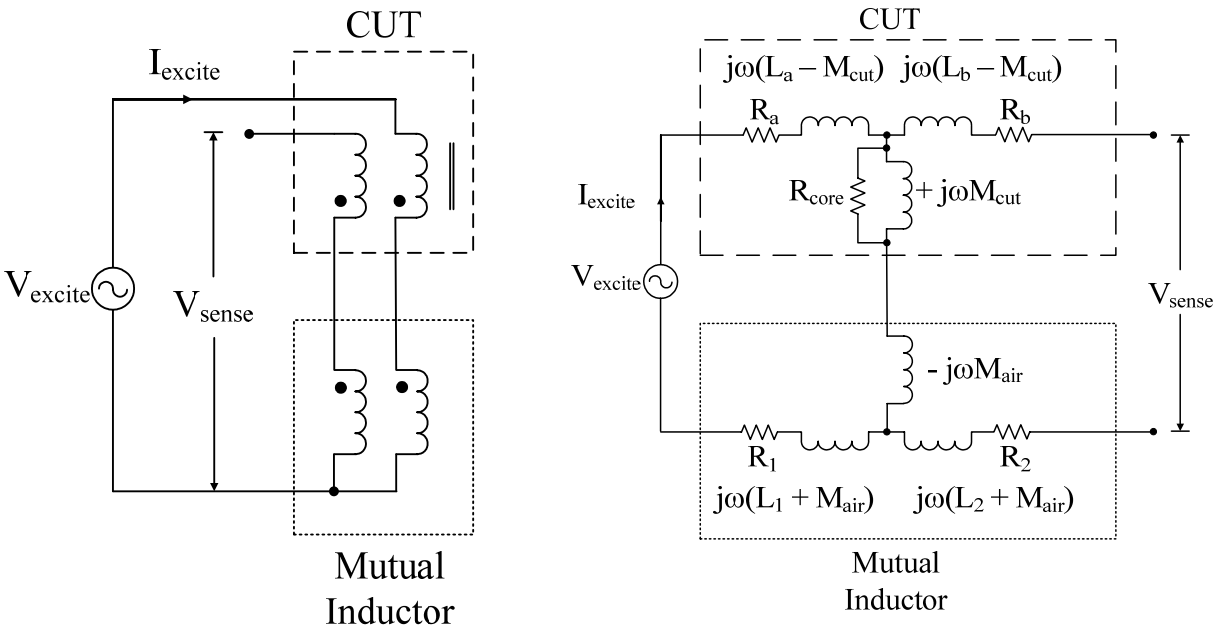

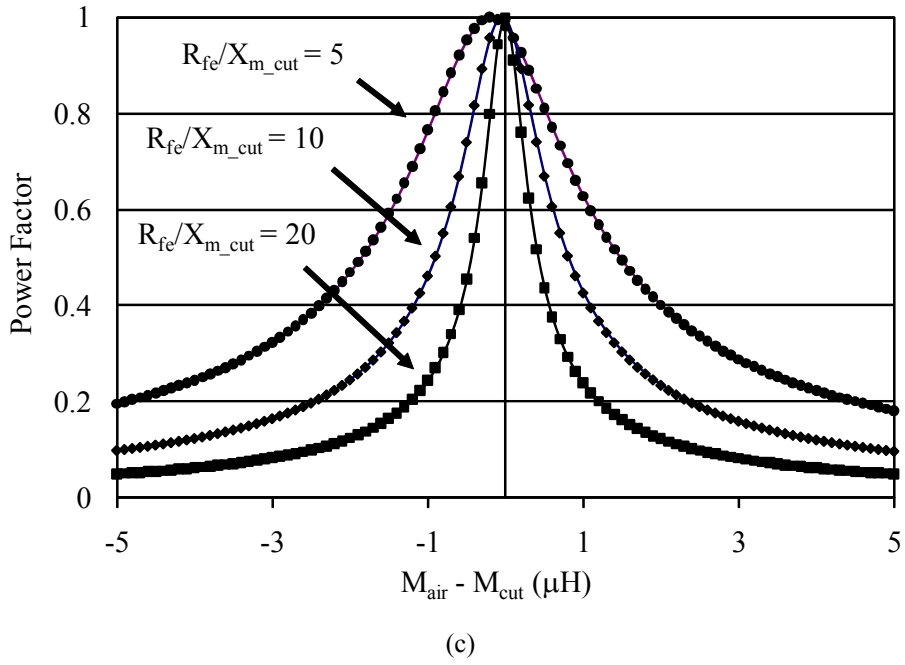

Fig. 5.2 (a) The mutual inductance neutralization circuit, (b) its equivalent circuit, and (c) variation of power factor with the difference between air and CUT mutual inductances for different R_c to X_{m_cut} ratios.

For Fig. 5.2(c) the sinusoidal excitation frequency is 100 kHz, M_{cut} is 5 μH, M_{air} is varied from 0 to 10 μH, and three different values of R_{fe} are used to give three ratios of R_{fe}/X_{m_cut}, where X_{m_cut} is the mutual reactance of the CUT. It is apparent that the smaller is $|M_{air} - M_{cut}|$

then the better is the p.f. between V_{sense} and I_{excite}. It is also apparent that the greater is the ratio of R_{fe}/M_{cut}, the more significant is the improvement to the p.f. in the uncompensated case, for which $|M_{air} - M_{cut}| = 5\ \mu H$, compared to that in the fully compensated case, for which the p.f. is equal to one. This shows that the potential benefit of the mutual inductance neutralization technique is greatest when low permeability, low loss cores are tested, for which the excitation VA drawn is high relative to the core loss.

The improvement to the p.f. that can be achieved is apparent in the measured waveforms shown in Fig. 5.3, for which the CUT is a MMG 25x15x10 mm ferrite toroidal in F49 material. In Fig. 5.3(a) the V_{sense} and I_{excite} waveforms measured using an uncompensated circuit are shown, and it is evident that the p.f. is poor with a phase shift close to 90^o. For the same CUT the V_{sense} and I_{excite} waveforms, measured using the mutual inductance neutralization circuit given in Fig. 5.2(a), are shown in Fig. 5.3(b). It is clearly evident that the V_{sense} and I_{excite} waveforms are close in phase, and that the magnitude of the V_{sense} waveform is dramatically reduced, indicating that the reactive component of V_{sense} has been largely cancelled. It is also evident that a strong third harmonic component remains, due to the non-linearity of ferrite. The harmonics have no impact on the core losses in this case. This is because I_{excite} is substantially sinusoidal in nature, as evident from Fig. 5.3(b), and therefore the product of I_{excite} with the harmonics of V_{sense} is negligible when averaged over one cycle.

Mutual inductance standards have previously been used in high accuracy bridge measurement circuits, and the impurity of these devices has been investigated. The impurity causes the phase angle between the open circuit secondary winding emf, and the primary excitation current waveforms of the mutual inductor to deviate from quadrature. Impurity is relevant to the air cored mutual inductor used in the mutual inductance neutralization technique proposed in this Thesis, because such a deviation results in a significant core loss measurement error if it is not minimized. The causes of impurity have been identified [10]-[14] as the self and inter-winding capacities of mutual inductor windings, in conjunction with winding resistances and/or dielectric losses, as well as the winding eddy current losses. Therefore, the mutual inductor was constructed so as to minimize, in particular, the inter-winding capacitance. This minimization was achieved by placing the primary and secondary windings end to end on a single layer. To further reduce inter-winding capacitance, as well as the associated dielectric

losses, the ends of the windings that were adjacent to each other were both brought to the circuit ground [15]. To minimize primary winding eddy current losses, the primary was wound using Litz wire. The secondary was wound using 0.25 mm diameter magnet wire, and the primary to secondary turns ratio was 2:21. The relatively low number of primary winding turns minimized the voltage drop across the primary winding impedance, so allowing most of the supply voltage to be used to excite the CUT. The high number of secondary winding turns was necessary in order for a sufficiently large reactive voltage drop across M_{air} to be developed to cancel that across M_{cut} and improve the p.f. The primary and secondary windings were wound atop separate pieces of mylar, which were slid along a glass former to adjust the gap between the windings to allow the mutual inductance to be varied to the optimal position. Such a variation was necessary in order to allow the measurement technique to be used with CUTs of different permeability's and under different temperature and excitation conditions.

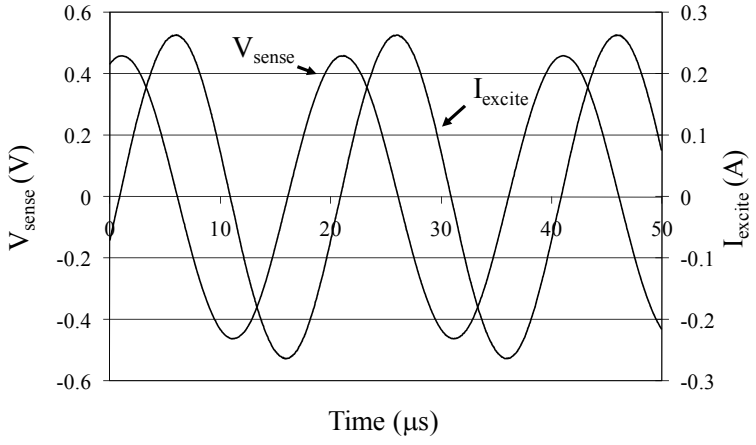

(a)

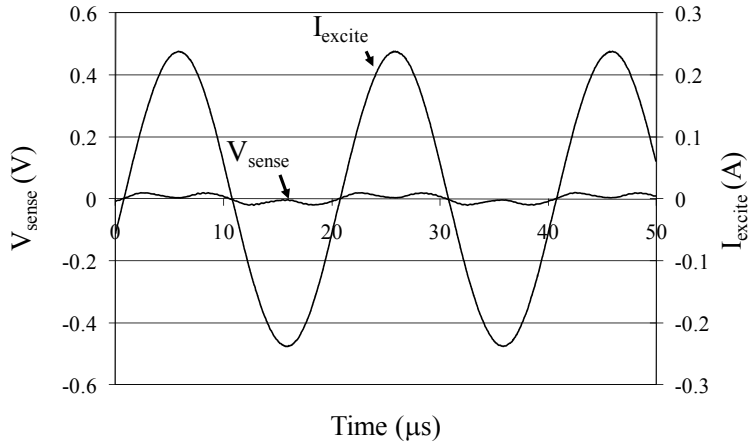

(b)

Fig. 5.3 (a) excitation waveforms in an uncompensated circuit, (b) the excitation waveforms in a compensated circuit

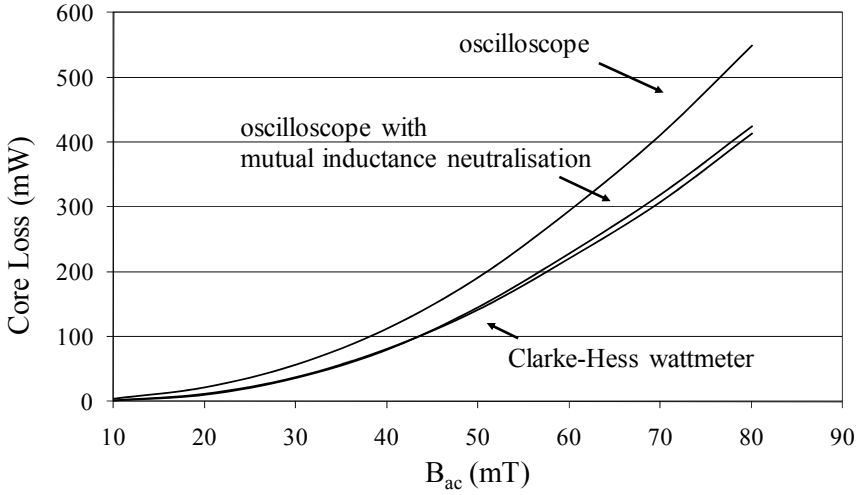

Fig. 5.4 Comparison of core loss measurements with no dc bias

The benefit of using the mutual inductor is shown in the results presented in Fig. 5.4, which gives the measured core losses as a function of the ac flux density, B_{ac}, of a MMG 25x15x10 mm toroidal in F49 material that is cut into two halves, with no spacer between the halves. The core loss measurements were made in an ambient temperature of 24^{o}C, at a frequency of 50 kHz, and in the absence of a dc bias. Three sets of measurements were made: firstly, using a Clarke and Hess 2335 wattmeter [16], secondly, using an Agilent DSO6034 oscilloscope [17] as a wattmeter and thirdly, using the same oscilloscope and the mutual inductance neutralization technique. The readings taken using the wattmeter were expected to be the most accurate, as this instrument is optimized for accurate high frequency power measurement at any p.f. through the high degree of phase/time matching between the current and voltage sensing channels. The specifications of the wattmeter are listed in Appendix C. By comparison with the wattmeter, the core loss data measured using the oscilloscope was strongly subject to errors resulting from poor phase/time matching between the current and voltage sensing channels. This poor matching was due primarily to the parasitic impedances introduced into the current sensing channel by the 0.22 Ohm thick film resistive current shunt that was used, and the 1m long probe leads connecting it to the oscilloscope. It is apparent that the core losses measured using the wattmeter, were significantly different from those measured using the oscilloscope. It is also apparent that, through the use of the mutual inductance neutralization technique, measurements made using the oscilloscope were dramatically improved in accuracy.

5.3.2 Core Loss measurements under dc Bias Conditions using Mutual Inductance Neutralization

To measure core losses in the presence of a dc bias the measurement circuit shown in Fig. 5.2(a) was modified to that shown in Fig. 5.5. In this circuit V_{sense} and I_{excite} were measured and multiplied together to calculate the total losses of two gapped ferrite CUTs at the same time. Two CUTs were used in order to allow dc bias windings to be placed on each with polarities such that the dc bias windings were effectively decoupled from the ac windings in the circuit. Decoupling is necessary in order for the dc bias to be constant and free from ac ripple as explained in Chapter 2. The primary windings of the CUTs were connected in parallel to ensure that each CUT was run at the same ac flux density, B_{ac}. The sense windings of the CUTs were connected in series rather than parallel to avoid the generation of circulating currents in these windings, which would generate winding losses that would be added to the core loss measurement and thus constitute an error.

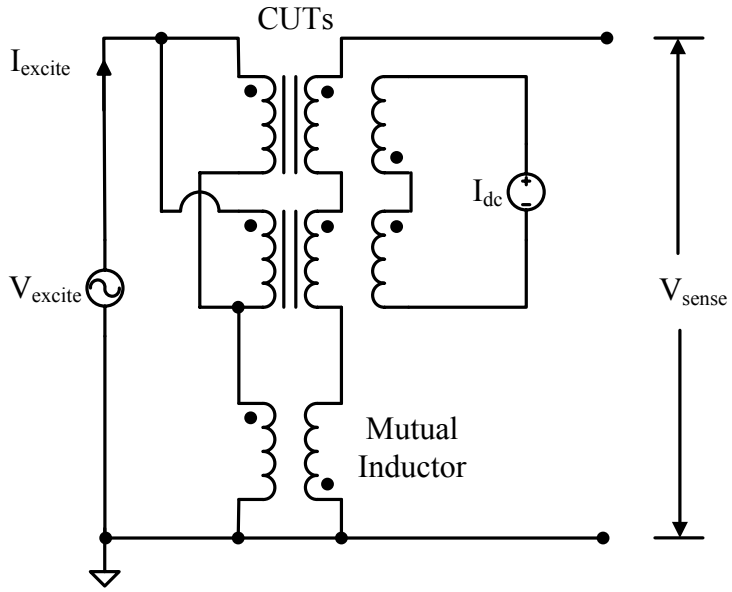

Fig. 5.5 The winding connection diagram of the core loss test circuit for dc bias conditions

Fig. 5.6 shows core loss results measured as a function of B_{ac}, and the dc magnetic field strength, H_{dc}, using the circuit given in Fig. 5.5. The measurements were made at 100 kHz in an ambient temperature of 24^{o}C, and the CUTs were gapped MMG 25x15x10 mm toroidals in F49 material. The total core gap used was 0.152 mm, which was found to be sufficient to reduce the tolerance on the relative permeability between the two gapped CUTs to within 3%.

Such a gap is necessary to ensure the CUTs operate at same dc flux density, B_{dc}, within a tolerance, for a given level of H_{dc}. A non-linear increase in the core loss characteristic with H_{dc} is clearly apparent.

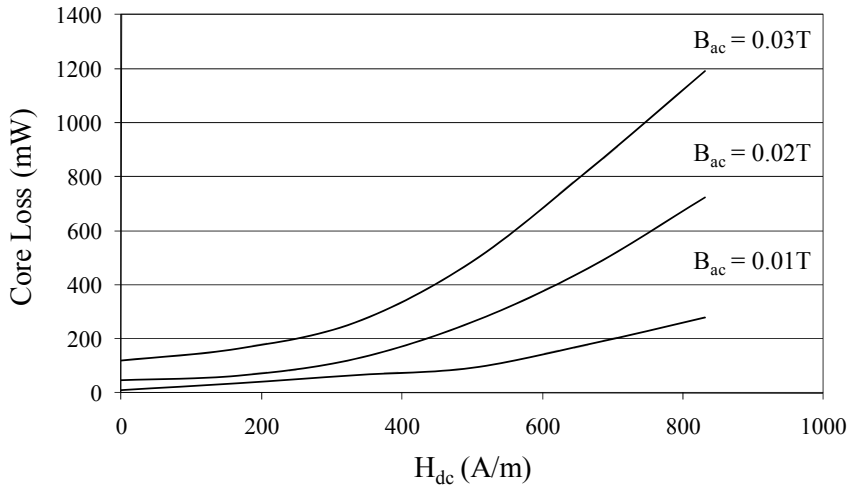

Fig. 5.6 Core loss measurements made under dc bias conditions

5.3.3 Evaluation of the Mutual Inductance Neutralization Technique

The mutual inductance cancellation of the reactive part of the voltage drop across V_{sense} can be used to greatly enhance the accuracy of core loss measurements. However, the technique suffers from disadvantages, including the need to gap each of the CUTs to ensure their relative permeability's are equal. Such a gap reduces the impedance of the core loss measurement circuit thereby increasing the VA demanded from the magnetic excitation supply. A further disadvantage is the need to adjust the mutual inductance between core loss measurements, which slows down the data gathering process. For these reasons the principle core loss measurements made under dc bias conditions, which are presented in Chapter 6, were not made using the mutual inductance neutralization technique.

5.4 The Zero-Voltage-Switching Technique

A core loss measurement technique, which overcomes many of the disadvantages of those previously described, is reported in this section. In this approach the switches of an extremely efficient ZVS half-bridge were used to circulate excitation energy through the CUT. A simplified schematic of the circuit is shown in Fig. 5.7. The dc input power to the circuit was

measured to directly determine the core loss, thereby eliminating the dependency of core loss measurement errors on the accurate determination of the phase shift between an ac voltage and current. The dc input power very closely approximated the core losses of the circuit, because circuit losses were minimized. Turn-off losses of the ZVS half-bridge were minimized by using core magnetization energy to commutate current from the FET just turning off, to that of the other half-bridge FET to be turned on, charging the junction and parasitic capacitances in a non-dissipative manner. Turn-on losses were eliminated by turning the next FET on 10-20 ns after a monitor had detected that V_{DS} had fallen below 1V. Oversized FETs were used to minimize conduction losses, and the FET drive and the control power were supplied from a separate source and did not affect the loss measurement. Furthermore, the technique allowed core loss measurement data to be quickly and easily obtained. The disadvantages of the technique due to practical switching considerations included upper limits on the input voltage, current, and the switching frequency of the test circuit to 90 V, 8 A and 2 MHz respectively. In addition, practical considerations required the inductance of the CUT to be within maximum and minimum values according to the input voltage and frequency. The minimum inductance was determined by the peak current ratings of the FETs, while the maximum value was limited by the zero voltage switching requirements of the circuit. Additional disadvantages included the fact that only square wave voltage waveforms could be used to excite the CUT, and the need to separate the residual circuit losses from the core losses. The residual circuit losses were due primarily to FET conduction losses, and secondarily to the CUT winding resistance, and the capacitor ESR. These losses were calculated by sensing the excitation current in the circuit to determine the residual circuit losses, then subtracting these losses from the measured dc power to determine the core loss.

The B_{ac} of the CUT could be simply calculated using the dc input voltage, excitation frequency, excitation winding turns, and core area. However, at high frequencies both lead inductance, and increasingly finite voltage rise and fall times began to result in significant calculation errors. To overcome this issue the excitation voltage was sensed directly through a separate 'excitation sense' winding on the CUT, and the average voltage was also used to maintain the correct flux density. An appropriately terminated 50 Ohm coax cable was used to couple the excitation sense signal to the control circuitry to prevent unwanted transmission line reflections.

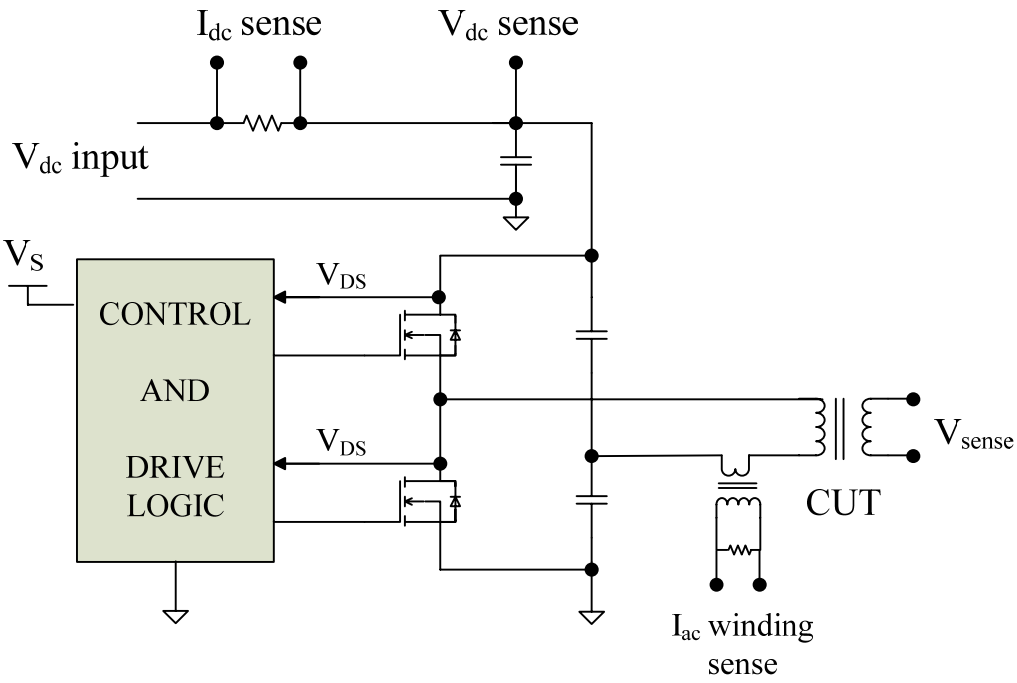

Fig. 5.7 Simplified schematic of the ZVS half bridge circuit

Using this circuit the measured results showing the variation of the core losses with temperature, and frequency in the absence of a dc bias are presented in Chapter 1 for MMG Mn-Zn ferrite cores in F49 material.

The core loss measurement technique shown in Fig. 5.7 can be adapted to measure core losses in the presence of a dc bias with the placement of a dc current carrying winding on the CUT. H_{dc} can be easily calculated through the measurement of this current, allowing core losses to be found as a function of H_{dc}. Core losses can also be measured as a function of B_{dc} within the CUT. However, the determination of B_{dc} is not a trivial matter as it depends not only on H_{dc}, but also the core permeability, μ_r, and B_{rem}, which can both vary considerably between cores of the same geometry and material, as well as with temperature. These variations, as well as the variation of μ_r with magnetic field strength, are significantly reduced by the placement of an air-gap in the flux path of the core, thus allowing B_{dc} to be calculated with greater precision. However, as shown in Section 5.2, core gaps significantly affect the accuracy of those core loss measurement techniques that multiply voltage and current waveforms together, and which are displaced by phase shifts of close to 90^o. Furthermore, the presence of a core gap is also disadvantageous to techniques requiring the subtraction of test

circuit losses from the total measured losses to determine the core loss. This is because core gaps introduce additional losses into the test circuit which, in some cases, are difficult to calculate, such as the higher winding eddy current losses induced by fringing flux from the magnetic field around the air gap. Other difficulties introduced by a core gap include: the existence of a fringing field around the gap which causes the actual B_{dc} to be greater than that calculated by theory, and the non-uniform distribution of flux in the CUT. The latter effect influences the measurement of core losses in two ways. Firstly, it limits the locations on a CUT where an ac sense winding can be placed if core losses are measured by sensing the winding emf; ideally such a winding should be placed on a portion of the CUT that is distant from the core gap(s) to accurately sense the flux in the core. Secondly, the non-uniform distribution of flux around an air gap means that those parts of the CUT in which flux has a greater concentration will experience higher, localized core losses, thereby distorting the total core loss measurement. Therefore, to keep the distribution of flux as uniform as possible, it is preferable to implement the total core gap using a number of smaller gaps to minimize fringing effects. By the placement of ac excitation, and dc bias windings over the core gaps, the fringing field can be minimized further.

As described in Chapter 2, the use of a dc bias winding can require the placement of a dc choke in the series with the winding to attenuate ac currents which are reflected from the ac excitation winding into the dc bias winding. For the measurement circuit presented in this section this requirement is overcome by using a technique similar to that described in Section 5.3, which implements the dc bias in a way that decouples the bias winding from all the other windings on the CUT. Using this technique two CUTs were used, with ac excitation windings wound on each. The CUTs were stacked, with cooling space in-between, and the ac excitation windings on each were connected out of phase with each other, and driven by the ZVS half-bridge to provide excitation. Sense windings, placed on each of the two CUTs, were also connected out of phase, and used to ensure that the correct B_{ac} was maintained. The dc bias winding was then wound over both CUTs together, and the losses were measured as the sum of the losses in the two cores. A diagram illustrating the connection of the windings is given in Fig. 5.8.

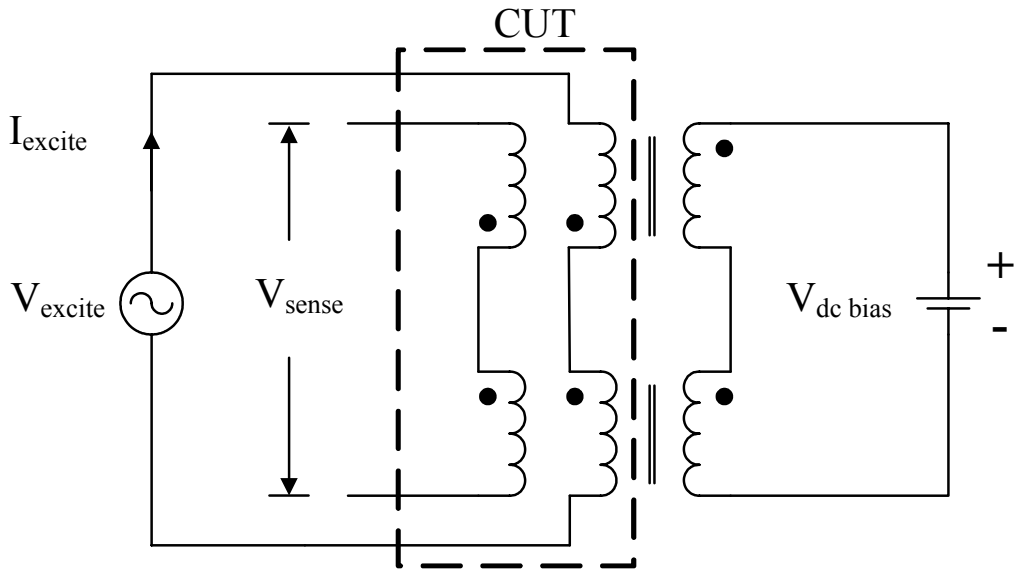

Fig. 5.8 Winding connection diagram of the core loss test circuit

While the circuit described in this section overcomes the disadvantage of the circuit presented in Section 5.3, in that it allows core loss measurements to be taken more quickly, it has a number of disadvantages, as noted in this section. The primary disadvantage is the measurement of residual circuit losses at the same time as core losses are measured, which must be precisely estimated to allow core losses to be accurately determined. Therefore a new core loss measurement technique is proposed in Section 5.5 to overcome this issue.

5.5 A Fast, High Accuracy Core Loss Measurement Technique

The technique presented in this section is that used to gather the core loss measurement results under dc bias conditions that are shown in Chapter 6. The experimental set-up consists of a drive circuit, which provides ac excitation to a CUT under dc bias, a high accuracy wattmeter, and a laser vibrometer measurement system.

5.5.1 The Drive Circuit and the Wattmeter

The drive circuit used to apply dc biased magnetic excitation to the CUT is shown in Fig. 5.9. This circuit is based around a weighted summing amplifier, OA1, implemented using an Apex PA19, 40 V, 4 A, 900 V/μs slew rate, high power op-amp [18], which is used to sum and amplify low power dc and ac signals together. Initially only the dc signal component is

applied to the inverting input terminal of OA1, and used to establish a dc current in the primary winding and, therefore, a dc magnetic field. The dc current in the circuit is controlled according to the reference level I_{ref} and the integrator implemented using OA2, which removes the ac current component from the control loop. After the dc magnetic field is setup a sinusoidal ac signal is then supplied to the inverting input terminal of OA1 and, as a result, sinusoidal ac magnetic excitation under dc bias conditions is applied. To ensure the level of the ac excitation is correct, the winding emf is closely monitored using the V_{sense} winding, and adjusted appropriately. The core losses are then measured using a Clarke and Hess model 2335 high frequency sampling wattmeter. This wattmeter is used specifically for its accuracy at high frequencies and very low p.f. levels, as described in Section 5.3. For core loss measurements made at elevated temperatures the CUT is placed within a Contherm 7050 Designer Series incubator with tight control of its internal temperature [19]. The temperature of the CUT is independently monitored using a type K thermocouple probe, which is attached to the surface of the CUT. To minimize the voltage dropped across the primary winding of the CUT, and therefore the level of excitation VA required, the primary winding is wound with 175 strand, 0.08 mm litz wire, and the winding lead-outs are made as short as possible.

The core loss test circuit shown in Fig. 5.9 is implemented in an aluminium enclosure to minimize noise pick-up in the circuit, and therefore avoid circuit instability. The power op-amp is mounted on a heatsink, which in turn is mounted on the outside of the aluminium enclosure.

All core loss measurements in the absence of a dc bias are made with a 2200 μF capacitor in series with the output of OA1, in order to block any dc current component. The magnitude of the dc bias is monitored through the measurement of the dc component of the voltage drop across R_{sense} in Fig. 5.9. Therefore, to ensure an accurate dc bias is set-up, R_{sense} is implemented using a low tolerance, high accuracy resistor. For the results presented in this Thesis two resistor types are primarily used to implement R_{sense}: a 0.47 Ohm (model HF003) resistor with a manufacturers specified phase shift of less than 0.0001^{o}/kHz [20], and a 1 Ohm resistor implemented by paralleling twenty, 20 Ohm low tolerance resistors together. For the 1 Ohm resistor a higher value was chosen in order to minimize the ratio of resistance to reactance, and a number of resistors were paralleled in order to minimize the parasitic inductance. Two different resistors are used to implement R_{sense} to allow each to act as a

check on the other. In addition to the role R_{sense} plays in setting the dc bias, the voltage drop across it is also measured using an oscilloscope and is used to determine the B-H loops of CUTs. The determination of the B-H loops also allows the wattmeter measurements to be checked.

The physical core loss test circuit is shown in Fig. 5.10, as setup for core loss measurements made at room temperature. This picture includes the high accuracy, high frequency wattmeter previously described in Section 5.3, the CUT mounted on a jig with a peg through its centre, and an EMI sniffer probe (model E101) [21] fitted to the back of the CUT. The sniffer probe touches the surface of the CUT, and is used to sense the stray magnetic field radiating from the core. The lead-outs from the V_{sense} winding are tightly twisted together before being brought to the wattmeter in order to avoid any noise pick-up in the V_{sense} signal from stray magnetic fields.

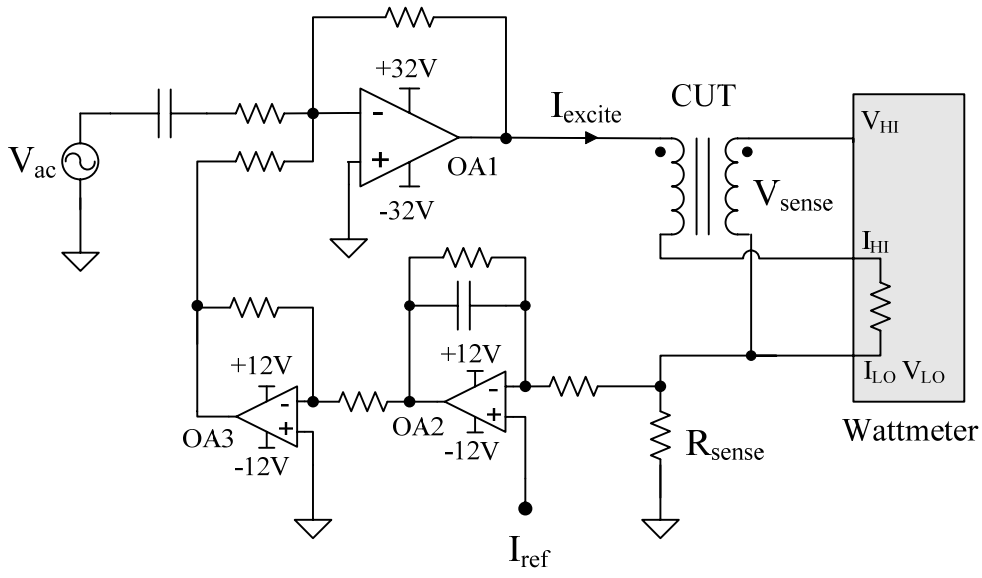

Fig. 5.9 The core loss test circuit schematic

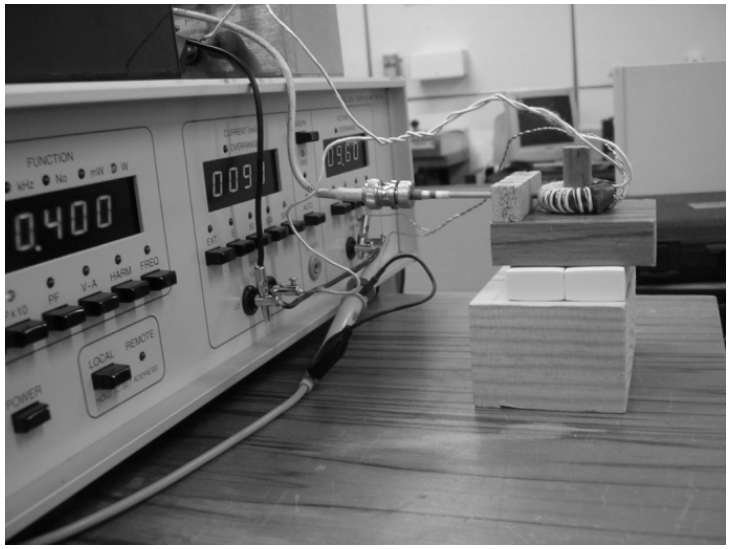

Fig. 5.10 The core loss test circuit

All core loss measurements presented in Chapter 6 are made under sinusoidal magnetic excitation conditions. This is due to the bandwidth limitations of the laser vibrometer system, which are described below, and also to ensure that the core loss measurements have the greatest accuracy. This accuracy is achieved because the sinusoidal voltage applied to the CUT under dc bias conditions means that V_{sense} is also sinusoidal. Consequently, when this voltage is multiplied with I_{excite}, the harmonics in I_{excite} cannot play a part in the core loss measurement and, therefore, cannot contribute to a high frequency measurement error in the core losses.

5.5.2 The Laser Vibrometer

At the same time as core losses are measured under dc bias conditions, the vibration of the CUT is also measured using a laser vibrometer to monitor the level of magnetomechanical interactions taking place. The laser vibrometer system consists primarily of a scanning head (model OFV 056), junction box (model PSV-Z-040-U) and a vibrometer controller (model OFV-30015) [22]. Inside the scanning head is an interferometer, which is positioned to measure the vibration induced by magnetostriction at a point on the CUT by means of a laser beam. The light from the laser beam is reflected back from the vibrating CUT to the scanning head to interfere with a reference beam. A photo detector is used to record the interference, and a resulting signal is processed in the vibrometer controller by a decoder. The decoder then produces a voltage proportional to the vibration parallel to the laser beam, with the

proportionality being dependent on a scaling factor pre-settable by the user. Lower scaling factors have the advantage of producing larger signals, which are less susceptible to noise distortion, but have the disadvantage of a low bandwidth of only 50 kHz. Therefore, in making vibrometer measurements there is a tradeoff between bandwidth and signal amplitude. For the tests undertaken for this Thesis, high levels of harmonic content could be observed in certain vibration waveforms. Consequently, a scaling factor of 10 mm/s/V was chosen; the smallest allowable while maintaining the maximum bandwidth of 200 kHz of the system.

(a)

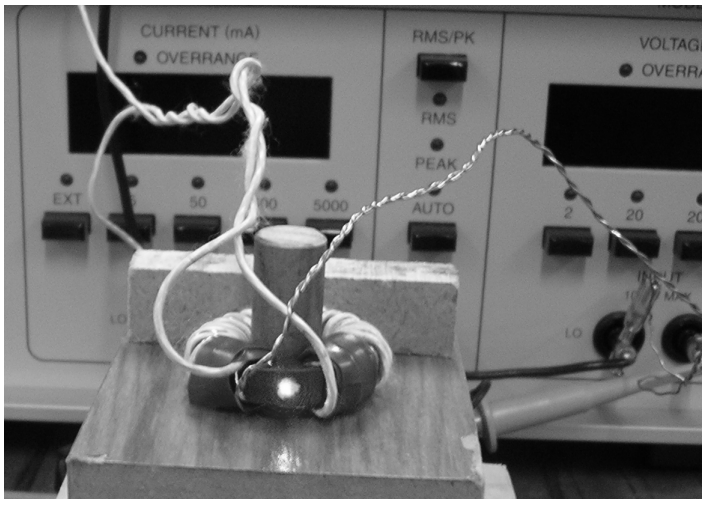

(b)

Fig. 5.11 (a) Computer screen view available to laser vibrometer user, (b) laser beam from vibrometer incident on CUT surface.

The output signal of the vibrometer controller, representing the vibration, is fed directly into an Agilent model DSO6034 oscilloscope [17], where it is heavily averaged to minimize any distortion produced by noise. In Fig. 5.11(a) the computer screen view available to the vibrometer user is shown; it includes the position controls used to focus and locate the laser beam, a signal strength indicator, and a camera shot of a ferrite CUT as the laser beam impacts upon it. The camera is located in the scanning head. A photograph of a ferrite CUT is shown in Fig. 5.11(b), which clearly shows that the beam from the laser vibrometer is incident directly on the CUT surface. The MMG F49 material ferrite CUTs, which are tested, are uncoated. However, small white dots are painted on the surface of each CUT at which the laser beam is aimed to ensure that measurements are made at the same locations for each set of tests, and also because the white dots appear to maximize the amount of light reflected back from the CUT to the laser vibrometer.

For the measurements presented in this Thesis the output of the laser vibrometer is not measured at exactly the same time as the I_{excite} and V_{sense} waveforms, as a small ground loop exists when the vibrometer output cable, and the EMI sniffer, I_{excite} and V_{sense} probes are all connected to an oscilloscope at the same time. Therefore, for measurements made at each level of dc bias, the EMI sniffer, I_{excite}, and V_{sense} waveforms are all recorded, before the vibrometer output cable is connected to the oscilloscope for the vibration measurement.

5.5.3 The Establishment of a known dc Bias

The establishment of a known dc bias in terms of H_{dc} is a trivial matter if an accurate, low tolerance resistor is used to measure the dc current applied to a CUT. However, the determination of the dc bias in terms of B_{dc} is problematic, as it includes components due to B_{rem}, in addition to the applied dc magnetic field, which are both difficult to measure. This can be overcome by gapping the CUT, which reduces the level of B_{rem}, as well as the variations of μ_r with temperature and the applied magnetic field, allowing B_{dc} to be calculated. However, gapping a CUT requires higher levels of VA to be drawn from the magnetic excitation supply and worsens the p.f. of the circuit. A technique for determining a known level of B_{dc} within a CUT, without the need for a core gap, is described below.

To set up a known B_{dc} within a CUT it is necessary to know its initial magnetization curve and, therefore, the H_{dc} that is required. To determine the initial magnetization curve, an un-gapped CUT is firstly demagnetized by exciting it deeply into saturation at a frequency of 10 kHz, before gradually reducing the excitation to a very low level. The low demagnetization frequency of 10 kHz is chosen for convenience, as it minimizes core self heating, and is used for all demagnetizations carried out for the results presented in this Thesis. After demagnetization the initial magnetization curve is measured through sensing the excitation response to the application of a step voltage waveform to the primary winding on the CUT. The flux response is sensed using an emf sense winding, V_{sense}, as shown in Fig. 5.12(a), and I_{excite} is sensed through a non-inductive 0.22 Ohm current shunt. A high number of primary turns are used in order to minimize the I_{excite} needed to achieve a given level of flux density; relatively fewer turns are used for the V_{sense} winding to allow the primary winding to fit on the CUT in a large wire gauge to minimize the primary winding voltage drop. The high number of primary turns also slows the rate of rise of the I_{excite} waveform and, thus, the rate of change in the magnetization of the CUT. This limits the core loss component inherent in the measured initial magnetization curve. The measured V_{sense} and I_{excite} current waveforms of an ungapped 25x15x10 mm Mn-Zn ferrite toroidal CUT in MMG F49 material are shown in Fig 5.12 (b). For these results eighteen turns are fitted for the primary winding, and five for the V_{sense} winding. The flux in the CUT is calculated through integrating the V_{sense} waveform, and I_{excite}, the number of primary number of turns and the average magnetic path length are used to calculate H. It is apparent that the V_{sense} waveform in Fig. 5.12 (b) is substantially constant until the CUT enters into saturation, when I_{excite} begins to rise sharply. Therefore, until saturation is reached the flux density can be accurately related to I_{excite} without the need to ensure very close phase/time matching between the I_{excite} and V_{sense} sensing channels. From the measured V_{sense} and I_{excite} waveforms, initial magnetization curves can be determined. Two initial magnetization curves of the same CUT, and measured at different temperatures, are shown in Fig. 5.12 (c). It is apparent that as the temperature is increased, both the large signal permeability, and the saturation flux density level are decreased. Also apparent is the high level of flux density able to be reached for the MMG Mn-Zn ferrite F49 material that is tested.

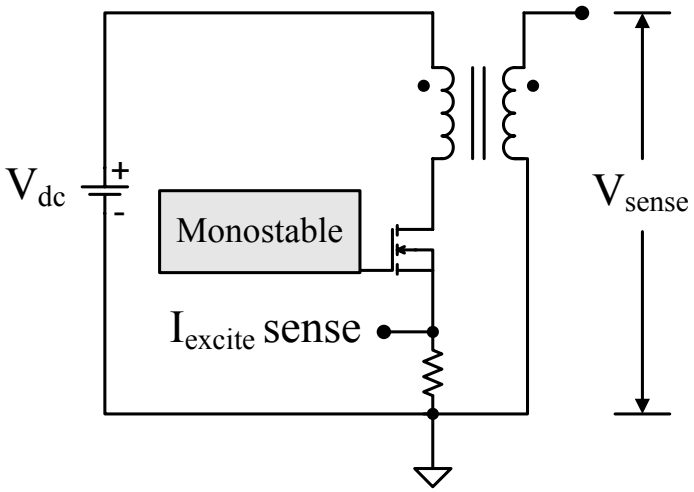

(a)

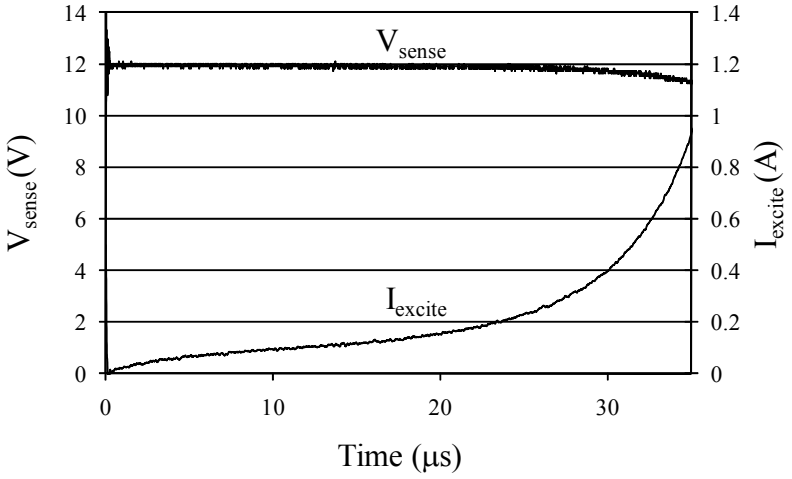

(b)

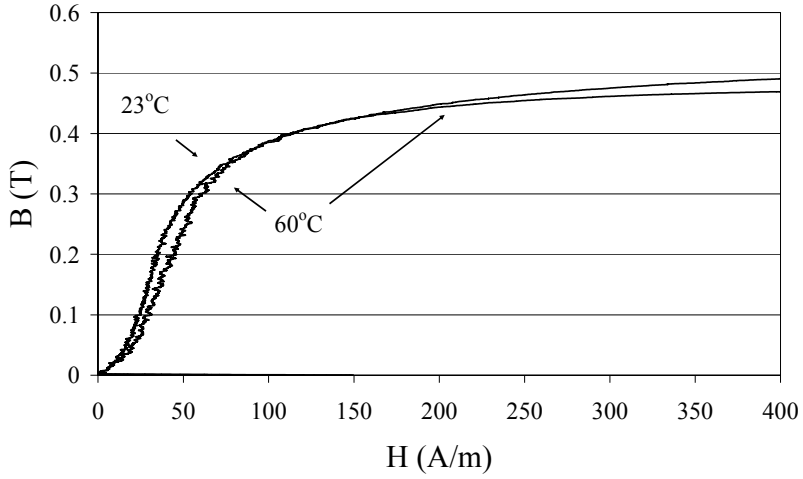

(c)

Fig. 5.12 (a) The magnetization curve measurement circuit, (b) measured V_{sense} and I_{excite} waveforms, (c) magnetization curves measured at 23°C and 60°C.

After the determination of the initial magnetization curve, the B_{dc} within a CUT for a given H_{dc} can be found. This is achieved by measuring the B-H loop of the CUT as it is excited under dc bias conditions, then adjusting the B-H loop upwards, or downwards, between the maximum and minimum values of its measured H-field. The adjustment continues until the tip of the B-H loop lies on the initial magnetization curve [23] as shown in Fig. 5.13. This graph shows measurements at 23°C of an initial magnetization curve and a B-H loop under dc bias conditions, varying between minimum and maximum values of -10 A/m and 79 A/m respectively. The maximum and minimum values of flux density, B_{max} and B_{min} can then be found, allowing B_{dc} to be calculated using:

$$B_{dc} = \frac{B_{max} + B_{min}}{2} \tag{5.4}$$

From Fig. 5.13 the value of B_{dc} is found to be 0.308 T.

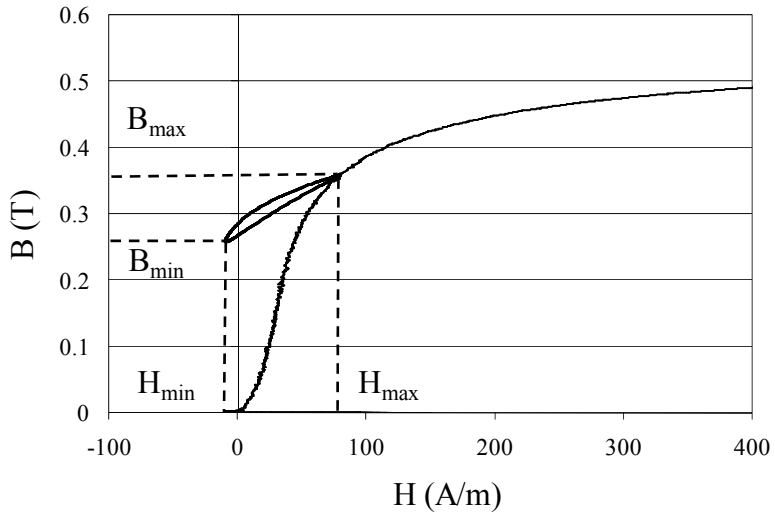

Fig. 5.13 The initial magnetization curve, and a measured B-H loop under dc bias conditions.

5.6 Summary

In Chapter 5 the difficulties associated with the measurement of ferrite core losses under dc bias conditions were described and elucidated in the form of numerical examples in the absence, and the presence, of core gaps. It was shown that the presence of a core gap increases considerably the difficulty of making accurate core loss measurements. With knowledge of these difficulties, various commonly used core loss measurement techniques

were reviewed. However, it was shown that all of these techniques suffer disadvantages, and three solutions were proposed, including: the mutual inductance neutralization technique, the ZVS technique, and the technique based around the power op-amp weighted summing amplifier used in conjunction with the high accuracy wattmeter. Using the mutual inductance neutralization technique it was shown that accurate core loss measurements could be made. However, the technique is disadvantageous in terms making measurements quickly and, therefore, was not used for the core loss measurements under dc bias that are presented in Chapter 6. The ZVS technique for measuring core losses under dc bias conditions was also critically evaluated, and although it allows loss measurements to be made quickly, it suffers the disadvantage of measuring residual circuit losses in conjunction with core losses. Due to the difficulty of separating these loss components, the ZVS technique was also not used. The technique based around the power op-amp and the high accuracy wattmeter does not suffer the preceding disadvantages, and allows core losses under dc bias conditions to be quickly and accurately measured. Using this technique accurate core loss measurements are presented in Chapter 6.

5.7 References

[1] B. Carsten, "Why a Magnetics Designer Should Measure Core Loss; with a Survey of Loss Measurement Techniques and a Low Cost, High Accuracy Alternative", *Proc. HFPC*, San Jose, California, pp. 103-119, May 1995

[2] W. V. Fam, "Poynting vector probe for measuring power at extremely low power factor", *IEE Proc.,* vol. 135, part A, no. 6, pp. 385-389, Jul. 1988

[3] J. Thottuvelil, T. G. Wilson and H. A. Owen Jr., "High Frequency Measurement Techniques for Magnetic Cores", *IEEE Trans. on Power Electronics*, vol. 5, no. 1, pp. 41-53, Jan. 1990.

[4] http://www.ferroxcube.com

[5] http://www.pack-feindraehte.de

[6] F. D. Tan, J. L. Vollin and S. M. Cuk, "Effective Control of the Error in a Direct Measurement of Core-Loss Power," *IEEE Trans. on Magn.*, vol. 31, no. 3, pp. 2280-2284, May 1995

[7] J. Hess, "Basics and Techniques of Power Loss Measurements in the frequency Range 10kHz up to 10MHz," Course Notes of the MMPA Soft Ferrite Users Conference, Chicago, Illinois, Oct. 24-25 1994

[8] M. Sippola and R. E. Sepponen, "Accurate Prediction of High-Frequency Power-Transformer Losses and Temperature Rise," *IEEE Trans. on Power Elec.*, vol. 17, no. 5, pp. 835-847, Sept. 2002

[9] T. G. Imre, W. A. Cronje, J. D. Van Wyk and J. A. Ferreira, "Loss Modeling and Thermal Measurement in Planar Inductors – a Case Study ," *IEEE Trans. on Ind. App.*, vol. 38, issue 6, pp. 1613–1621, Nov-Dec. 2002

[10] S. Butterworth, "Capacity and Eddy Current Effects in Inductometers", *Proc. Phys. Soc .of London*, 33, 1921, pp. 312-354 15

[11] L. Hartshorn, "The Properties of Mutual Inductance Standards at Telephonic Frequencies", *Proc. Phys. Soc. of London*, 38, 1925, pp. 302-320

[12] F. A. Laws, "Electrical Measurements", McGraw-Hill Book Co., New York and London, 1938

[13] D. Karo, "Electrical Measurements Part II", MacDonald & Co., London, 1953

[14] Z. Fei, "A New Construction of the Mutual Inductor used as Quadrature Standard", *IEEE Trans. on Inst. and Meas*., vol. IM-29, no. 4, Dec. 1980

[15] W. A. Edson, "The Single-Layer Solenoid as an RF Transformer", *Proc. IRE*, Aug. 1955, pp. 932-936.

[16] Clarke and Hess Communications Research Corp., www.clarke-hess.com

[17] Agilent Technologies, www.agilent.com

[18] http://apex.cirrus.com

[19] http://www.contherm.co.nz

[20] http://www.newtons4th.com

[21] http://www.bcarsten.com

[22] http://www.polytecpi.com

[23] S. Chikazumi, "Physics of Magnetization", John Wiley and Sons, New York, 1964,

Chapter 6

Vibration and Core Loss Measurements under DC Bias

6.1 Introduction

In Chapter 3 theoretical arguments were proposed co-relating Mn-Zn ferrite core losses under dc bias conditions to phenomena caused by magnetomechanical interactions over a wide frequency range. In Chapter 4 these phenomena were simulated within the framework of the J-A model. In this chapter the influence of magnetomechanical interactions on core losses under dc bias conditions is investigated experimentally using the core loss measurement circuit and laser vibrometer system described in Sections 5.5 and 5.6 respectively. The measurements are made using toroidal CUTs in two different Mn-Zn ferrite materials, and at a number of different frequencies and dc bias levels. The results for one of the ferrite materials show a clear correlation between dc bias levels, magnetostrictive vibration, and core losses, strongly suggesting a relationship exists under dc bias conditions.

6.2 Core Losses under dc Bias Conditions

This section presents the results of an experimental investigation of the core losses under dc bias conditions of MMG F49 Mn-Zn ferrite toroidal CUTs with dimensions 25x15x10 mm, and 30x18x6 mm. The CUTs were not forced air cooled in order to avoid the flow of turbulent air over the CUTs and, therefore, possible distortion of the vibration measurements made using the laser vibrometer system. As a consequence, self heating of the CUTs may have raised the core temperatures above ambient, and closer to 60^{o}C, at which core losses are a minimum according to the characteristic shown in Chapter 1. Therefore, the increase in core losses due to dc bias conditions may be slightly understated by the results that are shown.

Section 6.2.1 presents results which identify the magnetomechanical resonant frequencies of the CUTs, and it is shown that at these frequencies core losses are significantly higher than those at frequencies distant from resonance. Results are also presented showing that the level of magnetostrictive vibration of the CUTs increases with dc bias, and an obvious correlation with core losses is drawn. The investigation is extended in Section 6.2.2 to ac excitation frequencies distant from resonance, and results are presented showing a correlation between core losses and magnetostrictive vibration also exists at these frequencies. In Section 6.2.3 a CUT is potted in silicon elastomer, which is shown to have a significant influence on core losses under dc bias conditions. This influence is also explained with reference to magnetostrictive vibration.

6.2.1 Core Losses at Magnetomechanical Resonance

Fig. 6.1 shows the results of tests at an ac excitation level of 0.05 T, excitation frequencies of 20 kHz, 40 kHz, and 80 kHz, and various dc bias levels. For each test measurements were made at room temperature, and the CUTs were initially demagnetized before the dc bias of the ac excitation was monotonically increased. At 20 kHz and 40 kHz the measured core losses of each CUT were similar, with the differences being attributable to manufacturing variations in the ferrite material from one batch to another. However, at 80 kHz the core losses differed, with those of the 25x15x10 mm CUT significantly exceeding those of the 30x18x6 mm CUT. This difference can be explained by the proximity of the 80 kHz excitation frequency to the respective magnetomechanical resonant frequencies of each of the CUTs. The proximity in frequencies influences core losses because the ac magnetic excitation induces high levels of magnetostrictive vibration at resonance, which in turn induces high core losses [1]. Consequently, to show that

core losses increase with dc bias over a wide range of frequencies due to increased levels of magnetostrictive vibration, core losses were measured along with the magnetostrictive vibration at, near to, and distant from frequencies of magnetomechanical resonance.

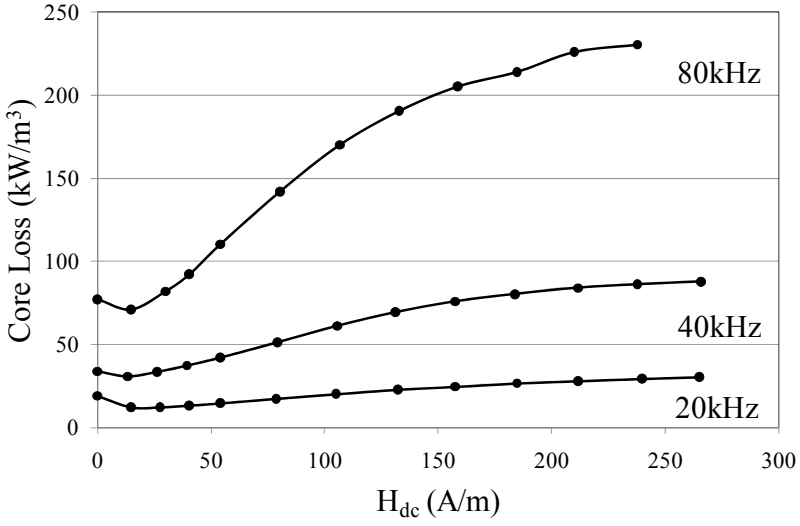

(a)

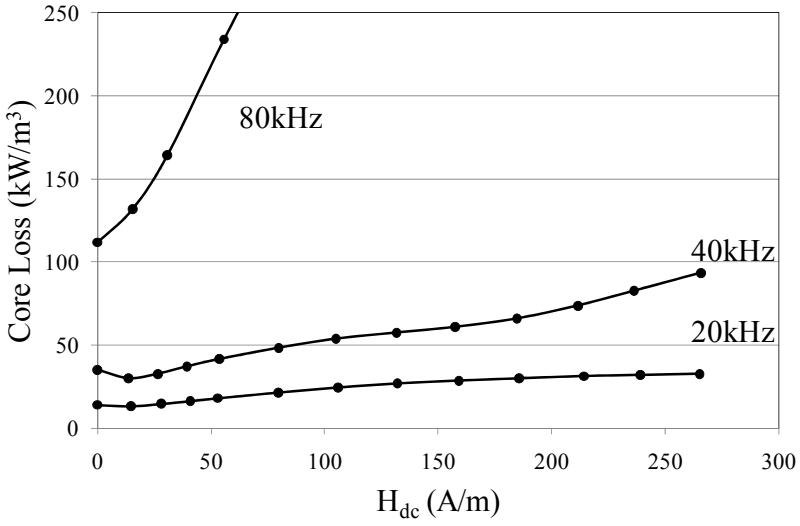

(b)

Fig. 6.1 Magnetostrictive vibration and core loss measurements made on (a) 30x18x6mm, (b) 25x15x10mm toroidals under various dc bias conditions and frequencies, and at 0.05 T

To identify the magnetomechanical resonant frequencies of the 25x15x10 mm CUT, the technique described in [1] was employed. This involved exciting the winding on the CUT, and measuring its impedance under various dc bias and low signal level ac excitation conditions using an Agilent 42841A bias current source in conjunction with an Agilent E4980A Precision LCR meter [2]. At resonant frequencies large changes in the winding impedance magnitude occurred,

as is evident in the results shown in Fig. 6.2(a). These measurements were made at dc bias levels of 50 A/m, 100 A/m and 200 A/m over a wide frequency range, and show that the magnetomechanical resonant frequency varied between 70 kHz and 80 kHz depending on the level of dc bias, with resonance occurring at 70 kHz given a 50 A/m dc bias. In Fig. 6.2(b) the winding impedance phase measurements are shown for the same CUT, and under the same dc bias conditions used for Fig. 6.2(a). These results show that magnetomechanical resonance dramatically affected the magnetic characteristics of the CUT, causing its excitation winding to exhibit a capacitive reactance. From Fig. 6.2(a) and Fig. 6.2(b) it is apparent that a resonant frequency occurs at 146 kHz, but only with a dc bias of 50 A/m. This is believed to be due to the CUT entering a mode of vibration which differed from that occurring between 70 kHz and 80 kHz, and which is only excitable at lower dc bias levels.

Using the Agilent 42841A bias current source in conjunction with an Agilent E4980A Precision LCR meter a frequency sweep of the impedance of an excitation winding on the 30x18x6 mm CUT was also undertaken. The results in terms of the impedance magnitude are shown in Fig. 6.2(c). The frequency range in which the largest changes in impedance occurred varied between 54 kHz and 58 kHz, depending on the dc bias level. The lower frequency range of magnetomechanical resonance of the 30x18x6 mm CUT in comparison to the 25x15x10 mm CUT can be explained by differences in the dimensions between the two CUTs. From Fig. 6.2(c) it is apparent that a number of significant changes in the impedance occur at various excitation frequencies under dc bias conditions. These are believed to be modes of vibration which differ from that arising between 54 kHz and 58 kHz.

To further examine the effect that magnetomechanical resonance has upon core losses, a frequency sweep of core losses under various dc bias conditions for the 25x15x10mm CUT was made, and is shown in Fig. 6.3. The core losses were measured at an ac flux density of 0.01 T, and resulted in resonant frequencies of 73 kHz, 76 kHz, and 79 kHz at dc bias levels of 50 A/m, 100 A/m and 200A/m, respectively. These resonant frequencies correspond closely to the resonant frequencies determined through the impedance frequency sweep, and which also varied between 70 kHz and 80 kHz. The results clearly show that core losses increase dramatically at magnetomechanical resonance, with the dc bias level influencing both the resonant frequency, as well as the level of the losses.

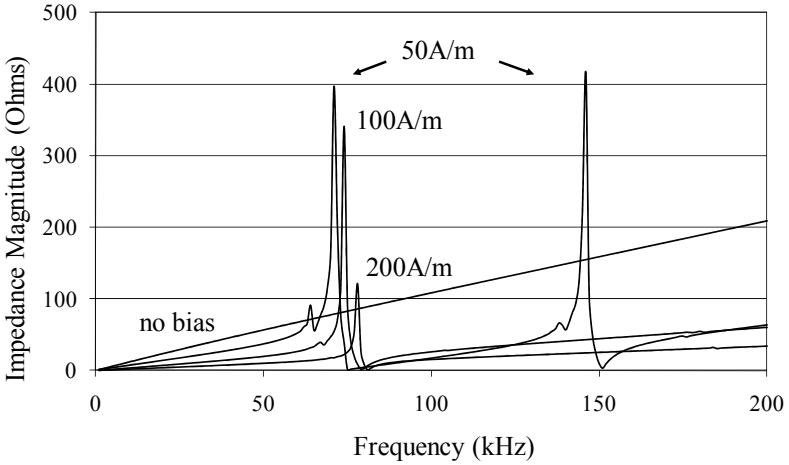

(a)

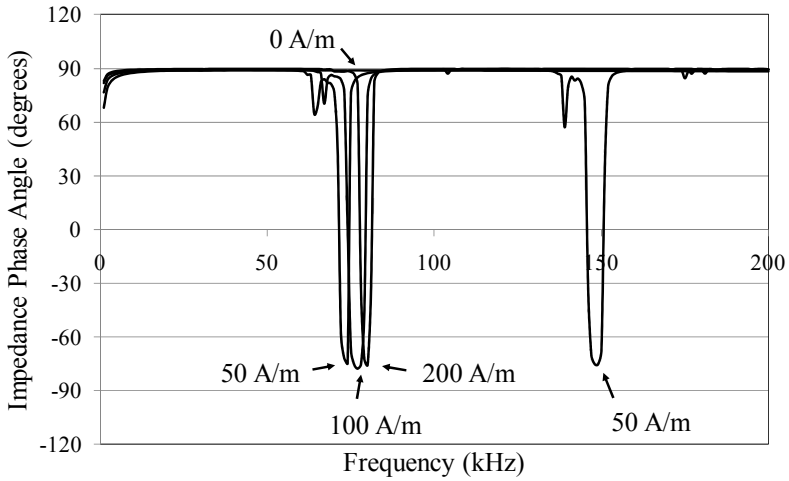

(b)

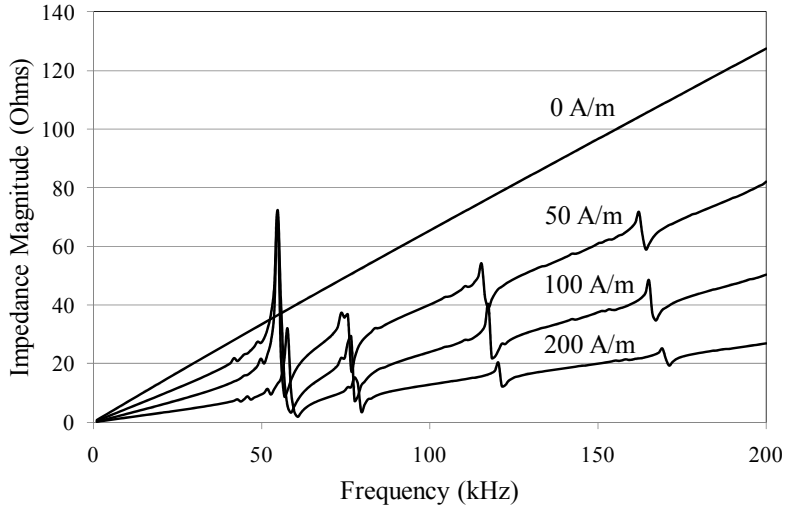

(c)

Fig. 6.2 Impedance measurements made on the 25x15x10 mm CUT under dc bias in terms of (a) the impedance magnitude, (b) the impedance phase angle. (c) Impedance magnitude measurements made on a 30x18x6 mm CUT

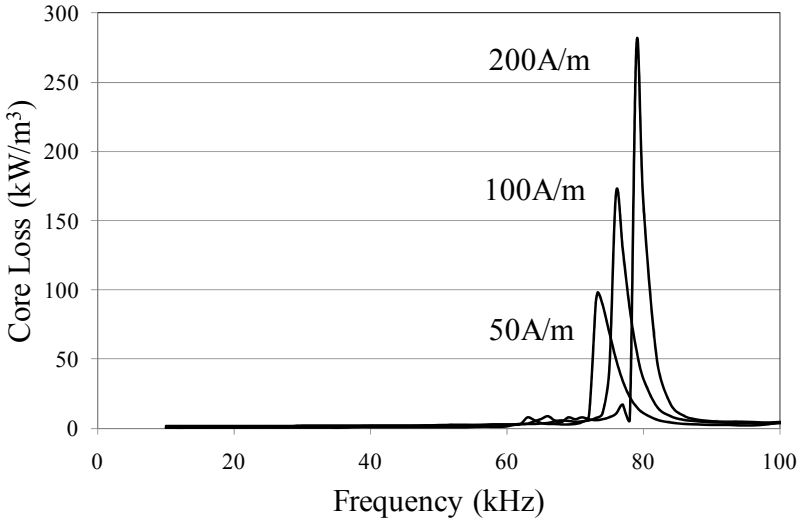

Fig. 6.3 Core Loss measurements made on the 25x15x10mm CUT under various dc bias conditions

To prove that magnetostrictive vibration is a mechanism which invokes core losses under dc bias conditions, the 25x15x10 mm toroidal CUT was tested with a dc biased, 0.05 T ac excitation waveform at 70 kHz. At this frequency it was expected that the measured vibration of the CUT would increase with the dc bias, up to the level giving magnetomechanical resonance. At dc bias levels beyond that giving resonance at 70 kHz, the vibration was expected to fall as the resonance was shifted to higher frequencies. Consequently, if core losses were measured to rise and fall with the vibration amplitude, this would indicate a correlation exists. The vibration measurements were made at position A, as shown in Fig. 6.4, using the laser vibrometer system described in Chapter 5. For these results the CUT was initially demagnetized, before the dc bias of the excitation waveform was increased monotonically from zero. The core loss and peak to peak magnetostrictive vibration measurement results are shown in Fig. 6.5. From these results it is evident that magnetostrictive vibration reaches a maximum at a dc bias of 80 A/m, which gives reasonable agreement with the value of 50 A/m predicted using the Precision LCR meter. As the dc bias was increased beyond 80 A/m the resonant frequency shifted to higher values, and the amplitude of the magnetostrictive vibration correspondingly decreased. From Fig. 6.5 it is clearly apparent that the measured core losses rose and fell in synchronism with the magnetostrictive vibration, proving an obvious correlation exists.

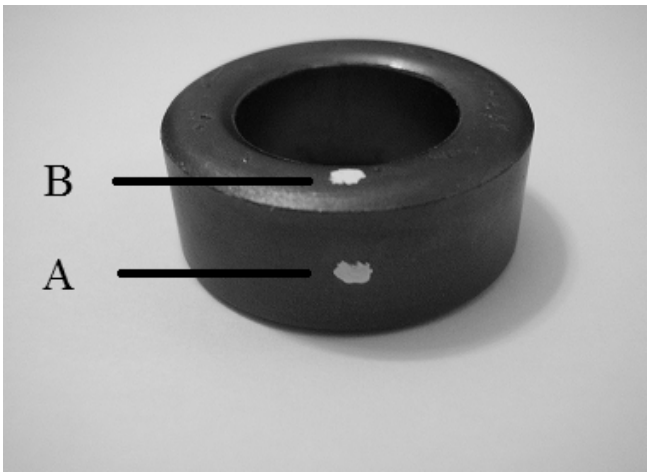

Fig. 6.4 Positions A and B at which magnetostrictive vibration measurements are made

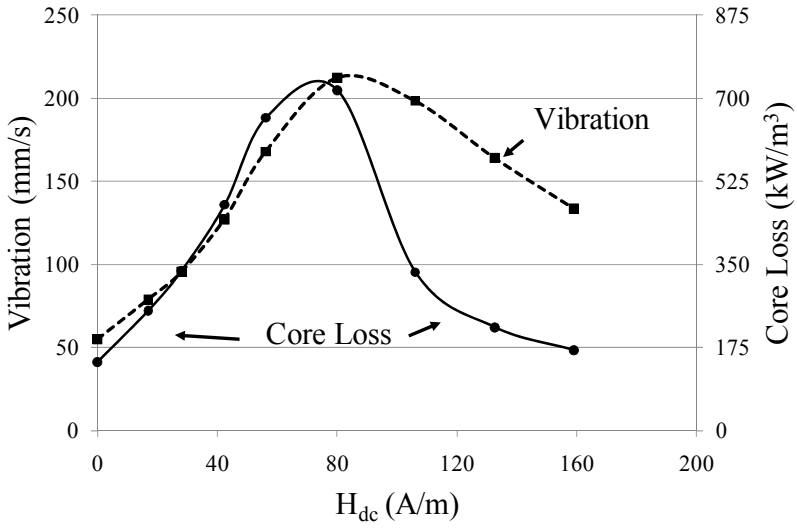

Fig. 6.5 Magnetostrictive vibration and core loss measurements made on the 25x15x10 mm toroidal at 70 kHz, 0.05 T and various dc bias levels

At the end of the test resulting in Fig. 6.5, the position of the CUT was changed allowing the vibration waveform to be measured at position B with a 160 A/m dc bias. This waveform is shown in Fig. 6.6(b), along with the magnetostrictive vibration waveform measured at position A in Fig. 6.6(a) at the same dc bias level. Through a comparison, it is evident that the CUT is vibrating largely in its axial plane as viewed from Fig. 6.4.

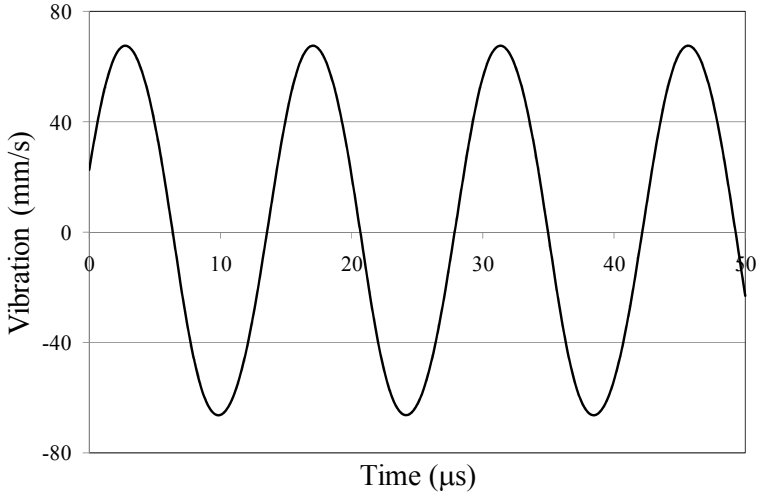

(a)

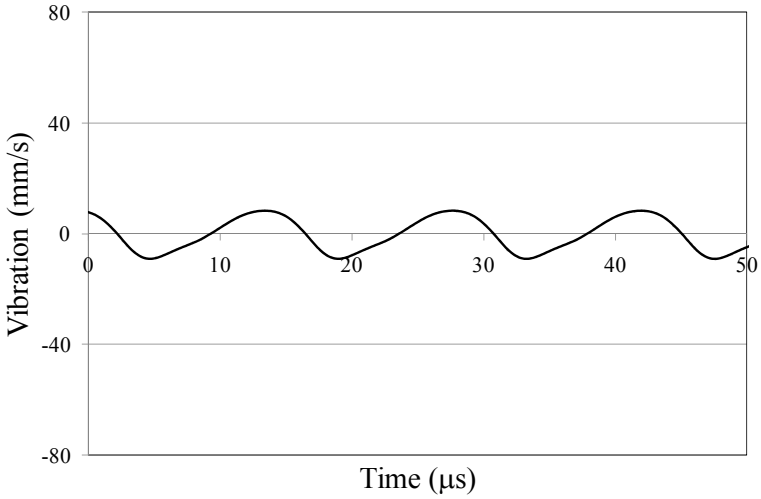

(b)

Fig. 6.6 Measured magnetostrictive vibration waveforms at (a) position A, and (b) position B for the 25x15x10 mm toroidal, 70 kHz, 160 A/m dc bias

For the magnetostrictive vibration waveforms measured at 70 kHz, the harmonic distortion was determined by taking the FFT of each waveform and applying:

$$\mathrm{THD} = \frac{\sqrt{\sum_{1}^{n} v_n^2}}{v_f} \tag{6.1}$$

where,

THD = total harmonic distortion of the magnetostrictive vibration waveform

v_f = vibration amplitude of the harmonic component at the ac excitation field

frequency (mm/s)

v_n = vibration amplitude of the nth harmonic component up to the fifth harmonic and excluding v_f (mm/s)

The THD content of the magnetostrictive vibration waveforms associated with Fig. 6.5 are shown in Fig. 6.7; it is apparent that the magnetostrictive vibration waveform is largely sinusoidal in nature except at 80 A/m dc bias, where the vibration highest. Therefore, through considering all the results in Fig. 6.5 except for that at 80 A/m, it can be concluded that core losses are dependent on the amplitude of the magnetostrictive vibration waveform when the harmonic content of this waveform is low. This conclusion is consistent with the proposal in Chapter 3 that domain wall pinning site densities within a CUT are dependent on the amplitude of the magnetostrictive vibration.

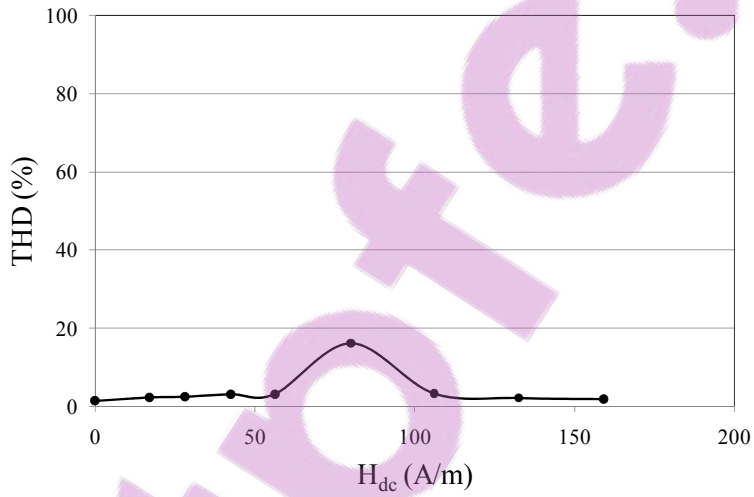

Fig. 6.7 THD content of magnetostrictive vibration waveforms at 70 kHz for the 25x15x10 mm toroidal

For the following tests in Section 6.2 vibration was measured at position A and the test procedure was the same that used for Fig. 6.5, with the exception that the dc bias was decreased back down to zero, after first being increased from zero to a maximum. Using this procedure the 25x15x10 mm toroidal was tested at 80 kHz, 0.05 T. The results, given in Fig. 6.8, show core losses increasing with the peak to peak magnetostrictive vibration and dc bias, as expected, before rising sharply at the very highest level of dc bias, where the vibration amplitude dramatically fell. However, at this highest level of dc bias the magnetostrictive vibration waveform changed its nature, containing a very large number of high amplitude harmonics, including those at frequencies below that of the applied ac magnetic field. These harmonics increased the THD of the vibration waveform significantly, as apparent in Fig. 6.8(c).

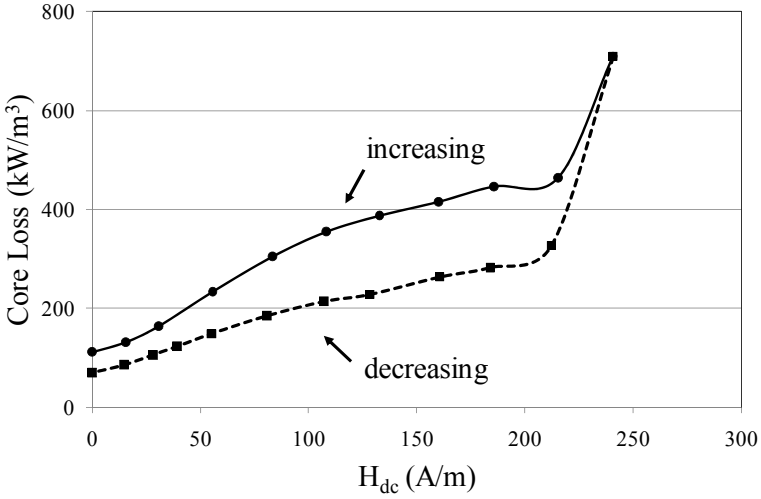

(a)

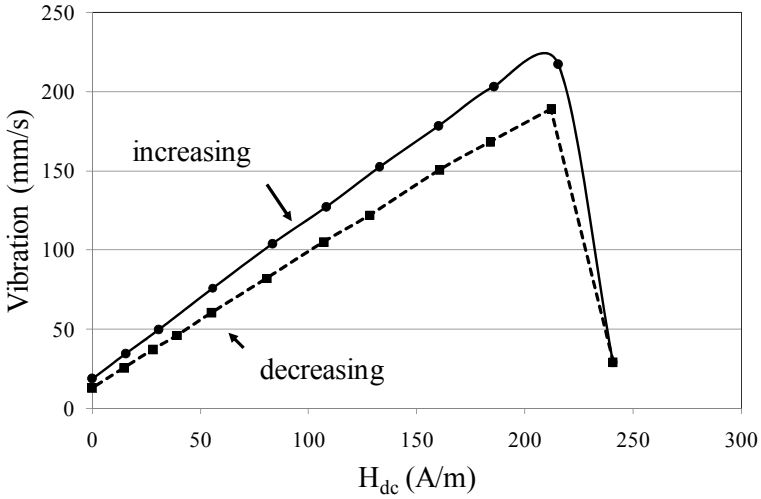

(b)

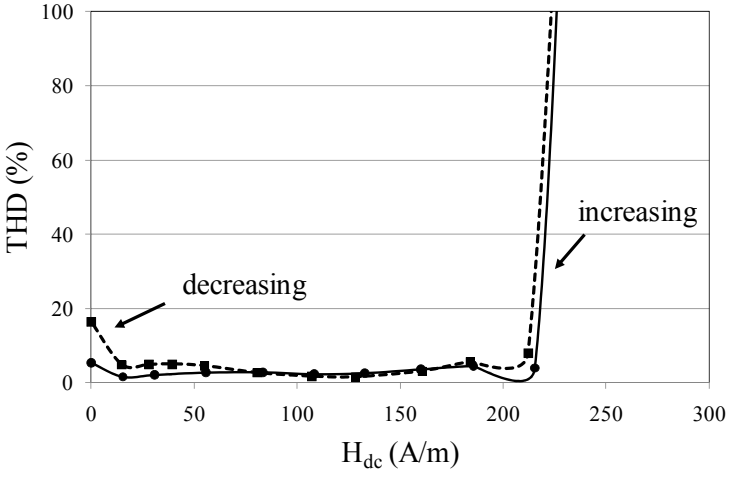

(c)

Fig. 6.8 Measured (a) core loss, (b) magnetostrictive vibration, (c) THD for increasing and decreasing levels of dc bias for 25x15x10 mm toroidal at 80 kHz, 0.05 T

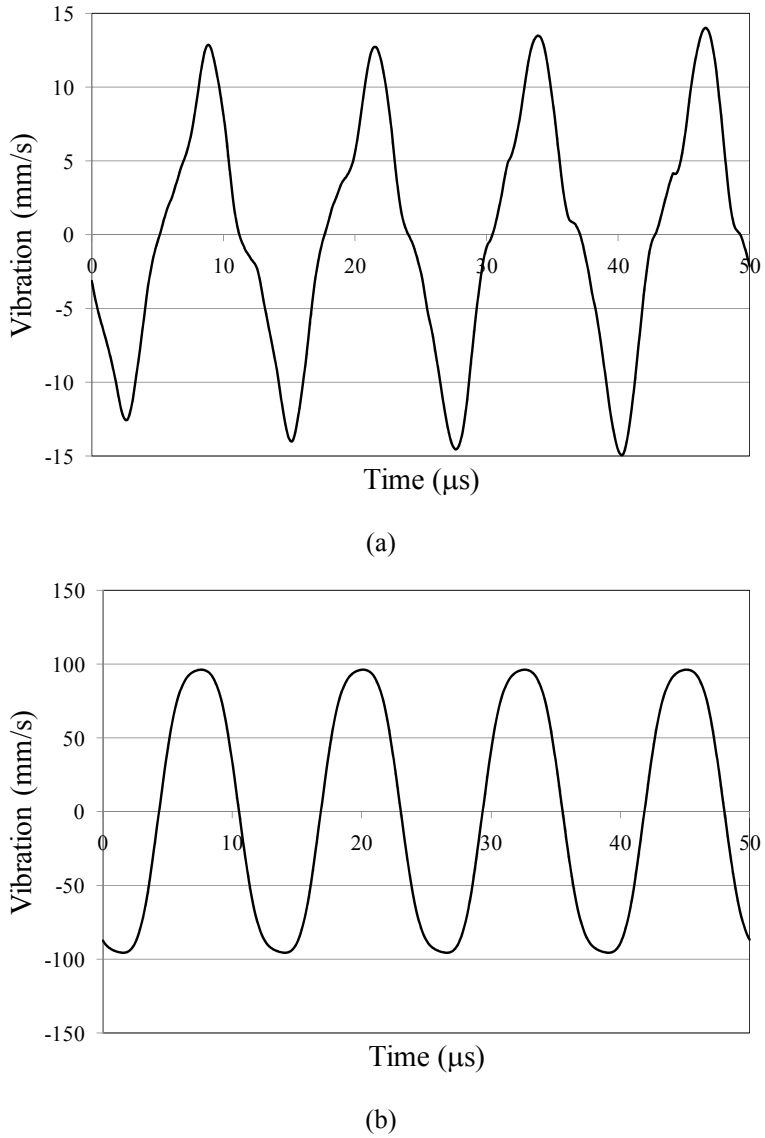

Fig. 6.9 Measured magnetostrictive vibration waveforms for the 25x15x10mm toroidal at 80kHz, 0.05T and dc bias levels of (a) 241A/m, (b) 212A/m

The influence the harmonics had on the magnetostrictive vibration waveform shape can be clearly observed through a comparison between the waveforms given in Fig. 6.9. The magnetostrictive vibration waveform shown in Fig. 6.9(a) was recorded at the highest level of dc bias of 241 A/m and contained both high frequency harmonics, resulting in a triangular shape, and harmonics below that of the ac excitation frequency, making the peak value of the waveform vary with time. The magnetostrictive vibration waveform recorded when the dc bias was decreased to 212 A/m is shown in Fig. 6.9(b), and the dramatic reduction in the harmonic content is obvious. These results clearly show that core losses are not only affected by the magnetostrictive vibration waveform amplitude, but also its harmonic content. Furthermore, the

results are consistent with the proposal in Chapter 3 that domain wall pinning site densities within a CUT are dependent on the frequency of the magnetostrictive vibration.

The results given in this section have shown that a correlation exists between core losses, and the nature of magnetostrictive vibration in terms of amplitude and harmonic content at magnetomechanical resonant frequencies. In Section 6.2.2 the investigation is extended to frequencies distant from magnetomechanical resonance.

6.2.2 Core Losses Measurements under dc Bias Distant from Resonance

To show a correlation between magnetostrictive vibration, core loss, and dc bias at frequencies distant from magnetomechanical resonance, core loss and vibration measurements were made at 20 kHz using the 25x15x10 mm CUT. From Fig. 6.2(a) it is apparent that this test frequency is distant from the magnetomechanical resonant frequencies of the CUT. The results, given in Fig. 6.10, show that core losses initially fell with dc bias, before rising as the dc bias was increased monotonically to a maximum. The initial dip in the core loss with the application of a dc bias can be explained with reference to the THD content of the magnetostrictive vibration waveform in Fig. 6.11. With no dc bias the this waveform contained a strong harmonic component at twice the frequency of the applied ac magnetic field. This is because the magnetostrictive vibration is a quadratic function of the field in the absence of a dc bias, as described in Chapter 3 [3]. Therefore, based on (6.1), the THD was very high as shown in Fig. 6.11. With the application of the dc bias the second harmonic rapidly fell in amplitude, and the core losses correspondingly decreased. However, as the dc bias increased beyond very low levels the variations in THD became less significant and, therefore, had a lesser influence on core losses; conversely, the magnetostrictive vibration amplitude increased with dc bias and, therefore, caused core losses increase. At high levels of dc bias a slight increase in the THD occurred as the CUT entered the non-linear region of its magnetization curve. This can be expected to increase core losses at the very highest levels of dc bias.

From the results given in Fig. 6.10 and Fig. 6.11 it is apparent that when the dc bias was decreased from a maximum back to zero, the peak to peak magnetostrictive vibration was greater than that at the start of the test, when the dc bias was also zero. Correspondingly, the core losses at the end of the test were also higher than at the start. This reinforces the proposed theory that

higher levels of magnetostrictive vibration cause increased core losses. The measured magnetostrictive vibration waveforms before, and after the application of the dc bias are shown in Fig. 6.12. The increased level of magnetostrictive vibration at the end of the test, after the dc bias had been decreased from a maximum, can be explained by the higher level of remanent flux density, B_{rem}, present in the CUT providing a dc bias of an internal nature. The results presented in Fig. 6.10, Fig. 6.11, and Fig. 6.12 are supported by the results shown in Fig. 6.8, and Fig. 6.13 through a comparison between the magnetostrictive vibration and core loss measurements with no dc bias at the starts and ends of each test.

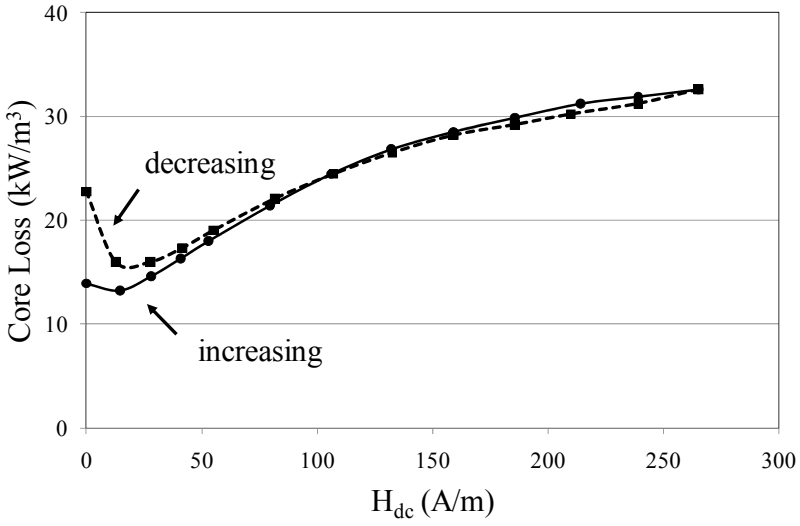

(a)

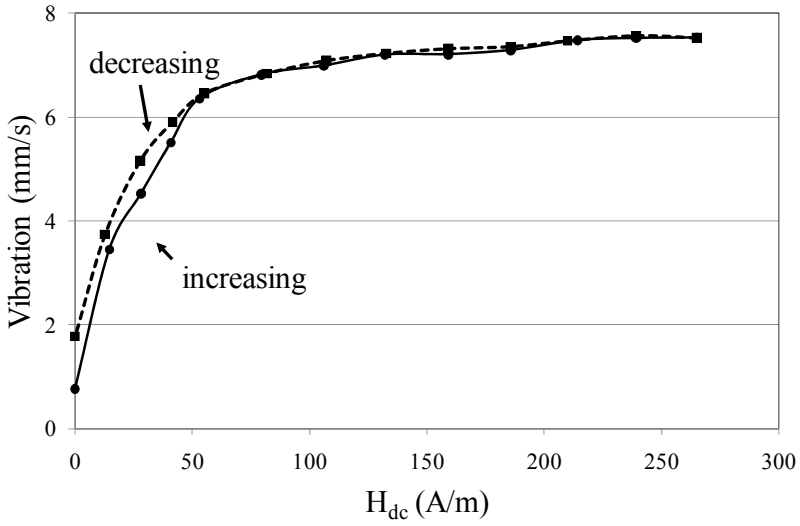

(b)

Fig. 6.10 Measured (a) core loss, and (b) magnetostrictive vibration for increasing and decreasing levels of dc bias for the 25x15x10 mm toroidal at 20 kHz, 0.05 T

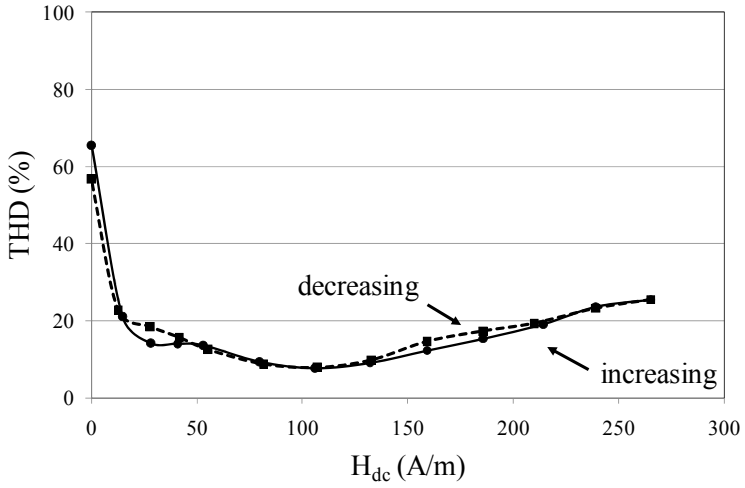

Fig. 6.11 Measured THD for increasing and decreasing levels of dc bias for 25x15x10 mm toroidal, 20 kHz, 0.05 T

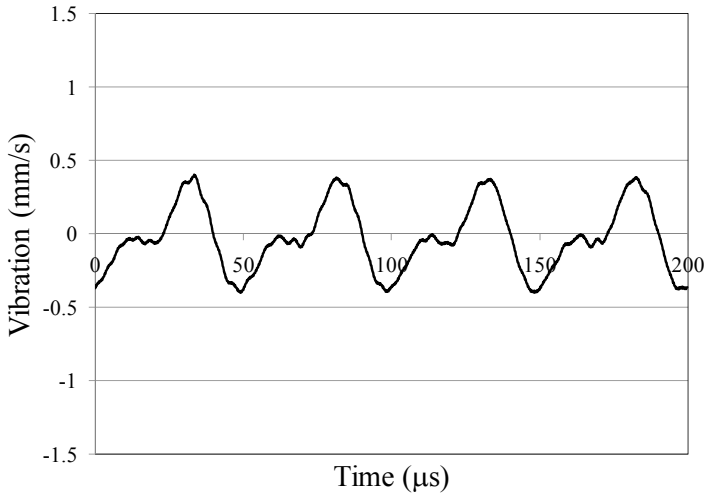

(a)

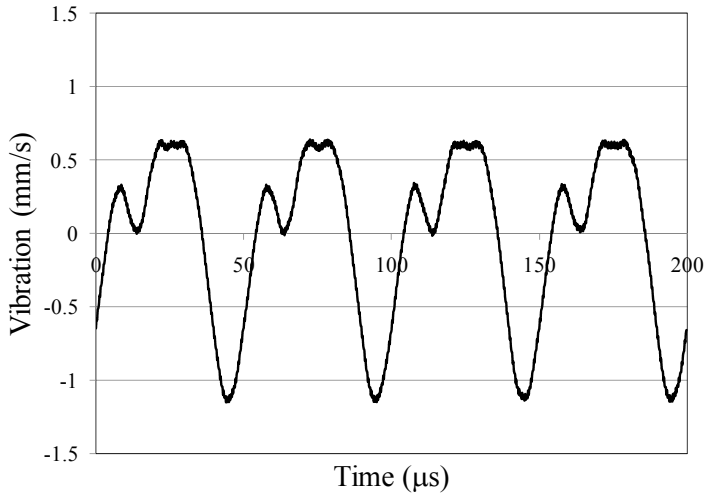

(b)

Fig. 6.12 Measured magnetostrictive vibration waveforms with no applied dc bias, and (a) with, (b) without B_{rem}, at 20 kHz, 0.05 T

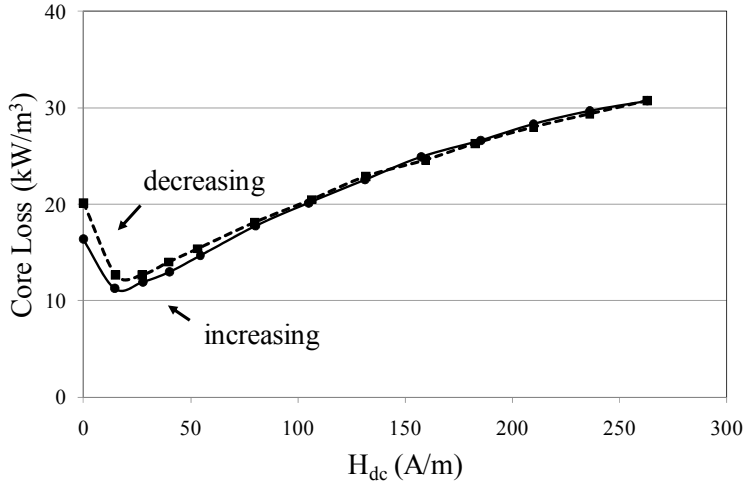

(a)

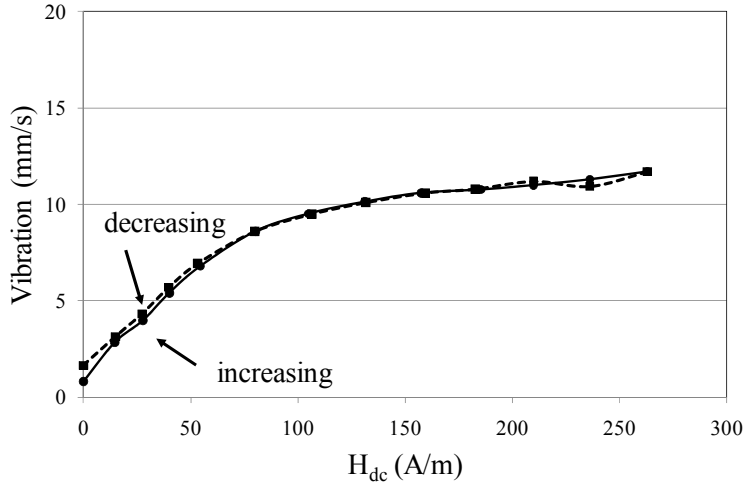

(b)

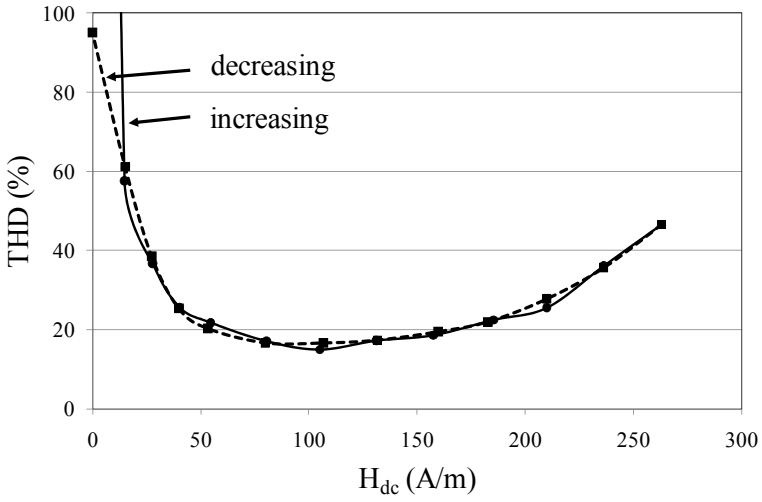

(c)

Fig. 6.13 Measured (a) core loss, (b) magnetostrictive vibration, (c) THD for increasing and decreasing levels of dc bias for the 30x18x6 mm toroidal at 20 kHz, 0.05 T

Fig. 6.13 shows the results of tests made under dc bias conditions on the 30x18x6 mm toroidal CUT at 20 kHz. This frequency is distant from magnetomechanical resonance, as apparent from the impedance magnitude vs. frequency characteristic measured under dc bias conditions for this CUT, which was previously shown in Fig. 6.2(c). The results in Fig. 6.13 exhibit similar characteristics to those presented for the 25x15x10 mm toroidal and, therefore, support the conclusions previously made in relation to that CUT.

6.2.3 The Effect of Potting on Core Losses under dc Bias

In this section the effect of potting on core losses under dc bias conditions is investigated through testing a 30x18x6 mm CUT in MMG F49 material before and after potting. The potting material used was Sylgard 184 silicon elastomer [4], and the CUT after potting is shown in Fig. 6.14. The CUT was demagnetized before potting, and not afterwards, in order to avoid loosening the core through the high magnetostrictive vibrations incurred during the demagnetization process. The tests under dc bias were performed with an ac excitation level of 0.05 T, at 20 kHz, and by increasing the dc bias level monotonically from zero to a maximum, before decreasing it back to zero. The core loss results before potting are shown in Fig. 6.15(a), and those after in Fig. 6.15(b). From these results it can be observed that at the start of the test, with no applied dc bias, the core losses of the potted CUT were significantly higher than those in the unpotted state. Under dc bias conditions a trend developed, with the difference between the losses in the potted and unpotted states increasing with the dc bias level, and reaching a maximum at the highest level of dc bias; this is evident in the characteristic shown in Fig. 6.16, which gives the difference between the potted and unpotted core losses at corresponding levels of dc bias, as the dc bias was reduced from a maximum down to zero. These results can be explained in terms of magnetomechanical interactions. As described in Chapter 3, a time varying applied magnetic field demands that the dimensions of a CUT change due to magnetostrictive vibration, with the level of the vibration increasing in the approach to saturation, as more of the magnetization process takes place through domain rotation. Therefore, the increasing difference between the potted and unpotted core losses with increasing dc bias levels can be explained by the higher levels of applied magnetic field energy demanded by the potted CUT, in order to allow it to vibrate against the force of the potting material.

Fig. 6.14 The potted 30x18x6 mm CUT

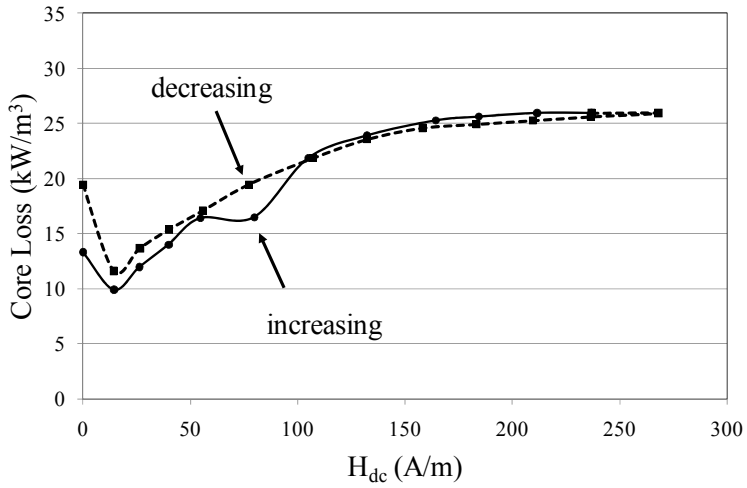

(a)

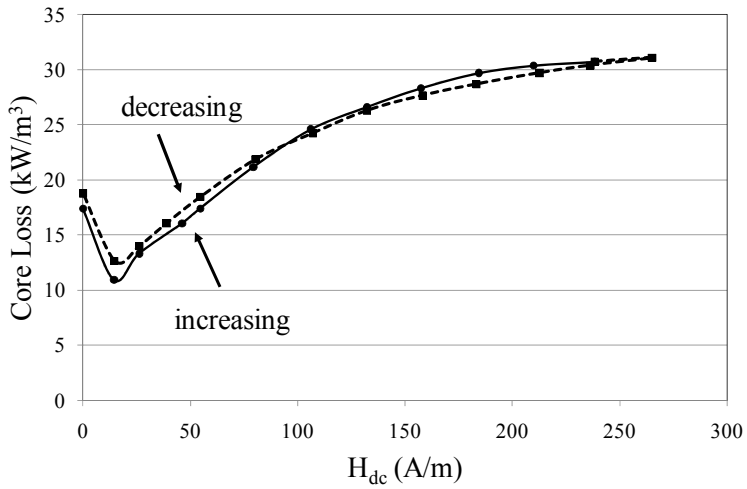

(b)

Fig. 6.15 Core loss measurements made on 30x18x6 mm toroidal CUT in MMG F49 material (a) before, and (b) after potting

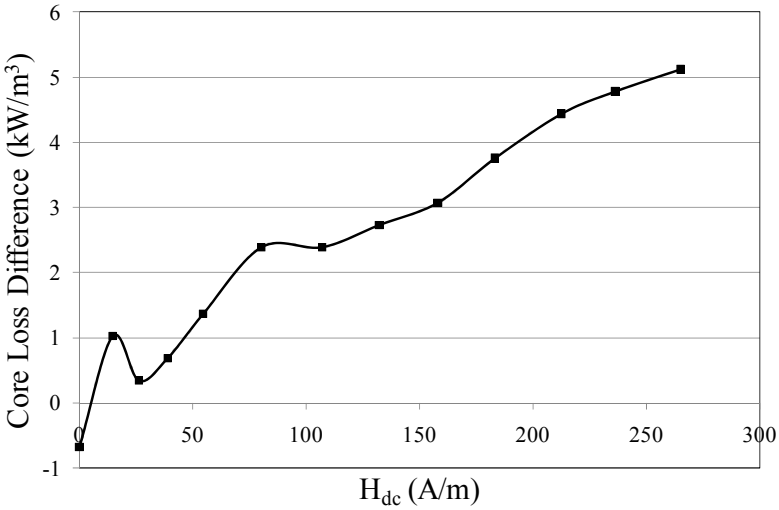

Fig. 6.16 Difference between potted and unpotted core losses as the dc bias is decreased from a maximum down to zero

6.3 Measurements under dc Bias for Type R Ferrite Material

To investigate a different Mn-Zn ferrite material under dc bias conditions to that tested in Section 6.2, a Magnetics Inc type ZR42915TC toroidal in R material [5], was used, and the results are presented in this section. To determine the frequency range at which magnetomechanical resonance occurs for this CUT, a frequency sweep of the impedance magnitude under dc bias conditions was performed. The results are given in Fig. 6.17, and show that magnetomechanical resonance varies between a lower frequency range of 72 kHz to 74 kHz, and a higher frequency range of 191 kHz to 192 kHz. By a comparison with the impedance measurements made on the MMG F49 material CUTs given in Fig. 6.2, it can be surmised that the influence of magnetomechanical resonance is less significant. This is supported by the results given in Fig. 6.18, which show the core loss and peak to peak magnetostrictive vibration measurements made under dc bias conditions with an ac excitation of 0.05 T, and at 20 kHz. These results show that the magnetostrictive vibration levels are low for the Magnetic Inc CUT in R material relative to those of both the MMG F49 material CUTs tested at the same frequency.

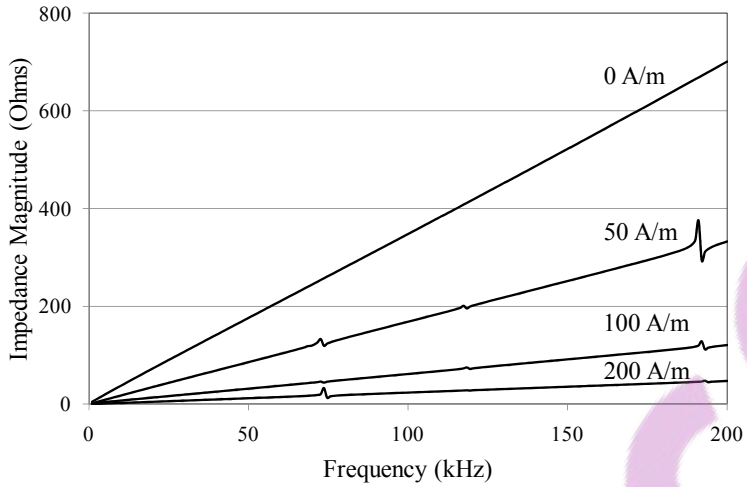

Fig. 6.17 Impedance magnitude measurements made on the R material CUT under dc bias

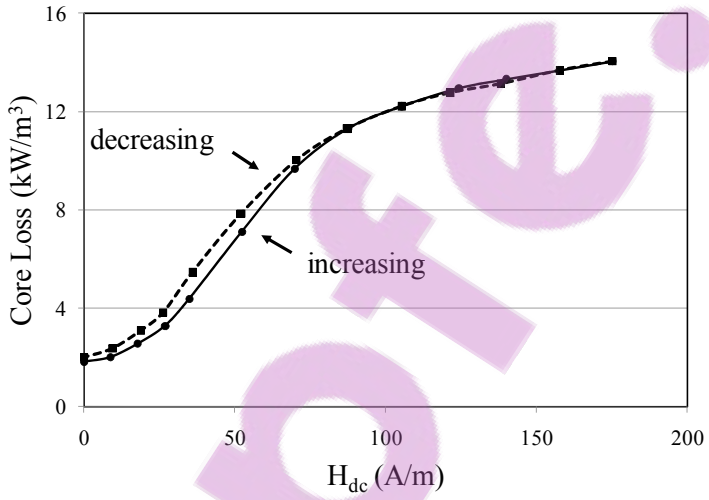

(a)

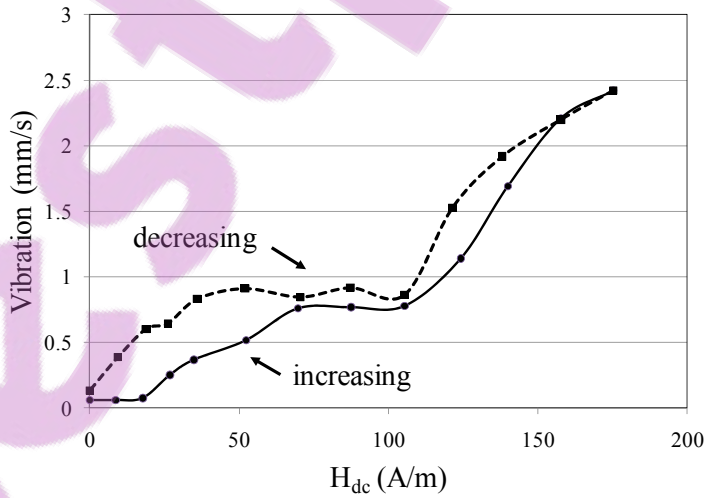

(b)

Fig. 6.18 Measured (a) core loss, (b) magnetostrictive vibration for the R material CUT at 20 kHz, 0.05 T under dc bias

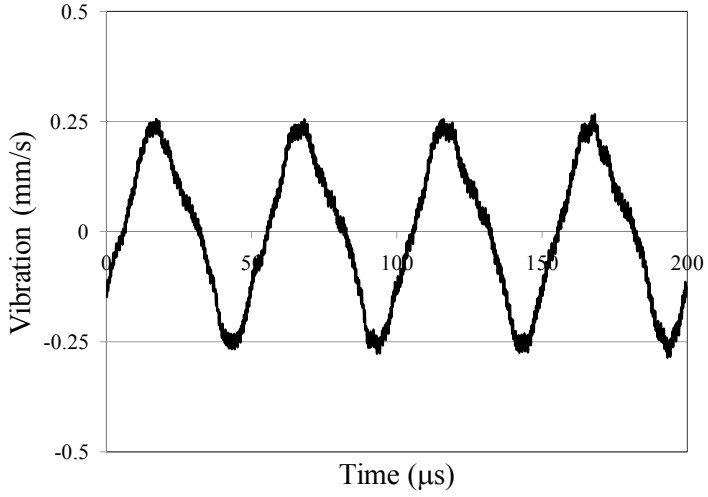

(a)

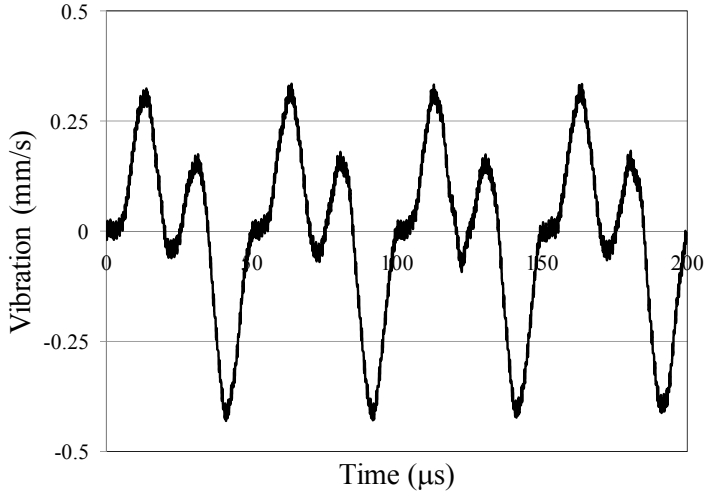

(b)

Fig. 6.19 Magnetostrictive vibration waveforms measured at 20 kHz, 0.05 T, at dc bias levels of (a) 52 A/m, (b) 70 A/m

From Fig. 6.18 it is apparent that the peak to peak amplitude of the magnetostrictive vibration waveform deviated from an upward trend for dc bias values in excess of 30 A/m on both the increasing, and decreasing parts of the dc bias tests. However, over the same interval the nature of the magnetostrictive vibration changed in terms of its harmonic content. This is apparent in Fig. 6.19, which gives the vibration waveforms measured at (a) 52 A/m, and (b) 70 A/m, at which level the harmonic content increased significantly, and the peak to peak vibration level began to deviate from an upward trend with the dc bias. This complicates drawing any conclusions from the results during this interval, because the high level of harmonics in the magnetostrictive vibration waveforms may account for an increase in core losses under dc bias despite the lower level of magnetostrictive vibration. Therefore, the characteristics shown in Fig. 6.18 were

examined only between 0 A/m and 30 A/m dc bias, as during this interval the harmonic content is relatively low. This allowed the influence of the vibration amplitude on core losses to be examined in isolation from the effect of harmonics in the magnetostrictive vibration waveform.

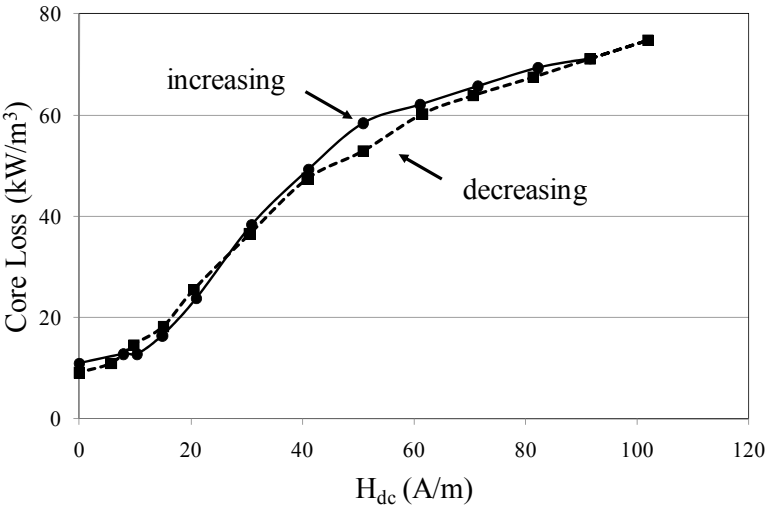

(a)

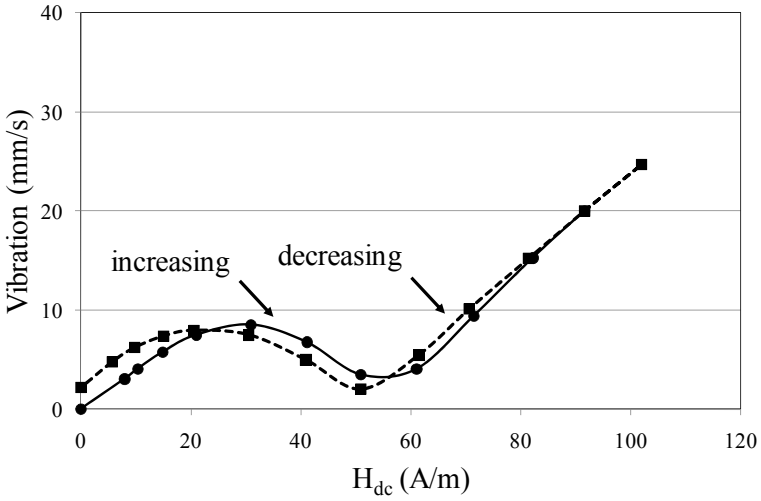

(b)

Fig. 6.20 Measured (a) core loss, (b) magnetostrictive vibration for the R material CUT at 80 kHz, 0.05 T_{ac} under dc bias

The results in Fig. 6.18(a) show that core losses at the start of the dc bias test, when the CUT had no B_{rem}, were similar to those at the end, when the CUT had a higher level of B_{rem}. Corresponding to the similar level of losses at the start and end of the test, were similar levels of magnetostrictive vibration. Although this provides a contrast to the results presented for the MMG F49 material, it does suggest a correlation exists between core losses and magnetostrictive vibration levels at frequencies distant from resonance for the R material. The existence of such a

correlation is further supported by the clear differences in the levels of magnetostrictive vibration between 0 A/m and 30 A/m. During the interval over which the dc bias was increased from zero up to 30 A/m, a lower level of magnetostrictive vibration was measured in comparison to the decreasing interval from 30 A/m down to 0 A/m. Corresponding to the lower level of magnetostrictive vibration during the increasing interval was a lower level of core loss.

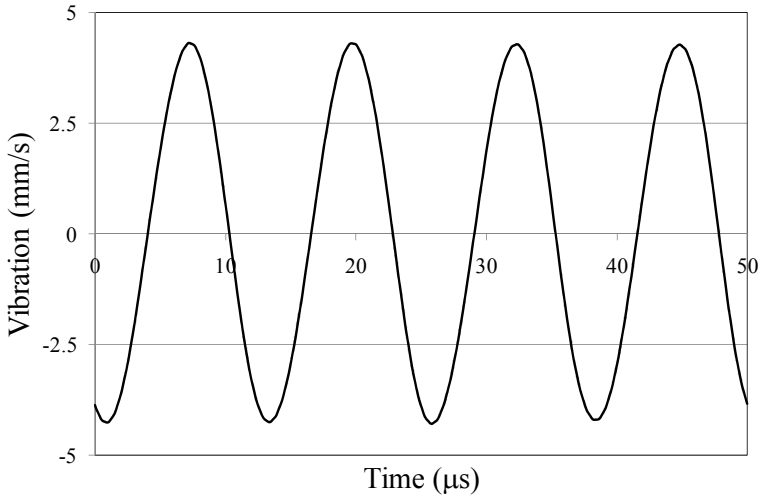

(a)

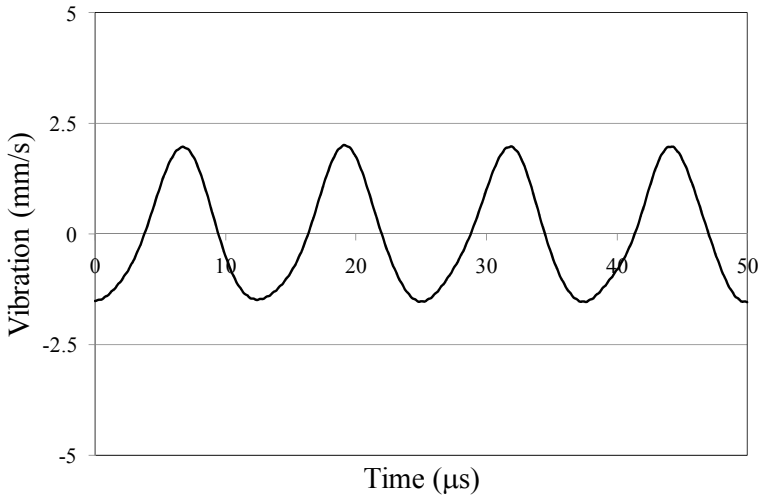

(b)

Fig. 6.21 Magnetostrictive vibration waveforms measured at 80 kHz, 0.05 T, at dc bias levels of (a) 31 A/m, (b) 51 A/m

To further test the proposed theory that core losses are correlated to magnetostrictive vibration levels, the R material CUT was also tested at 80 kHz, which is in close proximity to a magnetomechanical resonant frequency as shown by the results in Fig. 6.17. As evident in the results shown in Fig. 6.20, the magnetostrictive vibration levels were significantly higher than

those measured at 20 kHz and shown in Fig. 6.18, and also showed that significant variations in the amplitude of the magnetostrictive vibration waveform occurred. However, at the same time core losses did not deviate from their upward trend under increasing dc bias conditions, which is in complete contrast to the results presented in Fig. 6.5 for the F49 material 25x15x10 mm CUT. The magnetostrictive vibration waveforms recorded at the dc bias levels of 31 A/m and 51 A/m are shown in Fig. 6.21, and it is clear that a significant degree of asymmetry exists in the waveform measured at 51 A/m. Based on the measured results presented in Chapter 7, this may indicate that the CUT changed its mode of vibration, so that while the magnetostrictive vibration amplitude was found to decrease when measured in one axis, it may have increased in a different axis. However, this was not determined at the time the measurements were made. Therefore, no conclusions can be made with certainty with regard to the relationship between magnetostrictive vibration and core losses for the R material CUT that was tested.

6.4 Summary

In this chapter experimental results were presented relating core losses to the nature of magnetostrictive vibration under dc bias conditions. Initially, the magnetomechanical resonant frequencies of Mn-Zn MMG F49 ferrite material CUTs were identified, before core loss and magnetostrictive vibration measurements under dc bias conditions were made at specific frequencies; these frequencies were chosen to be close to, as well as distant from magnetomechanical resonance. The measurements clearly showed a strong correlation exists between core losses, and the amplitude and harmonic content of magnetostrictive vibration waveforms, thereby strongly supporting the theoretical work in Chapters 3 and 4. Furthermore, correlation between the nature of magnetostrictive vibration and core losses under dc bias conditions at frequencies distant from magnetomechanical resonance was also shown.

To further investigate the impact of magnetomechanical effects under dc bias conditions on Mn-Zn ferrite core losses, the core losses of a MMG F49 material CUT were tested before, and after potting in silicon elastomer. These results showed that the effect of potting was to raise the level of the core losses at the highest levels of dc bias and, therefore, magnetostrictive vibration. This result can be explained by the higher levels of H-field energy demanded by the potted CUT, in order to allow it to vibrate against the force of the potting material.

A conclusion as to the influence of magnetomechanical effects on the core losses under dc bias conditions of the Magnetic Inc R material CUT could not be reached, based on the experimental results that were presented. However, these results do not preclude the possibility that such a relationship exists.

The results in this chapter show that magnetomechanical effects in the form of magnetostrictive vibration can significantly influence Mn-Zn ferrite core losses. However, the influence these effects can exert upon other aspects of the magnetization process has not been investigated. This is addressed in Chapter 7, which gives experimental results showing the manner by which B-H loops under dc bias conditions can be distorted by magnetostrictive vibration.

6.5 References

[1] V. J. Thottuvelil, T. G. Wilson, and H. A. Owen, "High-frequency core-loss characteristics of biased Fe B S amorphous metallic alloy tape-wound cores," IEEE Trans. Magn., vol. MAG-20, no. 5, Sep. 1984, pp.1329–1331

[2] http://www.home.agilent.com

[3] E. du Tremolet de Lacheisserie, "Magnetostriction, Theory and Applications of Magnetoelasticity", CRC Press, 1993, ISBN 0-8493-6934-7

[4] http://www.dowcorning.com

[5] http://www.mag-inc.com/products/ferrite-cores

Chapter 7

Magnetomechanical Interactions and B-H Loop Shape

7.1 Introduction

In the previous chapter it was shown that magnetomechanical interactions can have a strong influence on the magnetization process in terms of the losses that are incurred. This influence can be explained by elastic stresses occurring at a microscopic scale, which increase with magnetostrictive vibration under increasing dc bias conditions and increase the strength and density of domain wall pinning sites. In this chapter experimental evidence of the influence of magnetostrictive vibration at a macroscopic scale is presented. As proposed in Chapter 3, the mechanism by which this influence manifests is through stress anisotropy acting on large numbers magnetic moments within a CUT in a uniform manner. Furthermore, this influence is observable in the form of figure-eight shaped B-H loops, as described in Chapter 3 and modeled in Chapter 4. Results are presented showing B-H loops distorted into figure-eight as well as other shapes, and it is shown that the distortion can be attributed to the manner in which a CUT vibrates within a certain frequency range of excitation. The CUTs tested for all results presented in this Chapter were manufactured in MMG Mn-Zn F49 ferrite material.

7.2 Figure-eight B-H Loops

This section presents measured B-H loops, which exhibit a distorted, figure-eight shape. The measurements show that this phenomenon takes place at high magnetic field strengths, and at frequencies varying between 30 kHz and 40 kHz under dc bias conditions. The results were measured using the technique described in Section 5.5.

7.2.1 Figure-eight Shaped B-H Loops between 30 kHz and 40 kHz

Initially a 30x18x6 mm toroidal CUT was excited at 30 kHz, with an ac flux density of 0.05 T and a high constant dc bias of 247 A/m. The frequency was then increased while maintaining the

ac flux density constant, and various B-H loops were observed between 30 kHz and 37 kHz. These are shown in Fig. 7.1 and are located about zero, with the dc bias is removed for ease of comparison between B-H loops. It is evident that at 34.6 kHz the B-H loop changed from having a typical shape, as measured at 34 kHz, to having a loop in its tail, resulting in a figure-eight shape This shape also occurred at 37 kHz, but at 39 kHz the B-H loop reverted back to a typical shape. The data gathered to graph the B-H loop at 34.6 kHz incurred a total core loss of 0.225 W, which was the summation of a positive loss component of 0.231 W in the B-H loop body, less a negative loss of 6.11 mW present in the tail. This total core loss, calculated using measured data, compared closely with the value of 0.222 W measured using the high accuracy wattmeter described in Chapter 5. This suggests that the gathered data and, therefore, the B-H loop shape, were measured accurately.

In Fig. 7.2 the magnetostrictive vibration waveforms measured by the laser vibrometer at position A, as shown in Fig. 6.4, are given for 30 kHz, 34 kHz and 34.6 kHz. From a comparison, three aspects are notable: the waveform amplitudes increase with frequency, the harmonic content at 34.6 kHz is much greater than that at the other two frequencies, and the amplitude of one half cycle at 34.6 kHz is significantly greater than the other, even though the average value over one cycle is very close to zero (0.00026 m/s). The average of the magnetostrictive vibration must be zero over one cycle because the CUT is stationary over time; therefore, the small average value that is measured is attributed to measurement error. However, although the net movement of the CUT over one cycle is zero, the variation in the instantaneous mechanical energy over one cycle is highly asymmetrical. This is evident in Fig. 7.3, which shows the magnetostrictive vibration waveform at 34.6 kHz and its square, which is proportional to mechanical energy by:

$$E = \tfrac{1}{2} mv^2 \qquad (7.1)$$

where,

E = energy (J)

m = mass (kg)

v = velocity (m/s)

The area under the square of the magnetostrictive vibration during the positive part of the cycle in Fig. 7.3, between 5.1 μs and 17.4 μs, is a factor of 1.72 times greater than that during the negative part between 17.4 μs and 34.2 μs. This implies the core is storing mechanical energy over the

steady state. However, it is believed that this is not the case; rather, it is believed that some of the excess mechanical energy per cycle is dissipated as heat, and some is transferred to another form of energy. Therefore, it is proposed that at least some of the excess mechanical energy generated during the positive part of one excitation cycle is released during the negative part by being converted to magnetic energy through magnetomechanical interactions. In this way the magnetic state of the core gains in energy and this accounts for the figure-eight shape of the B-H loop where, for a portion of the B-H loop at its tail, a gain in magnetic energy occurs.

The proposal that B-H loops are distorted into a figure-eight shape by magnetomechanical interactions is supported by experimental results given in Section 7.2.2.

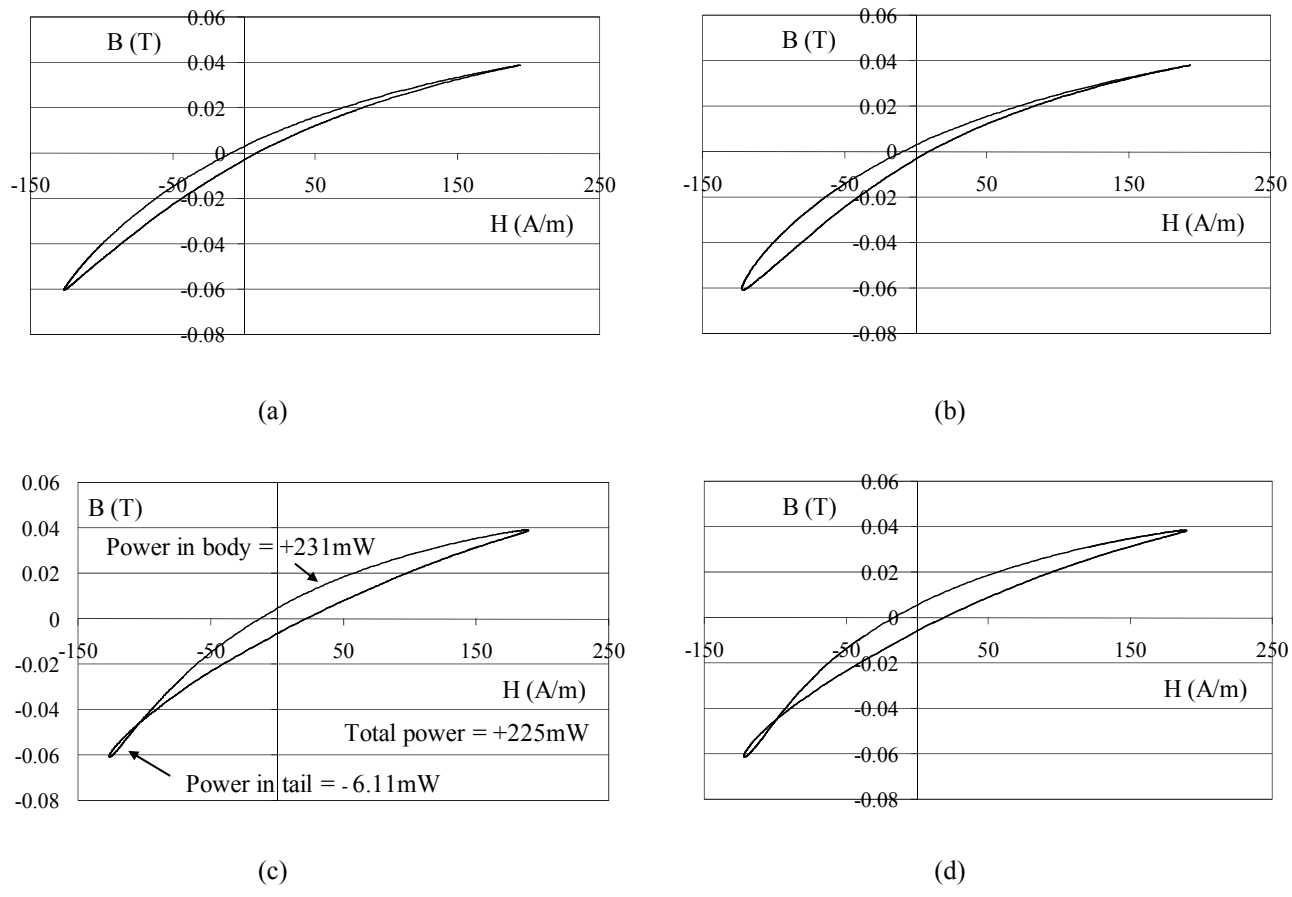

Fig. 7.1 B-H loops measured at an ac flux density of 0.05 T, and a constant dc bias of 247 A/m at (a) 30 kHz, (b) 34 kHz, (c) 34.6 kHz and (d) 37 kHz

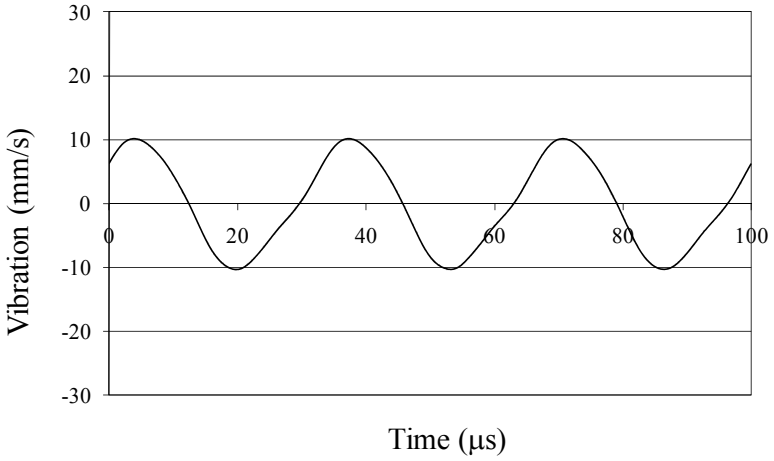

(a)

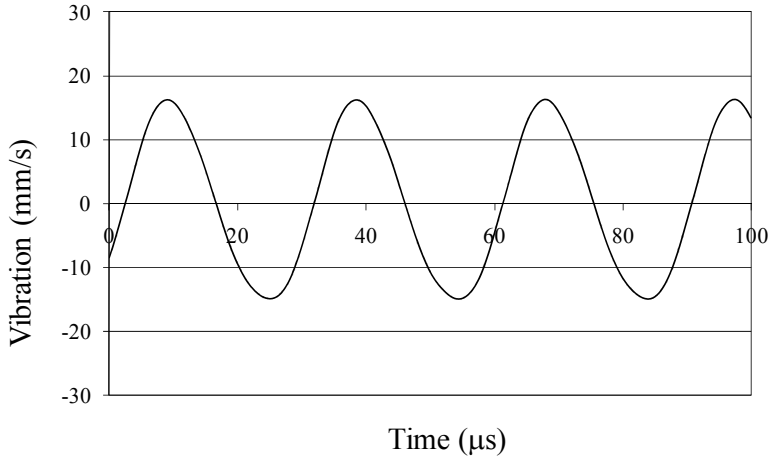

(b)

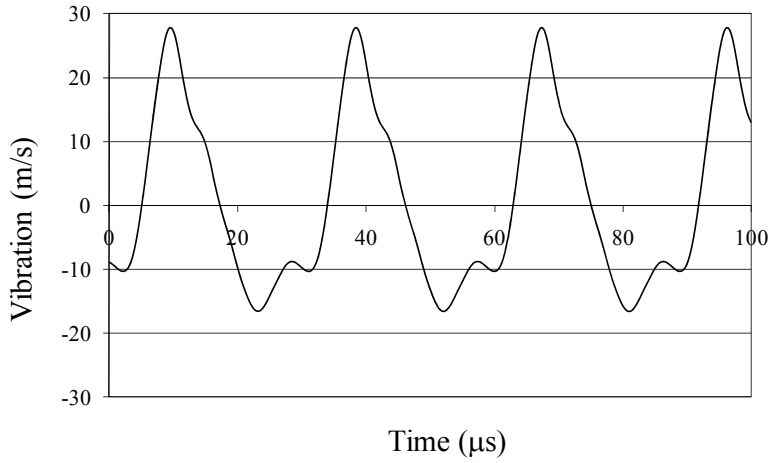

(c)

Fig. 7.2 Magnetostrictive vibration measured at (a) 30 kHz, (b) 34 kHz, and (c) 34.6 kHz

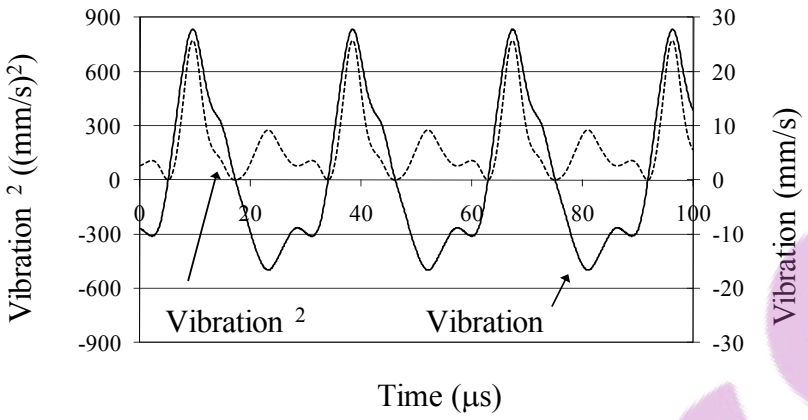

Fig. 7.3 Magnetostrictive vibration measured at 34.6 kHz, and its square

7.2.2 The Evolution of B-H Loops under dc Bias Conditions

After the tests in Section 7.2.1, the CUT was demagnetized then re-tested at 34.6 kHz, an ac flux density of 0.05 T, and at levels of dc bias which increased progressively from 0 A/m to 276 A/m. At various dc bias levels B-H loops were measured, and these are shown in Fig. 7.4. The B-H loops are presented with the dc bias removed, and located about zero for ease of comparison. With 0 A/m dc bias the B-H loop exhibited a typical shape, as shown in Fig. 7.4(a). As a dc bias was applied and increased to 40 A/m, the B-H loop attained a bulbous shape at the end exposed to the highest H-field and a tail at the end exposed to the lowest H-field, as shown in Fig. 7.4(b). These changes to the B-H loop became increasingly pronounced as the dc bias was increased until, at 128 A/m dc bias, the B-H loop crossed over on itself in its tail as shown in Fig. 7.4(c). This resulted in the figure-eight B-H loop shape, indicating that a small energy gain in the magnetic state occurred during part of the ac excitation cycle. The figure-eight shape continued to high levels of dc bias, as shown in Fig. 7.4(d) by the B-H loop measured at 276 A/m dc bias. From Fig. 7.4 it is obvious that the bulbous portions of the B-H loops contribute most to the loop area. Conversely, at the B-H loop ends, for which a tail firstly develops before the B-H loop crosses over on itself with increasing dc bias, core losses are constrained and then become negative. This suggests that during the bulbous portions of the B-H loop magnetic energy is not only dissipated in the form of losses, it is also converted to mechanical energy. Furthermore, during the portion of the B-H loop for which a tail develops, at least some of the mechanical energy previously developed is released through a conversion to magnetic energy. Through pressing down on the CUT while it is under a dc bias of 276 A/m, the B-H loop changed from the figure-eight shape to the undistorted shape shown in Fig 7.5. Pressing the CUT at 34.6 kHz under high dc bias conditions not only affected the B-H loop shape, it also affected the

magnetostrictive vibration and the stray field radiated from the CUT, which was measured using the EMI sniffer probe described in Chapter 5. This is evident in Fig. 7.6, which shows the stray field and vibration waveforms measured when the CUT was not pressed, in Fig. 7.6(a), and when it was pressed, in Fig. 7.6(b). These waveforms were measured under the same ac excitation and dc bias conditions used for Fig. 7.4(d), and measured at position A, as shown in Fig. 6.4. The results suggest that the shape of the stray field waveform is partly due to mechanical Barkhausen noise [1], and is dependent on the motion of the CUT.

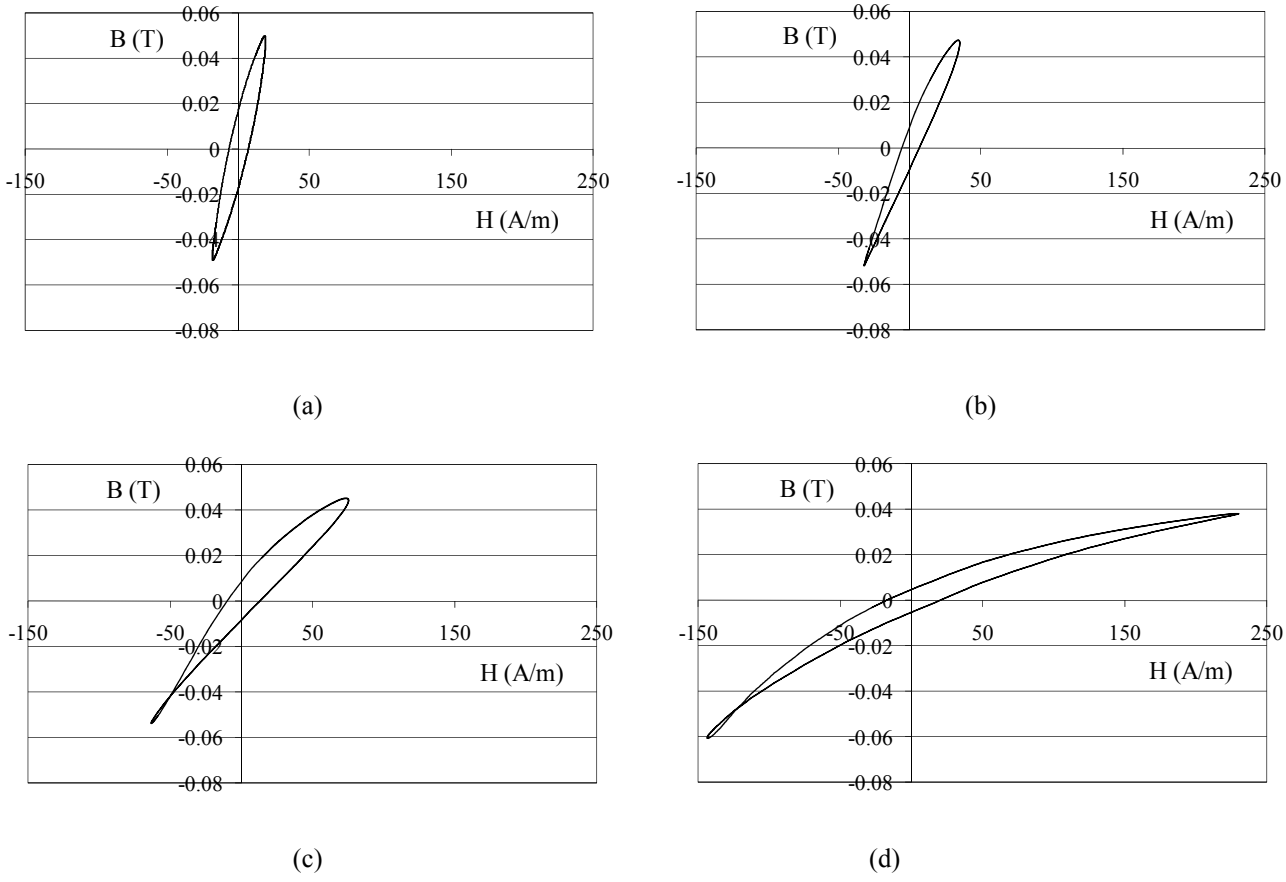

Fig. 7.4 B-H loops measured at 34.6 kHz, 0.05 T, with dc bias of (a) 0 A/m, (b) 40 A/m, (c) 128 A/m, (d) 276 A/m

The stray field waveform is also dependent on the proximity of the flux density of the CUT to its saturation level. This is evident in Fig. 7.7, which shows the relationship between the primary current waveform with the dc bias component removed, and the stray field waveforms at 30 kHz, an ac flux density of 0.05 T and a dc bias of 276 A/m. Under these conditions, for which the B-H loop has the conventional shape, the stray field waveform is similar to that in Fig. 7.6(b).

To test the transient nature of the figure-eight B-H loop condition, a CUT was excited under high dc bias conditions until a highly asymmetrical magnetostrictive vibration waveform and a

distorted B-H loop were generated. It was then left running for one hour. After this time the magnetostrictive vibration waveform was re-checked and was still found to be highly asymmetrical. Based on this result, it is therefore concluded that the figure-eight B-H loop condition can exist in the steady state.

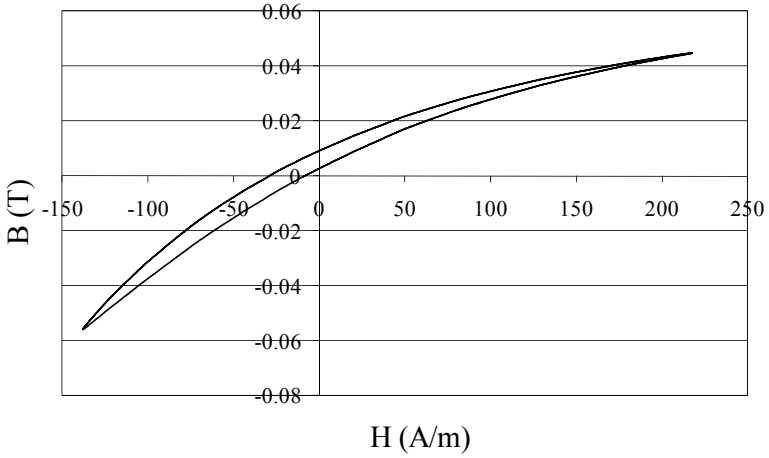

Fig. 7.5 BH loop when the CUT is pressed.

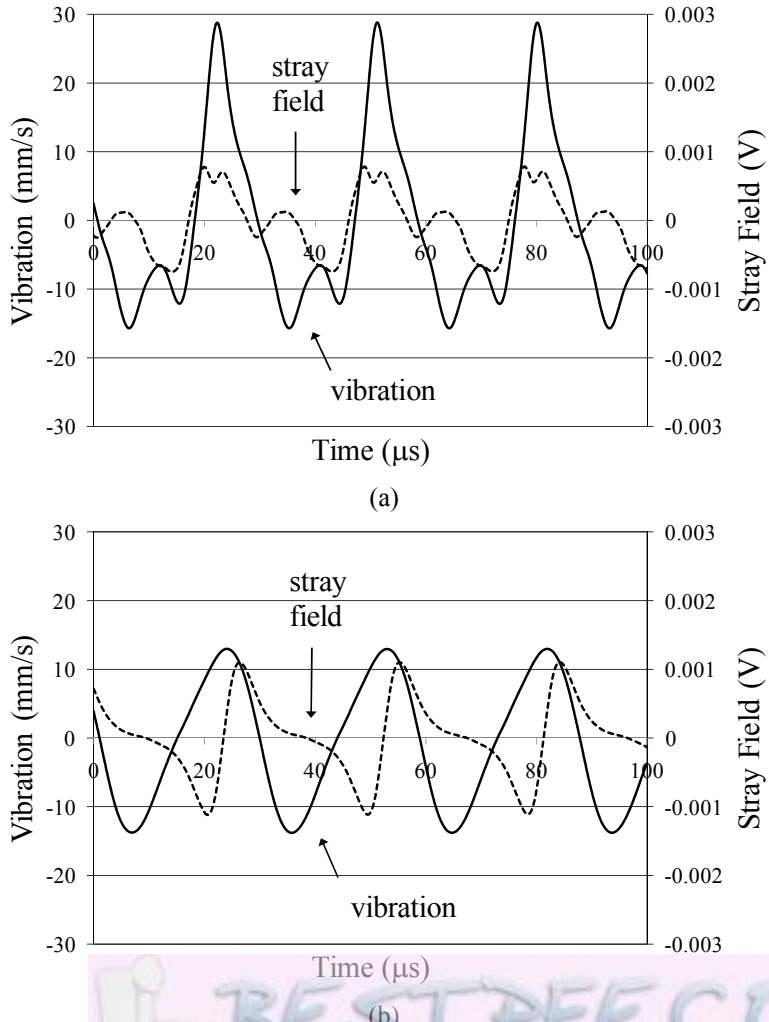

Fig. 7.6 Magnetostrictive vibration and stray field waveforms (a) not pressing, and (b) pressing on the CUT

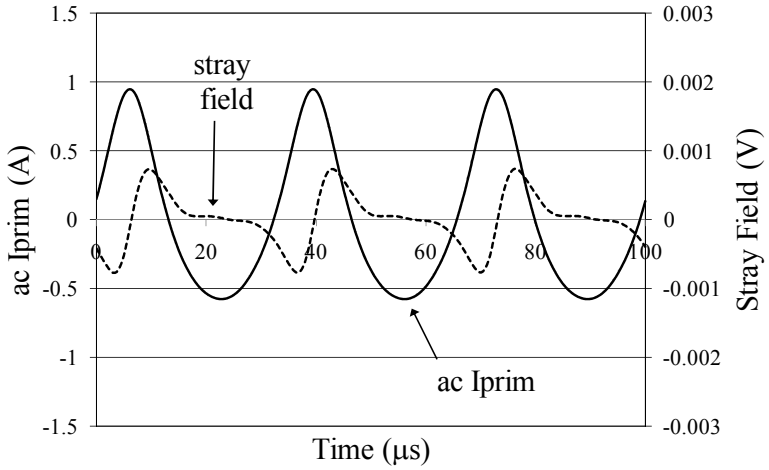

Fig. 7.7 ac primary current and stray field waveforms at 30 kHz

From the results presented in this section it is proposed that the asymmetrical nature and the harmonic content of the magnetostrictive vibration waveform cause the figure-eight B-H loop condition to occur through magnetomechanical interactions. The ability of the model proposed in Chapter 4 to simulate this phenomenon is discussed in Section 7.2.3.

7.2.3 Comparison to Model Results

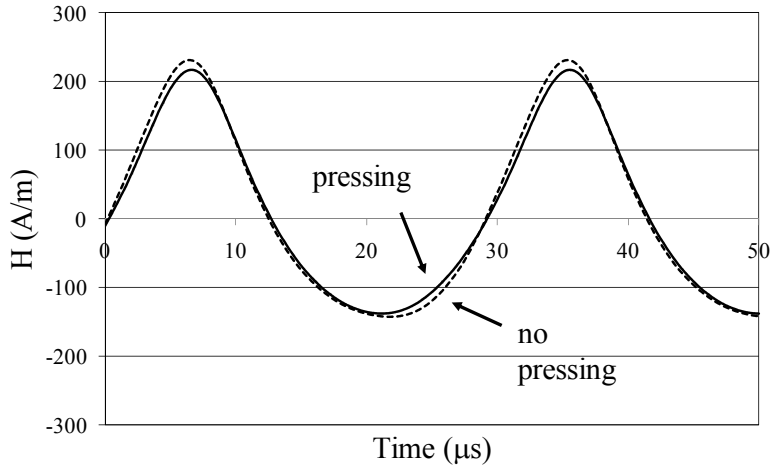

Fig. 7.8 Measured H-field waveforms when CUT is pressed and not pressed

As explained in Chapter 4, the experimental set-up used to obtain the results presented in this section operates to maintain a sinusoidal flux density in a CUT under dc bias conditions, irrespective of any magnetomechanical interactions that may be taking place. Therefore, variations in the magnetization process caused by magnetomechanical interactions are constrained to manifest through changes to the H-field. Accordingly, an inverse J-A model was

derived in Chapter 4, which operates with a B-field input, to simulate the figure-eight B-H loop phenomenon. Using this model it was possible to show that a phase shift of the H-field relative to the B-field occurs when figure-eight B-H loops are simulated. This effect can also be observed in experimental measurements. Fig. 7.8 shows measured H-field waveforms associated with the B-H loops measured when the 30x18x6 mm CUT was not pressed, as shown in Fig. 7.4(d), and when it was pressed, as shown in Fig. 7.5. From these results it can be observed that when the CUT was not pressed and, therefore, the magnetostrictive vibration of the CUT was not suppressed, a significant phase shift occurred in the lower portion of the H-field waveform. This measured result strongly supports the theory presented in Chapter 4, which states that the influence of magnetomechanical interactions on the magnetization process can be modeled through the addition of a stress field, $H_{\sigma i}$, to the effective field, H_e, within a CUT.

7.2.4 The Nature of the Vibration Measured at Different Points on the CUT

In this section magnetostrictive vibration waveforms are presented that were measured at positions A and B, as shown in Fig. 6.4, in order to further investigate the nature of the magnetostrictive vibration when typical, as well as distorted B-H loops are generated. The measurements were made on a 30x18x6 mm CUT under ac excitation conditions of 0.05 T, a dc bias of 247 A/m, and at excitation frequencies of 34 kHz and 34.6 kHz.

Fig. 7.9 shows magnetostrictive vibration waveforms measured at 34 kHz during the time a typical B-H loop was measured. From these measurements it is apparent that the CUT is largely vibrating in a sinusoidal manner in the horizontal plane, as viewed from Fig. 6.4. With an increase in the excitation frequency to 34.6 kHz, a distorted and figure-eight shaped B-H loop was measured, and the corresponding magnetostrictive vibration waveforms are shown in Fig. 7.10. From this figure it is apparent that the amplitude and harmonic content of the waveform changed at position A, as well as that at position B. Consideration of Fig. 7.9 and Fig. 7.10 together strongly suggests that the mode of vibration of the CUT changes when the figure-eight B-H loop phenomenon takes place.

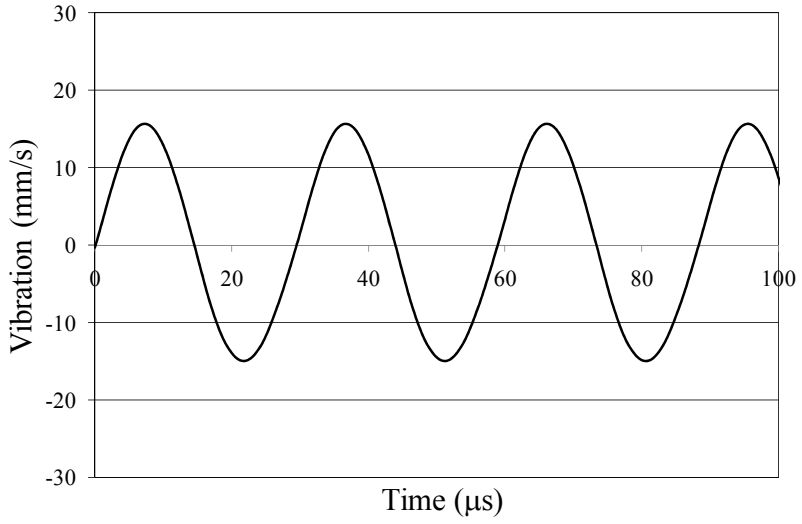

(a)

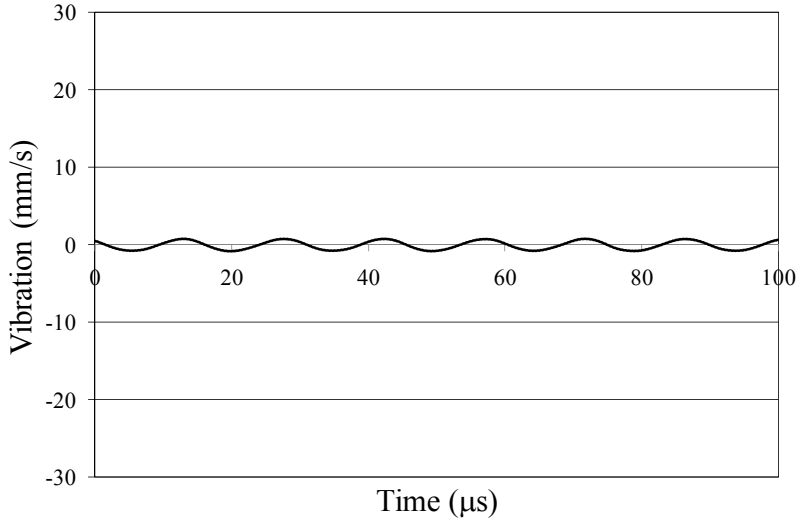

(b)

Fig. 7.9 Measured magnetostrictive vibration waveforms at 34 kHz at (a) position A, and (b) position B

7.3 Other Distorted B-H Loops under DC Bias Conditions

Distorted B-H loops, as well as those with a typical shape, have also been measured under dc bias conditions on a CUT in the same ferrite material as that tested previously in this chapter, but a different geometry. Results are shown in Fig. 7.11, which were measured at 40 kHz, an ac excitation level of 0.05 T and using a 25x15x10 mm toroidal CUT. In Fig. 7.11(a) a typical B-H loop is shown, which was measured with a dc bias of 133 A/m. The magnetostrictive vibration waveform measured at position A, as shown in Fig. 6.4, and associated with the B-H loop is given in Fig. 7.12(a), and it is apparent that the waveform is symmetrical.

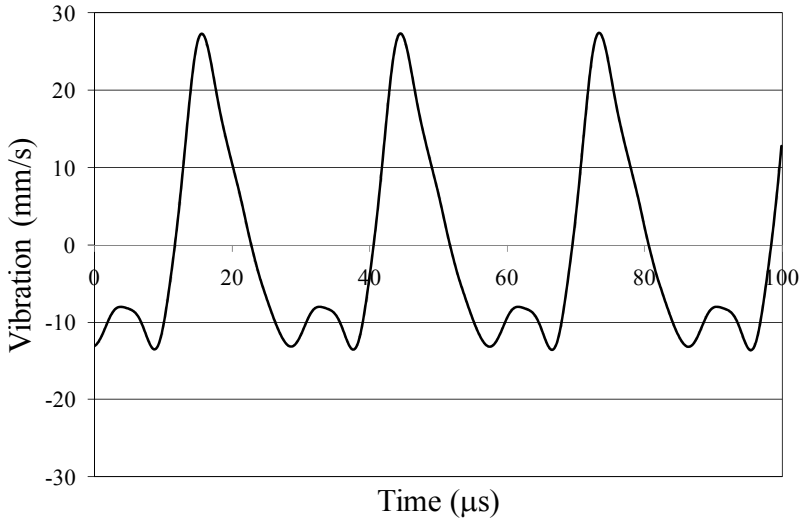

(a)

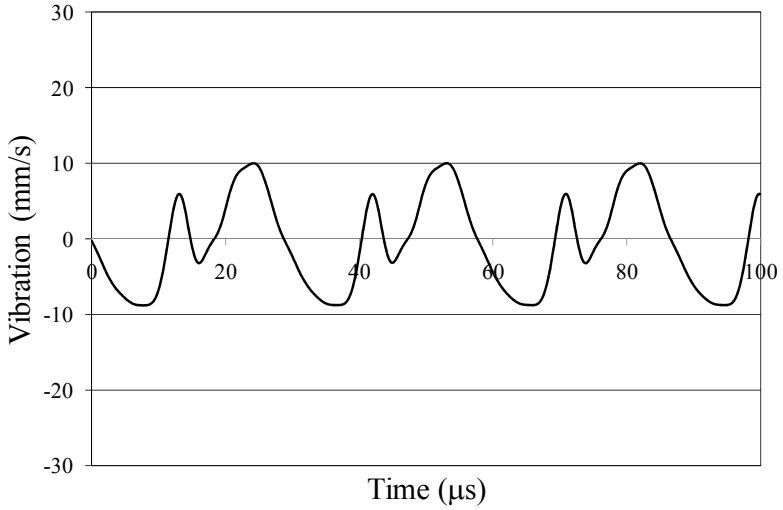

(b)

Fig. 7.10 Measured magnetostrictive vibration waveforms at 34.6 kHz at (a) position A, and (b) position B

However, with an increase of the dc bias to 159 A/m a change in the B-H loop shape occurred, as illustrated in Fig. 7.11(b), and the magnetostrictive vibration became asymmetrical, as shown in Fig. 7.12(b). In contrast to the figure-eight shaped B-H loops measured for the 30x18x6 mm CUT, it is evident that the crossover of the B-H loop occurs within the section located at the highest level of dc bias. This suggests that the energy conversion between magnetic and mechanical forms, which leads to distorted B-H loops, occurs during different parts of the respective excitation cycles of the 30x18x6 mm and 25x15x10 mm CUTs.

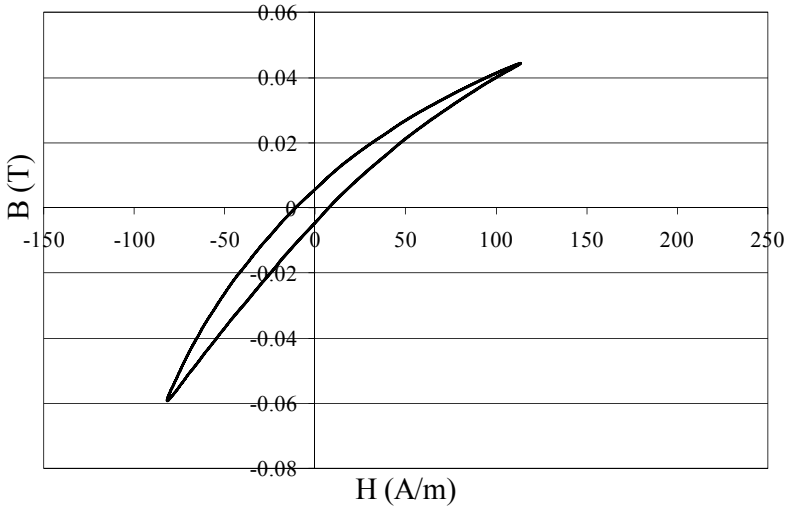

(a)

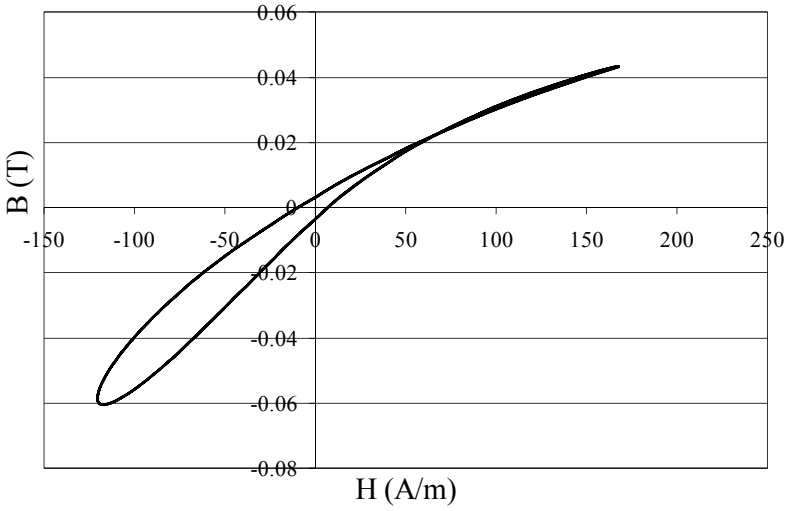

(b)

Fig. 7.11 B-H loops measured at 40 kHz and an ac flux density of 0.05T on the 25x15x10 mm CUT at dc bias levels of (a) 133 A/m, (b) 159 A/m

7.4 Summary

In this chapter experimental evidence has been presented showing the influence that magnetomechanical effects can have on B-H loop shapes under dc bias conditions, and at particular frequencies. Based on measured results, it is proposed that if a CUT is vibrating in a particular mode, for which the magnetostrictive vibration is asymmetrical, then significant distortion of the B-H loop can take place, as energy is converted between magnetic and mechanical forms. Experimental evidence has also been presented to show that the distortion to the B-H loop shape occurs through changes to the phase shift of the H-field of the CUT within portions of its cycle. This evidence strongly supports the model proposed in Chapter 4, which showed a similar phase shift in the predicted H-field also occurs when a $H_{\sigma i}$ field due to

magnetostrictive vibration is added to the H_e field within a CUT, as figure-eight shaped B-H loops are generated.

Evidence has also been presented to show that the influence of magnetomechanical interactions on B-H loop shapes can occur in toroidal CUTs of different geometries, albeit in the same ferrite material. Various other toroidal CUTs in different Mn-Zn materials have also been tested, and no distortion of the B-H loop shape for these materials has been found.

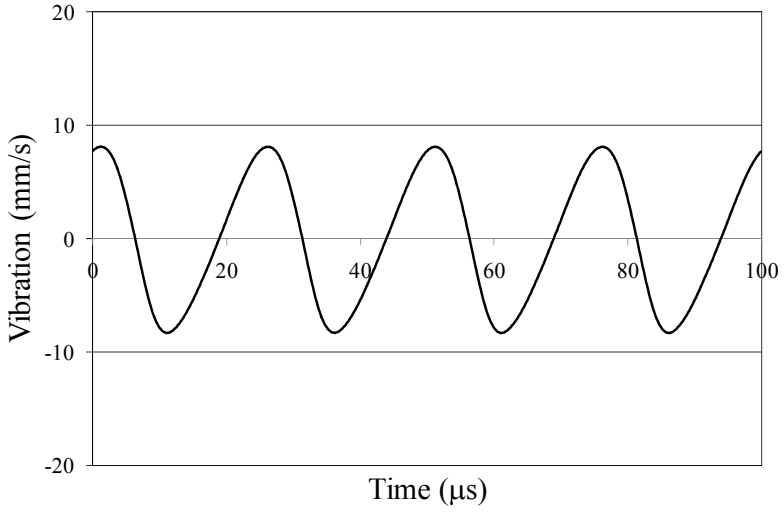

(a)

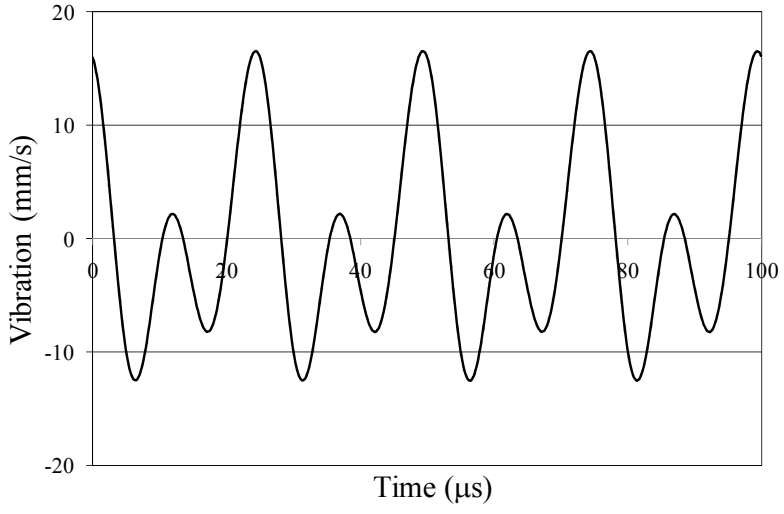

(b)

Fig. 7.12 Magnetostrictive vibration measured at 40 kHz and an ac flux density of 0.05T on the 25x15x10 mm CUT at dc bias levels of (a) 133 A/m, (b) 159 A/m

7.5 References

[1] J. Degauque, “Mechanical Spectroscopy”, Mat. Sci. Forum, vol. 366-368, 2001, pp. 453-482

Chapter 8

Conclusion and Suggestions for Future Work

8.1 General Conclusions

The nature of Mn-Zn ferrite material core losses under dc bias conditions has been investigated in this Thesis and, as a result, core loss mechanisms operative under dc bias conditions have been proposed. These mechanisms were incorporated into a mathematical model to allow the effect of dc bias conditions on hysteresis in the magnetization process to be predicted. Using the model it was also shown that B-H loops distorted into a figure-eight shape can be generated under dc bias conditions. The proposed core loss mechanisms associated with dc bias conditions, in additional to the mechanism causing figure-eight B-H loops to be generated, were validated through core loss and magnetostrictive vibration measurements made under dc bias conditions using a fully described circuit.

In Chapter 1 the importance of minimizing the energy losses of SMPS was explained, and used to show why it is important that an investigation into core losses under dc bias conditions should be undertaken. Aspects relating to the design of the dc filter chokes within SMPS were presented, and it was shown that the peak flux density at which the core of a dc filter choke is operated must be chosen to be as high as possible in order to maximize the energy density of the core. However, it was also stated that this involves a trade-off, because at higher levels of flux density and, therefore, dc bias levels, higher core losses will be encountered, thereby worsening the power supply efficiency.

In Chapter 1 a very brief introduction of the nature of hysteresis losses and the crystal structure of Mn-Zn ferrite materials was also given.

In Chapter 2 a literature review of previous studies on ferrite core losses under dc bias conditions was presented. The measurement circuits used to make these measurements were briefly described, and issues relevant to the accurate measurement of core losses under dc bias conditions were explained. In the majority of the previous studies measurements were presented showing that core losses increase in general with dc bias levels, and that this increase is significant. Empirical models that were presented in association with core loss measurements were criticized by the author on the basis that such models do not give physical insights. In other studies physical explanations and models were presented however, in the author's opinion, these explanations and models lacked detail. This was addressed in Chapter 3.

In Chapter 3 the nature of λ was described in the absence, as well as the presence, of a dc bias and related to mechanisms occurring at a microscopic level that impact upon the magnetization process. In the absence of a dc bias it was shown diagrammatically that the magnetostrictive vibration occurs at twice the frequency of the ac component of the applied magnetic field, and drops to the same frequency in the presence of a dc bias. It was then proposed that the decrease in the magnetostrictive vibration frequency contributes to an initial decrease in core losses with the initial application of a dc bias through a reduction of domain wall pinning sites within a CUT. However, with increasing levels of dc bias it was stated that an increase in magnetostrictive vibration takes place as domain rotation becomes more prominent in the magnetization process. Consequently, it was proposed that at some point the initial decrease in core losses due to the application of a dc bias is offset by the rising amplitude of the magnetostrictive vibration, which increases the strength and density of domain wall pinning sites and results in higher core losses.

A mechanism acting on the magnetization process at a macroscopic level under dc bias conditions was also proposed in Chapter 3. This mechanism was explained as the stress anisotropy resulting from magnetostrictive vibration, and acting on a large number magnetic moments within a CUT in a uniform manner. By this mechanism it was proposed that B-H loops distorted into a figure-eight shape under dc bias conditions could be generated.

In Chapter 4 it was shown that the phenomenon causing core losses to increase with dc bias conditions occurs at 1 kHz. It was also shown that 1 kHz is a quasi-static frequency for the Mn-

Zn ferrite material that was tested. This fact is important, because it allows the increase in core losses with dc bias conditions to be simulated using a rate-independent J-A model. Therefore, this model was described, with an emphasis placed on its parameters a and k, as well as the means by which M_{an} is derived, as it was proposed that these are significantly influenced by dc bias conditions. At a microscopic level it was proposed that under increasing dc bias conditions parameter k must correspondingly increase, as increased domain wall pinning sites are created for the reasons explained in Chapter 3. At a macroscopic level it was proposed that M_{an} is altered by the nature of the stress anisotropy generated by asymmetrical magnetostrictive vibration waveforms, which influences the shape of B-H loops. A modified inverse J-A model was then derived with the suitability to account for the phenomena induced under dc bias conditions, and used to predict the increase in core losses that occur under dc bias conditions, in addition to the figure-eight shaped B-H loop phenomenon described in Chapter 3.

In Chapter 5 the difficulties associated with the measurement of ferrite core losses under dc bias conditions were described and elucidated in the form of numerical examples in the absence, as well as the presence, of an air gap in the magnetic path of core. It was shown that the presence of a core gap increases the difficulty of making accurate core loss measurements. With knowledge of these difficulties, various commonly used core loss measurement techniques were reviewed. However, it was shown that all of these techniques suffer disadvantages and, therefore, three solutions were proposed. These included: the mutual inductance neutralization technique, the ZVS technique, and the technique based around the power op-amp weighted summing amplifier used in conjunction with the high accuracy wattmeter. Using the mutual inductance neutralization technique it was shown that accurate core loss measurements could be made. However, the technique was shown to be disadvantageous in terms making measurements quickly and, therefore, was not used to make the core loss measurements under dc bias conditions that were presented in Chapter 6. The ZVS technique for measuring core losses under dc bias conditions was also critically evaluated. This technique allows loss measurements to be made quickly, however it suffers from the disadvantage that residual circuit losses are measured at the same time as core losses. Therefore, in order to accurately determine core losses from the total losses that are measured, residual losses must be known to a precise value. Due to the difficulties associated with this disadvantage, the ZVS technique was not used to gather the results presented in this Thesis. For this task the technique based around the power op-amp and the high accuracy wattmeter was applied, which allowed core losses under dc bias conditions to be quickly and accurately measured.

In Chapter 5 a description was also given of the laser vibrometer system used to measure the magnetostrictive vibration of a CUT under dc bias conditions. This system allowed the proposed core loss mechanism to be monitored at the same time as core losses are measured under dc bias conditions. Consequently, it permitted the correlation between magnetomechanical effects and core losses under dc bias conditions to become apparent.

In Chapter 6 the relationship between core losses and magnetostrictive vibration under dc bias conditions was investigated experimentally. Initially, the magnetomechanical resonant frequencies of Mn-Zn MMG F49 ferrite material CUTs were identified, before core loss and magnetostrictive vibration measurements under dc bias conditions were made at specific frequencies; these frequencies were chosen to be close to, as well as distant from magnetomechanical resonance. The measurements clearly showed that a strong correlation existed between the amplitude and harmonic content of the magnetostrictive vibration and core losses, thereby strongly supporting the theoretical work in Chapters 3 and 4. Moreover, measurements made at frequencies distant from resonance were able to strongly support the theory describing why core losses initially fall with the application of a dc bias, before rising as the dc bias is increased above very low levels. To further investigate the impact of magnetomechanical effects under dc bias conditions on Mn-Zn core losses, the core losses of a MMG F49 ferrite material CUT were measured before, and after potting in silicon elastomer. These results showed that the effect of potting was to raise the level of the core losses at the highest levels of dc bias and, therefore, magnetostrictive vibration. This result can be explained by the higher levels of applied magnetic field energy demanded by the potted CUT, in order to allow it to vibrate against the force of the potting material.

In Chapter 7 experimental evidence was presented showing the influence that magnetomechanical effects can have on B-H loop shapes under dc bias conditions. Based on the evidence it was proposed that distorted B-H loop shapes can be encountered, as energy is converted between magnetic and mechanical forms. Experimental evidence also showed that the distortion to the B-H loop shape manifests through changes to the phase shift of the H-field of the CUT within portions of its excitation cycle. This evidence strongly supports the model proposed in Chapter 4, which showed a similar phase shift in the predicted H-field when predicted figure-eight shaped B-H loops were generated. Experimental evidence was also presented showing that distorted B-H loops can also be generated by CUTs of different toroidal geometries, albeit in the

same MMG F49 ferrite material. Various toroidal CUTs manufactured in Mn-Zn ferrite materials other then MMG F49 ferrite material have also been tested. For these materials distorted, figure-eight shaped B-H loops have not been measured.

8.2 Contributions

The main contributions of this study are listed below:

- The proposed theory that elastic micro-stresses increase with dc bias levels as magnetostrictive vibration increases, which generates a higher number of domain wall pinning sites and, therefore, increased core losses.
- The proposed theory that B-H loops can be distorted into figure-eight shapes under dc bias conditions due to the influence of magnetomechanical effects on the magnetization process.
- The modification of an inverse J-A model into a form that allows the increase in core losses with dc bias conditions, as well as distorted B-H loops, to be predicted.
- The development of three circuits allowing core losses to be measured under dc bias conditions.
- The presentation of accurate core loss measurements made under dc bias conditions.
- The presentation of measured B-H loops, distorted into a figure-eight shape.

The above contributions have resulted in the publication of four IEEE transactions papers, and two IEEE conference papers as listed below:

1. C. A. Baguley, B. Carsten, U. K. Madawala, "The Effect of DC Bias Conditions on Ferrite Core Losses," *IEEE Trans. Magn.*, vol.44, no.2, pp.246-252, Feb. 2008
2. C. A. Baguley, U. K. Madawala, B. Carsten, "A New Technique for Measuring Ferrite Core Loss Under DC Bias Conditions," *IEEE Trans. Magn.*, vol.44, no.11, pp.4127-4130, Nov. 2008
3. C. A. Baguley, U. K. Madawala, B. Carsten, "Unusual Effects Measured Under DC Bias Conditions on MnZn Ferrite Material," *IEEE Trans. Magn.*, vol.45, no.9, pp.3215-3222, Sept. 2009
4. C. A. Baguley, U. K. Madawala, B. Carsten, “The Impact of Vibration due to Magnetostriction on the Core Losses of Ferrite Toroidals under DC Bias”, *IEEE Trans. Magn*., accepted 2011

5. C. A. Baguley, U. K. Madawala, B. Carsten, "The Influence of Temperature and Core Geometry on Ferrite Core Losses under DC Bias Conditions", *IEEE Proc. SPEEDAM 2008*, 11-13 Jun. 2008, pp.355-359
6. C. A. Baguley, B. Carsten, U. K. Madawala, "An Investigation into the Impact of DC Bias Conditions on Ferrite Core Losses," *IEEE Proc. IECON 2007*, pp.1408-1413, 5-8 Nov. 2007

8.3 Suggestions for Future Work

Although the investigations presented in this Thesis show the significant influence that magnetostrictive vibration has upon the magnetization process in terms of increasing the core losses, this influence is not shown at its most detailed level. The author considers that this would require a comparison between dynamic domain wall movements observed in the presence, as well as the absence of a dc bias. Such a comparison should show that domain wall movement is increased in difficulty by dc bias conditions. A comparison of this type would also allow the geometry of domain wall pinning sites to be observed

In conjunction with the observation of moving domain walls in the presence and absence of a dc bias, it is also suggested that dynamic micro-stresses within a CUT should be observed. This would allow the increased difficulty of domain wall movement under dc bias conditions to be clearly associated with an increase in micro-stresses.

In Chapter 7 it was shown when figure-eight shaped B-H loops are generated the magnetostrictive vibration of the CUT is asymmetrical in two axes. However, the laser vibrometer used to measure the vibration of the CUT is limited in that it does not allow the vibration to be fully characterized in the space, or the time domains. Therefore, this task remains to be completed. It is also suggested that the modeling of the figure-eight phenomenon may be improved through the use of a modified version of a vector J-A model. Further investigation is also required on the manner by which an asymmetric magnetostrictive vibration waveform may be incorporated into a model under dynamic conditions.

The ideal measurement relating to the figure-eight B-H loop phenomenon would involve monitoring the magnetization component due vibration, in its vector form, in conjunction with the magnetization component due to the applied magnetic field. Such a measurement should

show that the magnetization component due to the applied magnetic field should reduce as it comes into alignment with the magnetization component due to the magnetostrictive vibration.

The results of the XRD test undertaken on the MMG F49 ferrite material show its composition is not extraordinary in terms of the elements it contains. However, despite its apparently standard composition in this respect MMG F49 ferrite material is able to generate highly distorted B-H loops. Furthermore, and to the knowledge of the author, such distorted B-H loops have not previously been reported for any other type of Mn-Zn ferrite material. Therefore, the author believes that the properties allowing the F49 material ferrite to generate highly distorted B-H loops may lie derive from the process by which it is manufactured. However, this remains to be confirmed.

In this Thesis it is proposed that core losses can be at least partially explained by the influence of magnetostrictive vibration on domain wall movement in addition to domain rotation processes. However, no distinction is drawn as to the relative contribution of each of these processes. Some insight into the relative contribution may be able to be drawn through testing magnetic materials under dc bias conditions for which the magnetization process occurs largely through domain rotation.

Appendix A:

Properties of MMG F49 Mn-Zn Ferrite Material

Symbol	Quantity	Test Condition	Value
μ_i	Initial permeability (nominal)	10 kHz B<0.1 mT 25°C	1000 ± 30%
B_{sat}	Saturation flux density (typical)	H=796A/m 25°C	580 mT
		100°C	480 mT
μ_a	Amplitude permeability (nominal)	B=400mT 25°C	1800
		B=320mT 100°C	2000
B_r	Remanent flux density (minimum)	10kHz 25°C	230 mT
H_c	Coercivity (typical)	10kHz 25°C	25 A/m
T_c	Curie Temperature (minimum)	10kHz B<0.1 mT	290°C
ρ	Resistivity (typical)	1 V/cm 25°C	100 Ω/cm
P_v	Total power loss density (maximum)	25 kHz B=200mT 80°C	200 mW/cm^3

Appendix B:

Inverse J-A Parameter Determination Algorithm

- Determine parameter k
  Estimate parameter k using:
  $k = H_c$

- Determine α
  if error > limit

$$M_{an}(M_r) = M_s\left(\coth\left(\alpha \times \frac{M_r}{a}\right) - \left(\frac{a}{\alpha \times M_r}\right)\right)$$

  where,
  M_r = magnetization at remanence (A/m)

$$f(\alpha) = M_{an}(M_r) - M_r + \frac{k}{\frac{\alpha}{1-c} + \frac{1}{X_r - c\frac{dM_{an}(M_r)}{dH}}}$$

  Use secant method to evaluate α

  1. $\alpha_{n-2} = \alpha_{n-1}$
     $\alpha_{n-1} = \alpha_n$
  2. $\alpha_n = \alpha_{n-1} - \frac{\alpha_{n-1} - \alpha_{n-2}}{f(\alpha_{n-1}) - f(\alpha_{n-2})} f(\alpha_{n-1})$
  3. If $\left|\frac{\alpha_n - \alpha_{n-1}}{\alpha_n}\right|$ > admissible error return to 1, else $\alpha = \alpha_n$

- Determine a
  $H_e = H_m + \alpha H_m$

  where,
  H_m = maximum value of H at tip of B-H loop (A/m)

$$M_{an}(H_e) = M_s\left[\coth\frac{H_e}{a} - \frac{a}{H_e}\right]$$

$$g(a) = M_{an}(H_e) - M_m - \frac{(1-c)kX_m}{\alpha X_m + 1}$$

where,

M_m = maximum value of magnetization at tip of B-H loop (A/m)

X_m = differential susceptibility at tip of B-H loop

Use secant method to evaluate a

1. $a_{n-2} = a_{n-1}$

   $a_{n-1} = a_n$

2. $a_n = a_{n-1} - \frac{a_{n-1} - a_{n-2}}{g(a_{n-1}) - g(a_{n-2})} g(a_{n-1})$

3. If $\left| \frac{a_n - a_{n-1}}{a_n} \right|$ > admissible error return to 1, else $a = a_n$

- Determine c

$$c = \frac{3aX_{in}}{M_s}$$

where,

X_{in} = differential susceptibility at low levels of magnetization

Appendix C:

The Table below gives the manufacturer specified power measurement uncertainty for the Clarke and Hess model 2335 wattmeter for any power factor from 0–100% of the full scale range.

Specified Uncertainty of Clarke and Hess 2335 Wattmeter

Frequency	+/-(% of VA + % of Range)
DC	+/- (0.2+0.1)
5-250kHz	+/- (0.2+0.1)
250-500kHz	+/- (0.4+0.2)
500-1MHz	+/- (0.8+0.4)